A New Method To Measure True Two-Photon Correlation of Soft X-ray Synchrotron Radiation

Renzhong Tai

March 24, 1999

Department of Synchrotron Radiation Science
School of Mathematical and Physical Science
The Graduate University for Advanced Studies

The Doctoral Thesis Summary

Two-photon correlation measurement provides a promising way to experimentally demonstrate the statistical nature of a light source, which is very significant for the deep understanding of the photon-generating process and the diagnosing of the coherence property. Quantitatively two-photon correlation is described by second-order coherence. Usually the behavior of the second-order coherence against any of the parameters defining the phase volume is different for different photon statistics. The Poisson photon statistics for coherent light gives its second-order coherence as a flat response; The Bose-Einstein photon statistics for chaotic light gives its second-order coherence as a bunching effect; While the Sub-Poisson photon statistics for non-classical light gives its second-order coherence as an anti-bunching effect. Therefore the measurement of two-photon correlation is proved to be a good finger print to check whether light is in coherent state or incoherent state such as thermal state or non-classical state.

Historically the measurement of two-photon correlation was first performed by Hanbury-Brown and Twiss (HBT) in 1956. They used a linear mixer to realize the correlation of the two currents from the photoelectric detectors illuminated by a stationary thermal light souece, a mercury arc, and the photo-bunching effect was first successfully observed in the visible region of 435.8 *nm*.

HBT method is no doubt a good way to extract the small excess two-photon correlation for a stationary light because the background, that is the DC components, has been cut off automatically by the broad band amplifiers, which is in fact the key of the success of HBT experiment. However there exists a general problem, to which no attention has ever been paid, in measuring the two-photon correlation of non-stationary light such as synchrotron radiation (SR) by the HBT method. Here the "non-stationary" means a sense of classical mechanics that the observed intensity has some deterministic time structure. The systematic time structure of SR decided by the bunch distribution of the electric current in a storage ring will give rise to a large amount of unexpected accidental correlation, which in fact has nothing to do with the inherent photon statistics of light source and usually 1000~10000 times larger than the true two-photon correlation due to the

short bunch separation length ($2ns$) and the short coherence time ($\sim 0.1ps$) which is not comparable to the time resolution ($1ns$) of the measuring system. The existence of the accidental correlation would severely prevent us from observing the bunching effect of the true two-photon correlation.

Therefore to suppress the much larger accidental correlation and to extract the small true two-photon correlation, a novel intensity interferometer has been developed for soft X-ray synchrotron radiation. This intensity interferometer consists of an optical vacuum chamber and an electric correlator. All the essential optical elements which includes a wire scanner, a precise diffraction slit, a grating monochromator with a coherence time modulator, a beam divider and two fast-response photon detectors (microchannel plates) are mounted in this high vacuum chamber. The electric correlator completes the multiplication of the two broad band electric currents coming from the photoelectric detectors. The basic idea to suppress the much larger accidental correlation is to modulate the coherence time by modulating the entrance slit width of the monochromator by a piezoelectric translator. The two sets of light intensity are simultaneously modulated too. When the frequency of modulation is f, the third harmonics $3f$ is detected with a loch-in amplifier because the $3f$ components include only the true two-photon correlation. Practically it is difficult to modulate with frequency f without any higher order harmonics distortion which might add some false $3f$ components. To overcome this difficulty we have used a sharp bandpass filter of 100~350 MHz in each branch of the correlator, which is lower than the RF frequency 500 MHz and much higher than 1.6 MHz, the revolution frequency of the stored beam of the 2.5 GeV storage ring.

This new apparatus has been operated successfully in the measurement of the horizontal two-photon correlation for the first harmonic of undulator radiation with photon energy of 70 eV at the Photon Factory, KEK. By narrowing the precise slit width which correspondingly changes the spatial coherence of the incident SR, a bunching effect of the normalized excess two-photon correlation has been clearly observed. This explicit bunching effect implies that synchrotron radiation is chaotic radiation.

Further investigation shows that although second-order coherence is completely determined by the first-order coherence for the case of chaotic light, the measured information from the light source is essentially different.

The two-photon correlation of synchrotron radiation does not depend on the response time of the detectors but gives the information of instantaneous emittance of the stored beam with the time scale of coherence time τ_c. By fitting the experimental data, the horizontal instantaneous emittance of the stored beam is estimated to be 40*nmrad*.

This intensity interferometer can be utilized to characterize the coherence properties of incomplete FELs, such as SASE, because if they are fully coherent light sources the normalized excess two-photon correlation would have a flat response, but not showing a photon-bunching effect.

Contents

1 Introduction

1.1 Historical review of two-photon correlation

1.1.1 Hanbury-Brown and Twiss experiment

The first experimental evidence for the existence of correlations between the outputs of two photoelectric detectors illuminated by a partially coherent light was obtained in a series of experiments performed by Hanbury-Brown and Twiss in the 1950s [1][2][3][4][5], with the apparatus shown in Fig. 1-1.

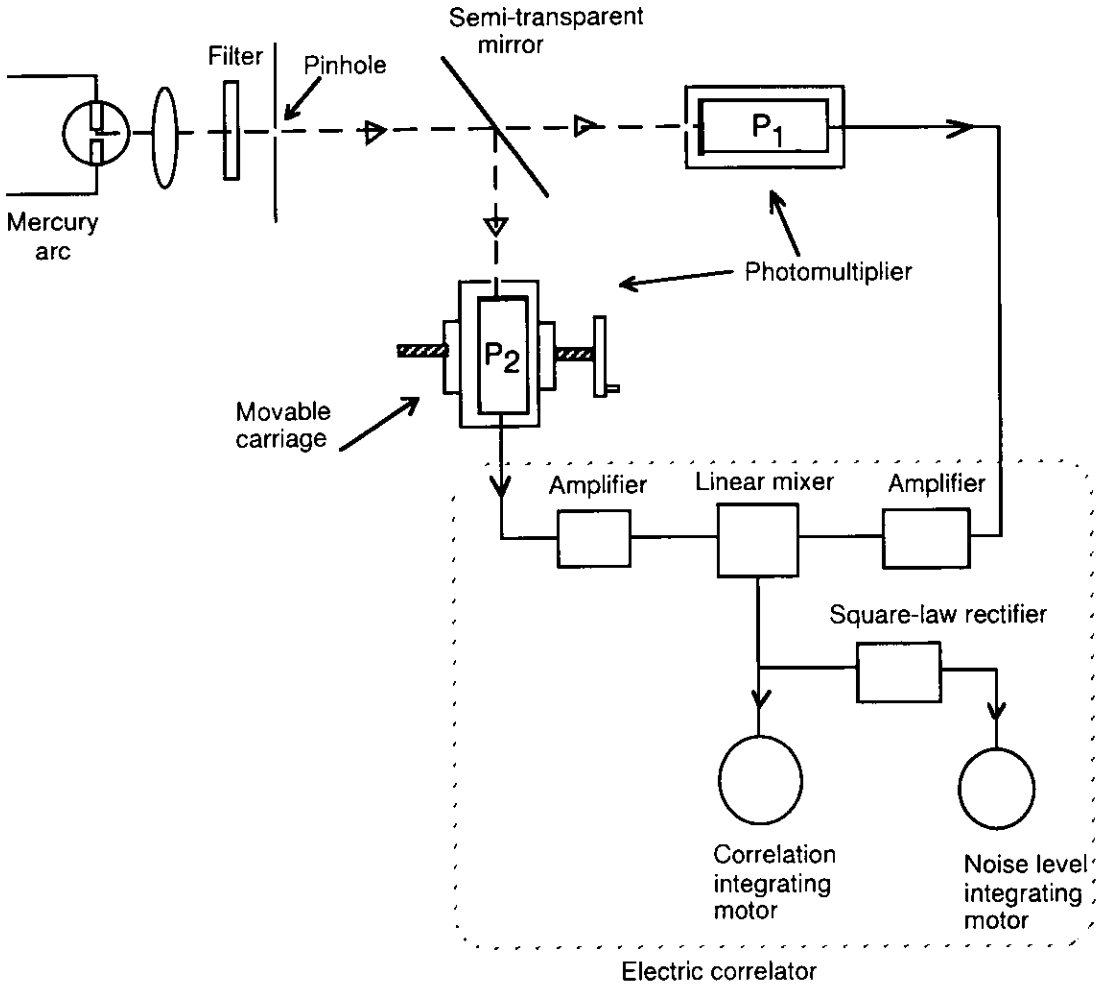

Fig. 1-1 A simplified outline of Hanbury-Brown and Twiss intensity interferometer

A secondary light source was formed by a circular pinhole on which the image of a high-pressure mercury arc was focused by a lens. The 435.8 *nm* line of mercury was isolated by a liquid filter. The beam of light from the pinhole was divided by a semi-transparent mirror to illuminate the cathodes of the photomultiplier P_1, P_2. The degree of coherence of the light at the cathodes could be varied by traversing one photomultiplier (P_2) horizontally and normal to the incident light.

The fluctuations in the anodes currents of the photomultipliers were transmitted to a correlator through coaxial cables of equal length. The photo-electric correlation was done by a linear mixer (multiplier). The average value of this correlation product, which was recorded on the revolution counter of an integrating motor, gave a measure of the correlation in the fluctuations. Another noise-level integrating motor, which recorded the average of the square of the correlation product, was used to measure the background that was indeed the product of average current of each branch. The signal to noise ratio, as was called by Hanbury-Brown and Twiss, gave the normalized correlation signal which is independent of the inevitable small changes in the light and of the changes in the gain of the correlator. As a result, a strong positive correlation was observed when the cathodes are superimposed but not when they are widely separated. This is the well-known bunching effect nowadays of the second-order coherence of thermal light.

The apparatus in Fig.1-1 was later developed to the application to astronomy and the angular sizes of stars were successfully measured with a precision higher to several orders than the ones by conventional method of Michelson's stellar interferometer [2][6]. The reason is that HBT electric correlator actually measures the "wave noise" correlation. This "wave noise" is just the light intensity fluctuation originating from the thermal nature of light sources (stars). Although the atmospheric scintillations, which had seriously affected the precision in Michelson's stellar interferometer, could introduce an additional disturbance fluctuation to the light, they are uncorrelated at all.

The great significance of Hanbury-Brown and Twiss experiment is that it provides a basic method to measure two-photon correlation. Two-photon

correlation is a measure of second-order coherence. It is essentially different from the familiar interference effects such as Youngs double-slit interference effect or Michelson interference effect(rigorously speaking they belong to first-order coherence). Hanbury-Brown and Twiss experiment might be a milestone in the development of quantum optics. It made one reconsider the concept of coherence quantum mechanically and directly resulted to the outgrowth of the quantum theory of optical coherence developed by R. J. Glauber in 1963 [7][8].

1.1.2 Two kinds of measuring methods

Up to now to measure two-photon correlation, there are two basic methods. One is *photoelectric currents correlation* as shown in Fig.1-1 (or called *HBT* method, because it was first performed by Hanbury-Brown and Twiss), where a linear multiplier is used to realize the correlation of two fluctuating photoelectrc currents. The other is *coincidence-counting method*. Fig.1-2 shows its basic arrangement .

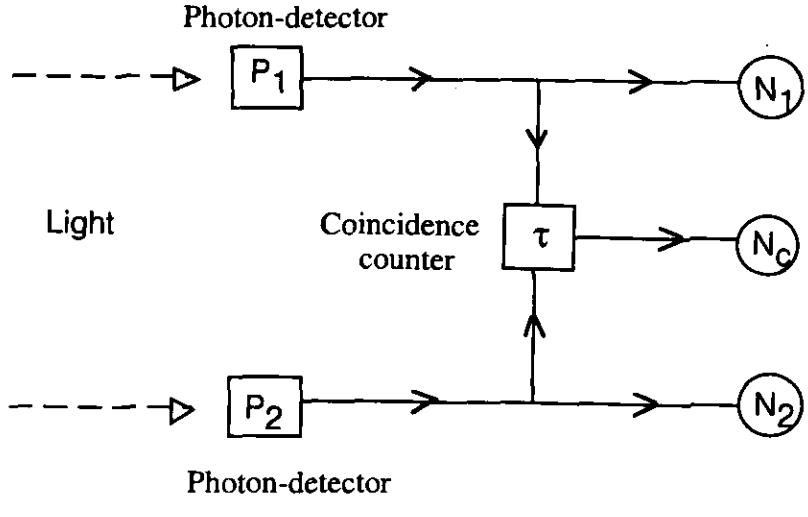

Fig.1-2 A coincidence-counting intensity interferometer

The two counters N_1 and N_2 register the number of photoelectrons in each channel and the counter N_c register a coincidence when two pulses arrive within a time τ. N_1 and N_2 are usually used for the normalization of N_c but not the only way, depending on the properties of light.

The coincidence N_c in Fig.1-2 includes not only the excess two-photon correlation but also the random Poisson coincidence, which requires that the coherence time should not be too smaller than the response time of photon-detectors, otherwise the much larger Poisson random coincidence would severely affect the extraction of the excess two-photon correlation and its measuring precision. On the other hand in *photoelectric currents correlation* method (*HBT* method) the large DC correlation has been cut off automatically by the broad band amplifiers and only the excess two-photon correlation is recorded, which would give a relatively higher measuring precision.

In *photoelectric currents correlation* method (*HBT* method), increasing of the light intensity helps improvement of signal to noise ratio, while it does not help in coincidence method due to the finite resolving time of practical detectors and counters which severely limit the number of photoelectrons per second that can be counted separately [6].

1.1.3 Two-photon correlation of X-ray synchrotron radiation

After Hanbury-Brown and Twiss's pioneering work, a number of experiments of two-photon correlation were performed both by photoelectric correlation and coincidence-countering technique in the visible region [9][10]. The application to the X-ray region was suggested by Lewis et al in 1963 [11]. But because degeneracy parameter is proportional to the third power of wavelength, it was apparently getting too difficult to detect the intensity correlation in a shorter wavelength region until the appearance of high brightness light source.

The advent of synchrotron radiation bring one a new ambition. First in 1975 Shuryak proposed the observation of two-photon correlation with synchrotron radiation [12]. Later in 1992 Ikonen gave a detailed argument of the possibility of detecting two-photon correlation of independent Gamma rays with the aid of the third-generation synchrotron radiation source, that is, high-brilliance undulator radiation [13]. In the same year a soft X-ray intensity interferometer was constructed for undulator radiation by Gluskin et al [14][15][16][17][18] by completely following the method of Hanbury-Brown and Twiss's electric correlator. But unfortunately the huge DC drift

severely prevented them from observing the small true two-photon correlation. According to our present study it has become clear that the huge DC drift is just the accidental correlation caused from the non-stationary time structure of synchrotron radiation [19][20].

The first success in the measurement of X-ray two-photon correlation from a synchrotron radiation source was reported by a Japanese group in 1997 by using the photoelectric coincidence technique [21]. The highly monochromatic hard X-ray with the photon energy 14.4 KeV and its energy width 6.4 meV came from a high-brilliance undulator radiation of the Tristan Main Ring, KEK, Japan. The block diagram of their photon-counting system is shown in Fig. 1-3. The output pulses from two detectors were fed into the coincidence unit and then scaler 1 counted the number of coincidences. In the delay circuit the delay time for the output pulse from one detector was set at the circulation period of electron bunch, 10μs. Poisson random coincidence events, which were the coincidence between one photon emitted from a certain electron bunch and another photon emitted from the same electron bunch after making one revolution, was recorded at scaler 2.

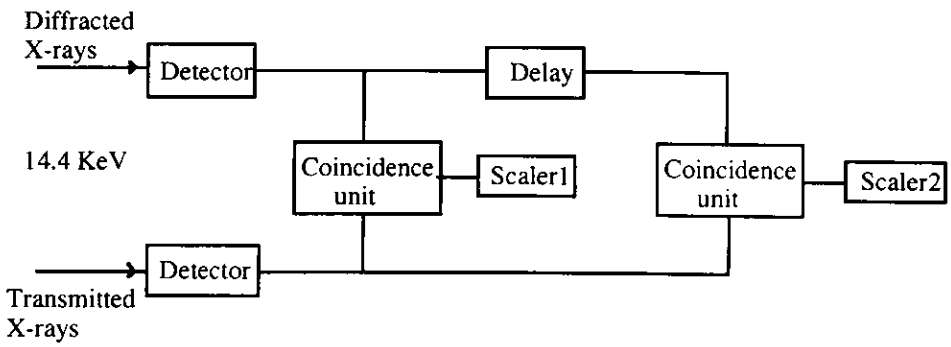

Fig. 1-3 The photon-counting system used by Y. kunimune et al [21]

After changing the width of a precise slit, which change the spatial coherence of incident synchrotron radiation, a bunching effect was observed.

Any way the strong background, that is the poisson random coincidence, severely decrease the measuring precision due to the finite response time of detectors compared with the coherence time.

1.2 Non-stationary light and accidental correlation

So far as we know there has been no report of successful measurement of two-photon correlation of synchrotron radiationin in soft X-ray region. Due to the considerations described in last two sections we believe that the *photoelectric currents correlation* (*HBT* method) might be an efficient way in the measurement of two-photon correlation of soft X-ray synchrotron radiation no matter how high its Bose degeneracy would be.

However the complete following after *HBT* method would inevitably lead to a failure in the measurement just as Gluskin did. This is because synchrotron radiation is a kind of non-stationary light. Here the "Non-stationary" means in sense of classical mechanics that the observed intensity has some deterministic time structures which are determined by the bunches distribution of electric current in the storage ring. This time structure will give a large amount of unexpected accidental correlation. It is caused by the fact that when one detector catches a photon signal, the other detector has more chance to get a photon signal through systematic time variation of radiation intensity modulated by the bunch structure. Usually this false correlation is 1000~10000 times larger than the true correlation due to the short bunch separation length ($2ns$) and the short coherence time($0.01ps$) which is not comparable to the time resolution($1ns$) of the measuring system. The accidental correlation is a positive correlation. It has nothing to do with the inherent photons statistics and will give a flat response. However the strong background formed by this accidental correlation would severely prevent us from observing the bunching effect of true two-photon correlation.

1.3 Motivations of this work

1.3.1 Exploration of a new experimental method

The existence of accidental correlation is a general problem in the measurement of two-photon correlation of non-stationary light by *HBT* method. Therefore how to suppress this *accidental correlation*, how to extract the *true two-photon correlation* is a new challenge to us.

To meausure *the true two-photon correlation* a most important step is to select an appropriate way to eliminate the influence of the systematic time structure. In fact a new intensity interferometer for soft X-ray synchrotron radiation based on a coherence time modulation technique has been developed and been successfully operated in the measurement of *true two-photon correlation* at the undulator beam line BL16B of Photon factory of KEK.

1.3.2 Study of photon statistics

Two-photon correlation measurement provides a promising way to experimentally demonstrate the statistical nature of a light source. Although rigorous appraisal of a totally coherent light needs to measure the coherence higher than the second-order, at least from the measurement of second-order coherence, thermal light (chaotic light) and squeezed light could be distinguished. Bose-Einstein photon statistics in thermal light gives the bunching effect of its second-order coherence; Sub-Poisson photon statistics in squeezed light gives the anti-bunching of its second-order coherence; while Poisson photon statistics in coherent light gives a flat response (a constant) of its second-order coherence. As it is shown later, the information of photon statistics is very significant for deep understanding of photon-generating process and mechanism.

According to our experimental result, it is first experimentally verified that soft X-ray synchrotron radiation is indeed a chaotic radiation and its photons obey Bose-Einstein distribution.

In fact the concept of second-order coherence has been nowadays generalized to not only photons, but a Bose-Einstein condensed atomic gas,

where the released atoms behaves completely like coherent photons from a laser. [22]

The measurement of second-order coherence can be utilized as an important experimental method to diagnose FELs, such as SASE. If it is a complete FEL its second-order coherence would exhibit a flat, but not bunching response.

1.3.3 Measurement of instantaneous emittance for synchrotron radiation

By the information of two-photon correlation, Hanbury-Brown and Twiss succeeded in measuring the angular size of stars with a higher precision. That was attributed to the second-order coherence which has a lot of advantages than the first-order coherence. Through the present study we found, in case it is known at advance that synchrotron radiation is chaotic radiation, the instantaneous emittance of synchrotron radiation could be measured with the time scale of coherence time τ_c by measuring two-photon correlation.

2 Mechanism of synchrotron radiation

Since our light source is synchrotron radiation, it is very necessary to review briefly the mechanism of synchrotron radiation, where incoherent collective effect - superposition of a large amount of spontaneous emissions happens. Such an incoherent superposition produces a low-efficiency radiation of the stored relativistic electrons in the storage ring and should be the origin of the chaotic characteristics of synchrotron radiation. The various time responses of electrons in a bunch are also reviewed with relation to the possible influences on the measurement of two-photon correlation of synchrotron radiation.

2.1 One-electron classical theory

A relativistic electron which is accelerated in a macroscopic field will radiate electromagnetic energy at a rate which is proportional to the square of the accelerating force. The rate depends on the angle between the force and the electron velocity and is larger by the factor ($\gamma_e^2 = (E / mc^2)^2$) when the force is perpendicular to the velocity than the force is parallel to the velocity. The radiated field is well described by the Maxwell equations and could be expressed in an analytic form in the far field limit [see Appendix C] [23][24].

2.1.1 Bending-magnet radiation

For an extremely relativistic electron following a circular trajectory (as in the bending magnets of a storage ring as Fig. 2-1 shows), the Fourier component of the radiated field in the observation direction $\mathbf{n}(0, \sin\psi, \cos\psi)$ can be expressed as follows in the far field limit,

$$\mathbf{E}(\mathbf{n}R_0, \omega) = \frac{e}{2\sqrt{2\pi}\varepsilon_0 c R_0}(-i)\mathbf{A}(\omega) \qquad (2-1)$$

$$\mathbf{A}(\omega) = \begin{bmatrix} \mathbf{A}_\sigma \\ \mathbf{A}_\pi \end{bmatrix} = \frac{\sqrt{3}}{2\pi}\gamma_e \frac{\omega}{\omega_c}(1+X^2)(-i)\begin{bmatrix} K_{2/3}^2(\eta) \\ \dfrac{iX}{\sqrt{1+X^2}} K_{1/3}^2(\eta) \end{bmatrix} \qquad (2-2)$$

where R_0 is the observation distance, ψ is the vertical observation angle, the electric field has been decomposited into two components $(\mathbf{e}_\sigma, \mathbf{e}_\pi)$ in the transverse plane against **n**. In order not to confuse with the coherence degree γ, we here use γ_e to stand for the normalized electron energy by its rest mass. $K_{1/3}(x)$ and $K_{2/3}(x)$ are modified Bessel functions with the orders of 1/3 and 2/3 respectively.

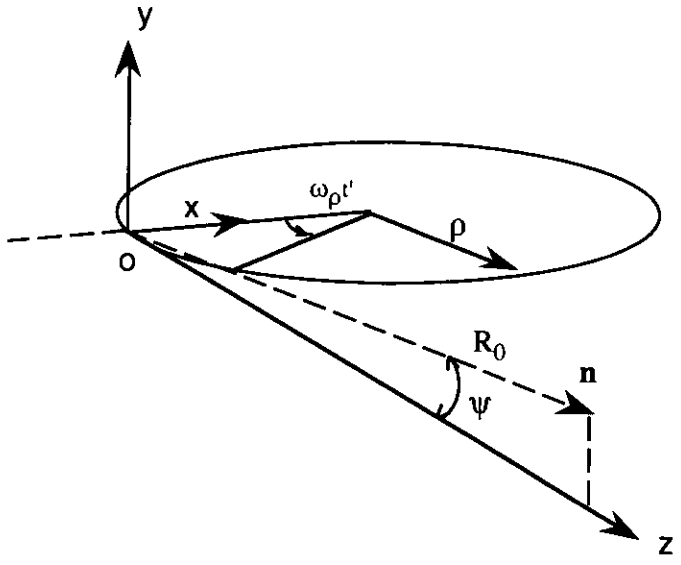

Fig. 2-1 The orbit and coordinate system for bending-magnet radiation

In Eq.(2-2) the parameters X and η are defined as follows,

$$X = \gamma_e \psi \qquad (2-3)$$

$$\eta = \frac{\omega}{\omega_c}(1+X^2)^{3/2} \qquad (2-4)$$

where ω_c is called critical frequency and decided by the bending radius ρ and electron energy γ_e,

$$\omega_c = \frac{3}{2}\gamma_e^3 \omega_\rho = \frac{3\gamma_e^3 c}{2\rho} \qquad (2-5)$$

In the case of bending-magnet radiation electron produces a smooth spectrum as Eq.(2-2) shows, and the emitted power is within a narrow cone of angular width γ_e^{-1} in the direction of the motion.

2.1.2 Undulator radiation

If a relativistic electron is accelerated in a periodic magnetic structure of period λ_u and under a condition of its K parameter $K \leq 1$, where K is defined as $K = eB_0\lambda_u / 2\pi mc$ and B_0 is the peak value of magnetic field, the electron will produces strong undulator radiation, and the radiated spectrum is not continuous again due to the interference effect.

Qualitatively the discrete spectrum can be understood simply as a grating effect [25].

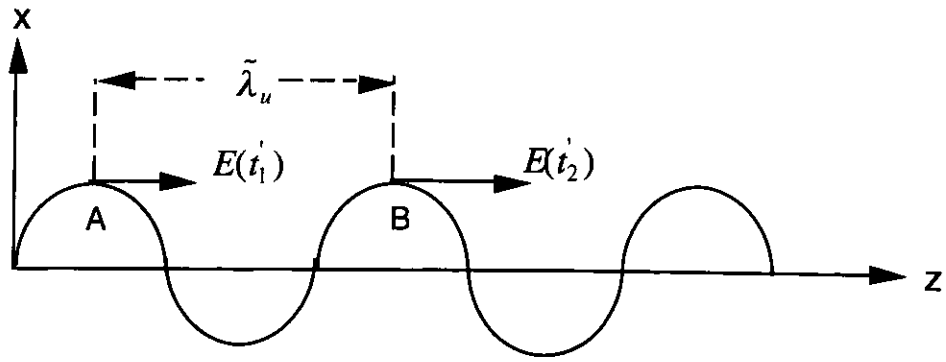

Fig.2-2 Orbit of an electron in x-z plane with a period of $\tilde{\lambda}_u$, when moving in a periodic y-direction magnetic field of a period λ_u with a number of periods, N.

The time-dependence of x and z components in Fig. 2-2 can be easily got from the equation of motion [22][23] and the results are shown as follows,

$$\begin{cases} x(t') = -\dfrac{K}{\gamma_e}\dfrac{\lambda_u}{2\pi}\sin\left(\dfrac{2\pi ct'}{\lambda_u}\right) \\ z(t') = \left(1 - \dfrac{1+K^2/2}{2\gamma_e^2}\right)ct' - \dfrac{K^2}{8\gamma_e^2}\dfrac{\lambda_u}{2\pi}\sin\left(\dfrac{4\pi ct'}{\lambda_u}\right) \end{cases} \qquad (2\text{-}6)$$

where t' is the local time, K is the undulator parameter, and λ_u is the period of the external periodic magnetic field . As Fig. 2-2 shows, the constructive interference between A and B happens when the optical path deference is the integral times of the radiated wavelength. From Eq.(2-6) we can easily get the emitted discrete wavelength as follows,

$$\lambda = \frac{\lambda_u}{n}\frac{1+K^2/2}{2\gamma_e^2} \qquad (n=1,2,3\ldots.) \qquad (2-7)$$

The difference from the classical grating in calculating the optical path difference is that relativistic effect must be considered in getting Eq.(2-7) from Eq.(2-6).

More general from Maxwell equations the Fourier component of the radiated electric field can be expressed as follows under the condition of far field limit ,

$$\begin{pmatrix}\mathbf{A}_\sigma\\ \mathbf{A}_\pi\end{pmatrix} = \frac{\omega}{\omega_1(0)}\frac{\gamma_e K}{(1+K^2/2)}\frac{\sin\left(\frac{N\pi\omega}{\omega_1(\theta)}\right)}{\sin\left(\frac{\pi\omega}{\omega_1(\theta)}\right)}\begin{pmatrix}\mathbf{B}_\sigma(\omega,\phi,\psi)\\ \mathbf{B}_\pi(\omega,\phi,\psi)\end{pmatrix} \qquad (2-8)$$

where

$$\begin{pmatrix}\mathbf{B}_\sigma(\omega,\phi,\psi)\\ \mathbf{B}_\pi(\omega,\phi,\psi)\end{pmatrix} = \frac{1}{\pi}\int_{-\pi}^{\pi} d\xi \begin{pmatrix}\gamma_e\phi/K\\ \gamma_e\psi/K\end{pmatrix} e^{i\left(\frac{\omega}{\omega_1(\theta)}\xi + q\sin(2\xi) + q\sin(\xi)\right)} \qquad (2-9)$$

where ϕ and ψ are observation angles, $\theta^2 = \phi^2 + \psi^2$. The nth hamonics is expressed as follows,

$$\omega_n(\theta) = \frac{2\pi cn}{\lambda_u}\frac{2\gamma_e^2}{1+K^2/2+\gamma_e^2\theta^2} \qquad (n=1,2,3\ldots) \qquad (2-10)$$

Therefore Eq.(2-7) is just a special case of Eq. (2-10) where $\theta = 0$. Undulator radiation is squeezed into discrete spectrum satisfied by Eq. (2-10) and an narrower emission angle of an order about $(\gamma_e \sqrt{N})^{-1}$ due to the interference of radiation from different parts of the trajectory.

2.2 Collective effects

The electric fields emitted at different positions by one electron could produce interference or total coherence which results to the quasimonochromatic spectral distribution of undulator radiation. Usually in one bunch the number of electrons is about 10^9 and the interference effect of the fields emitted by different electrons which are regarded as a large amount of radiators is to be discussed in the following sections for two extreme cases: incoherent superposition for synchrotron radiation and constructive interference for FELs [26]~[30].

2.2.1 Incoherent superposition - Chaotic synchrotron radiation

Synchrotron radiation, no matter whether it is bending-magnet radiation or undulator radiation, essentially belongs to spontaneous radiation. Therefore for more than one electron, each radiator (relativistic electron) radiates with its own phase, and these phases are completely random with respect to one another.

Let us consider one bunch with N electrons as one ensemble,. For a certain Fourier component (say angular frequency ω_o) emitted by each individual electron, it has a fixed amplitude E_0 and an unknown random phase φ, then the total electric field amplitude is

$$\begin{aligned} E(t) &= E_1(t) + E_2(t) + \ldots E_N(t) \\ &= E_0 e^{-i\omega_0 t}(e^{i\varphi_1} + e^{i\varphi_2} \ldots e^{i\varphi_N}) \\ &= E_0 e^{-i\omega_0 t} a e^{i\varphi} \end{aligned} \qquad (2\text{-}11)$$

The formal summation of the phase factors carried out in the final line of Eq.(2-11) is illustrated in Fig.2-3. For the case of the stored electron bunch in Photon factory of KEK, the average distance between two neighboring

electrons is of the order of 1 μm, which is much larger than the wavelength of the observed soft X-ray photon (for example λ=17nm for the photon of 70 eV). So any small fluctuation of the relative position of the electron in a bunch will lead to a large variation of the phase of the photon it emitted. Therefore the amplitude a and the phase φ in Eq. (2-11), which comes from the superposition of large amount of complex random phasors, will be appreciably different for different ensemble due to the fluctuation of two-electron's distance. Fig. (2-3-a) illustrates the resultant amplitude a and phase φ from one electron bunch, and Fig. (2-3-b) is the case from another electron bunch. It is worth noting here that, even for the same electron bunch, the resultant amplitude a and the phase φ will also become significantly different after one revolution due to the complicated random motion of the electron in the bunch, which results to the strong fluctuation of its relative position.

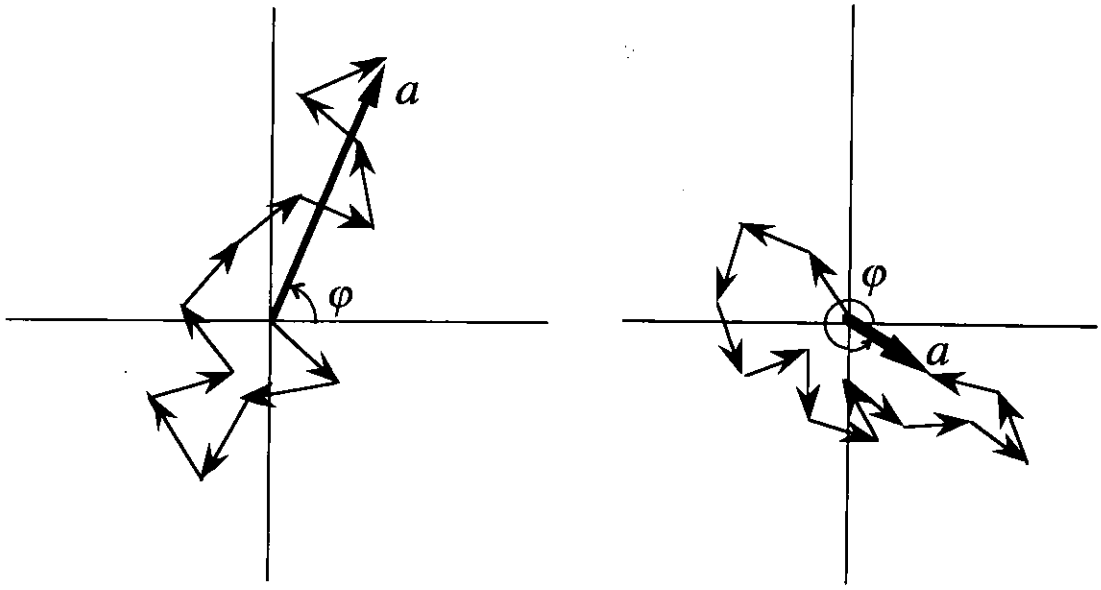

(a) electron bunch 1 (b) electron bunch 2

Fig. 2-3 Argand diagram to show the amplitude a and phase φ of the resultant vector formed by a large number of unit vectors, each of them has a randomly chosen phase angle.

Let $p(a)$ be the probability that the end-point of a two-dimensional random walk of N step lies in unit area around the point specified by coordinate a and φ in Fig.2-3, then the result given by the random-walk theory [31] for the present problem is,

$$p(a) = \frac{1}{\pi N} \exp\left(-\frac{a^2}{N} \right) \qquad (2-12)$$

Clearly $p(a)$ obeys to a Guassian distribution and exhibit the maximum at a=0. Because φ is randomly distributed between 0 and 2π, which naturally leads to the zero ensemble average of the total electric amplitude,

$$\langle E(t) \rangle = 0 \qquad (2-13)$$

The ensemble average of the intensity is also readily calculated from Eq.(2-11) as follows,

$$\langle I(t) \rangle = \langle E^*(t) E(t) \rangle = N E_0^2 \qquad (2-14)$$

From Eq.(2-11 ~ 2-14) we can get an important formula for the probability distribution of instantaneous intensity measurement for a chaotic radiation,

$$p(I(t)) = \frac{1}{\langle I \rangle} \exp\left(-\frac{I(t)}{\langle I \rangle} \right) \qquad (2-15)$$

The negative exponential distribution as Eq.(2-15) shows is a typical characteristics of a chaotic radiation. Although the thermal radiation from a thermal equilibrium gives the same distribution as Eq.(2-15), the terminology of "chaotic radiation" is more general whenever the excitation has an appropriately random quality, no matter how far the radiator is from thermal equilibrium just as synchrotron radiation does. There is no heat reservoir in an electron storage ring but it really belongs to chaotic radiation due to the spontaneous radiation and the incoherent superposition.

2.2.2 Constructive interference - complete FELs

The basic principle of FEL is to cause all electrons to have approximately the same phase, thereby producing constructive interferences (stimulated emission).

Still we consider Eq.(2-11), if all electrons are forced to emit with roughly the same phase, $\varphi_k \cong \varphi_j = \varphi$ for all k and j in one bunch, then the total electric field amplitude is

$$E(t) = NE_0 e^{-i\omega_0 t} e^{i\varphi} \qquad (2-16)$$

The ensemble average intensity is written as follows,

$$\langle I(t) \rangle = \langle E^*(t)E(t) \rangle = N^2 E_0^2 \qquad (2-17)$$

There are two important features for FELs. One is the high efficiency of the radiation. By comparison with Eq.(2-14), the radiated intensity by a complete FEL is N times larger than that by conventional synchrotron radiation. The other is the high stability of the radiated intensity. From Eq.(2-16) we can see that if electrons number in one ensemble is unchanged, the radiated intensity for different ensemble is also unchanged. Therefore the complete FEL is a kind of very quiet, well-stabilized light.

2.3 Time response of various dynamical motion of electrons in a bunch [32]

A systematic intensity variation of synchrotron radiation would cause an unexpected accidental correlation in the measurement of two-photon correlation. So it is necessary to survey the various time responses of an electron in the storage ring and their influences to the intensity modulation.

In general a relativistic electron runs not strictly along an ideal circular orbit in a storage ring, but has betatron oscillation and synchrotron oscillation. Betatron oscillation comes from the focusing properties of the guide field, which drives all electrons toward an ideal design orbit. Fig. 2-4 just shows the trajectory of one electron's betatron oscillation in the horizontal plane. Usually in order to avoid resonance of this oscillation, after

one revolution the electron cannot return back to its initial starting point. The electron will begin to repeat its past trajectories again after a certain time (several revolutions) which is called here betatron oscillation revolution time t_β. This could be calculated from the betatron tune of beam parameters.

For the PF storage ring, the electron bunch revolution frequency is about 1.6 MHz, the horizontal betatron tune is 9.85, and the vertical betatron tune is 4.20, then

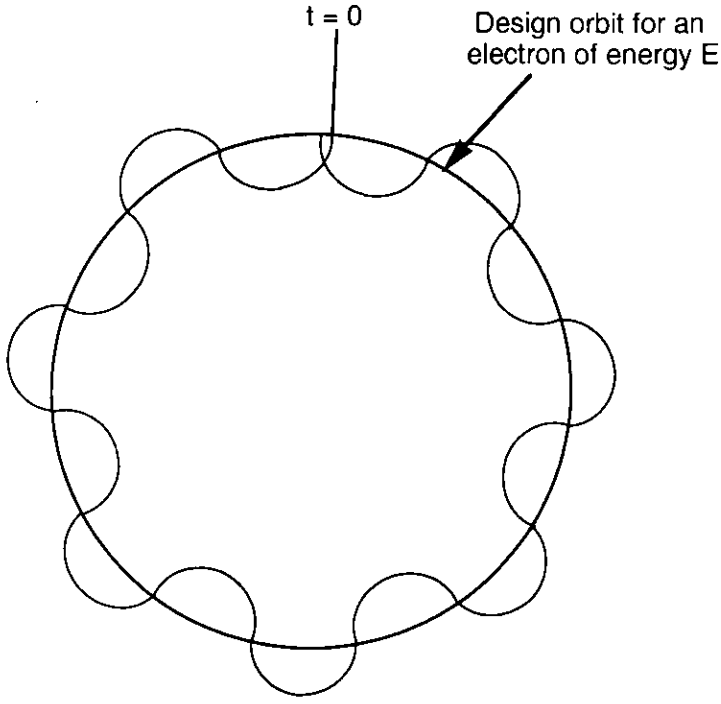

Fig. 2-4 Illustrating the lateral betatron oscillation around an ideal closed orbit

$$t_{\beta-H} = \frac{1}{0.85 \times 1.6 \times 10^6} = 0.735 \mu s \qquad (2-18)$$

$$t_{\beta-V} = \frac{1}{0.2 \times 1.6 \times 10^6} = 3.125 \mu s \qquad (2-19)$$

Synchrotron oscillation is actually energy oscillation which arises from the radiation loss and the energy gain from the rf system. This oscillation is usually very slow and causes the circular orbit as Fig.2-4 shows to oscillate around its initial orbit. The oscillation period t_{syn} for PF storage ring is calculated from its synchrotron tune (0.023) as follows,

$$t_{syn} = \frac{1}{0.023 \times 1.6 \times 10^6} \approx 0.027ms \qquad (2-20)$$

In stationary conditions a balance is reached between quantum excitation and radiation damping, leading to a statistically stationary distribution of the oscillation amplitudes and the phases of the electrons in a bunch. The bunch then has a stationary size and shape, although the motion for each individual electron is complicated, So it is reasonable to think that these time responses discussed above give no contributions to the systematic intensity modulation of synchrotron radiation, which is in fact justified by our measurement of the spectral distribution of SR intensity as Fig.4-14 shows. However these complicated microscopic oscillations (betatron oscillation and synchrotron oscillation) should be responsible for the fluctuation of two-electron's distance for different ensemble, as is described in section 2.2.1. In addition, the betatron oscillation is a kind of *high-frequency non-harmonic* oscillation (for the case of the PF storage ring, the horizontal oscillation frequency is about 15.8 MHz, the vertical oscillation is about 6.7 MHz), which might give some contributions to the chaotic nature of synchrotron radiation and could be checked by experiment as is described in section 9.

3 Theory of optical coherence [7][8][26][27]

3.1 Field correlations

The basic elements of field theory are expressed as the separated positive-frequency field operator and negative-frequency field operator,

$$\hat{\mathbf{E}}(\mathbf{r},t)=\hat{\mathbf{E}}^{+}(\mathbf{r},t)+\hat{\mathbf{E}}^{-}(\mathbf{r},t), \qquad (3-1)$$

where the positive frequency part of the electric field operator is given as follows,

$$\hat{\mathbf{E}}^{+}(\mathbf{r},t)=i\sum_{k}(\frac{1}{2}\hbar\omega_{k})^{1/2}\hat{a}_{k}\mathbf{u}_{k}(\mathbf{r})e^{-i\omega_{k}t}, \qquad (3-2)$$

and in general

$$\hat{\mathbf{E}}^{-}(\mathbf{r},t)=\left(\hat{\mathbf{E}}^{+}(\mathbf{r},t)\right)^{*}. \qquad (3-3)$$

In Eq.(3-2) $\hat{a}_k$ is the annihilation operator, and the mode function $\mathbf{u}_k(\mathbf{r})$, which corresponds to frequency ω_k, is usually determined by physical considerations and may be taken to satisfy the wave equation at interior points if the volume contains no refracting materials,

$$\nabla^{2}\mathbf{u}_{k}+\frac{\omega_{k}^{2}}{c^{2}}\mathbf{u}_{k}=0. \qquad (3-4)$$

In the classical coherence theory this expression as Eq.(3-1) shows in itself is just that of the analytical signal and could be considered to be a convenient mathematical trick that allows us to work with exponential functions with complex variable rather than with sines and cosines. But in the quantum theory of light they have different interpretations. The positive frequency part, $\hat{\mathbf{E}}^{+}(\mathbf{r},t)$, as it is shown in Eq.(3-2), is regarded to be a photon *annihilation operator*[33] . Applied to a n-photon state it produces a (n-1)-

photon state. Its Hermitian adjoint, $\hat{\mathbf{E}}^{-}(\mathbf{r},t)$, must be a photon *creation operator.*

The *m*th-order field correlation function is defined as follows,

$$G^{(m)}(X_1,\cdots X_m,X_{m+1},\cdots X_{2m})=\left\langle \hat{\mathbf{E}}^{-}(X_1)\cdots\hat{\mathbf{E}}^{-}(X_m)\hat{\mathbf{E}}^{+}(X_{m+1})\cdots\hat{\mathbf{E}}^{+}(X_{2m})\right\rangle,$$

(3 - 5)

where $X_i=(\mathbf{r}_i, t_i)$ stands for the *i*th time-space point within the field and it has been assumed that all the field operators have the same polarization for convenience of discussion. The angular bracket $\langle\cdots\rangle$ stands for an ensemble average. In classical mechanics this average is taken over six-dimensional phase space, while it is $Trace(\hat{\rho}\cdots)$ in quantum mechanics where $\hat{\rho}$ is density operator of the field.

3.2 Fully coherent optical field

If for an arbitrary positive integer *n*, the field correlation function can factorize as follows, it is said that this field has arbitrarily higher-order coherence or it is totally coherent field. If *n* is fixed, this field is said to have *n*th-order coherence.

$$G^{(m)}(X_1,\cdots X_m,X_{m+1},\cdots X_{2m})=\varepsilon^{*}(X_1)\cdots\varepsilon^{*}(X_m)\varepsilon(X_{m+1})\cdots\varepsilon(X_{2m})$$

(3 - 6)

for all $m \le n$. Where $\varepsilon(X_m)$ represent a complex function.

A quantum field in a pure coherent state $|\alpha\rangle$ has such properties as Eq.(3-6) shows. It can be easily verified because the coherent states for the *k*th mode are the eigenstates of the annihilation operator of this mode, and correspondingly the coherent states for the entire field are the eigenstates of the positive-frequency field operator,

$$\hat{a}_k|\alpha_k\rangle=\alpha_k|\alpha_k\rangle \qquad (3-7)$$

$$\hat{\mathbf{E}}^{+}(\mathbf{r},t)|\alpha\rangle = \varepsilon(\mathbf{r},t)|\alpha\rangle \qquad (3-8)$$

where the positive-frequency field operator has been shown in Eq. (3-2) for a multi-mode field and the set of coherent states for the entire field are given as follows,

$$|\alpha\rangle \equiv \prod_{k} |\alpha_k\rangle_k \qquad (3-9)$$

The eigenvalue function $\varepsilon(\mathbf{r},t)$ in Eq. (3-8) is given as

$$\varepsilon(\mathbf{r},t) = i\sum_{k}(\frac{1}{2}\hbar\omega_k)^{1/2}\alpha_k \mathbf{u}_k(\mathbf{r})e^{-i\omega_k t} \qquad (3-10)$$

The density operator can be readily written as

$$\hat{\rho} = |\alpha\rangle\langle\alpha| \qquad (3-11)$$

In this case the complex function $\varepsilon(\mathbf{r}_i,t_i)$ is interpreted as just the counterpart of the complex amplitude of classical field. To show an explicit form for $|\alpha_k\rangle_k$ in terms of the photon-number state, we write,

$$|\alpha_k\rangle_k = e^{-|\alpha_k|^2/2}\sum_{n}\frac{\alpha_k{}^n}{\sqrt{n!}}|n\rangle \qquad (3-12)$$

This form immediately gives the probability of finding n photons (the photon statistics) in the kth-mode coherent state as

$$\mathrm{p_n} = |\langle n|\alpha_k\rangle|^2 = e^{-|\alpha_k|^2}\frac{|\alpha_k|^{2n}}{n!} \qquad (3-13)$$

which obeys a Poisson distribution.

3.3 First-order coherence

The simplest and the most well-known coherence is first-order coherence, because it is also defined for a Fermion system, such as electrons. It is the case of $m = 1$ in Eq.(3-5). The degree of first-order coherence is defined as

$$\gamma_{12}(\tau) = \frac{\left\langle \hat{\mathbf{E}}^{-}(\mathbf{r}_1,t)\hat{\mathbf{E}}^{+}(\mathbf{r}_2,t+\tau)\right\rangle}{\sqrt{\left\langle \hat{\mathbf{E}}^{-}(\mathbf{r}_1,t)\hat{\mathbf{E}}^{+}(\mathbf{r}_1,t)\right\rangle \left\langle \hat{\mathbf{E}}^{-}(\mathbf{r}_2,t+\tau)\hat{\mathbf{E}}^{+}(\mathbf{r}_2,t+\tau)\right\rangle}} . \quad (3-14)$$

According to the definition of Eq.(3-6) if a radiation field is first-order coherent then

$$|\gamma_{12}(\tau)| = 1 , \quad (3-15)$$

It is easily shown from the definition of Eq. (3-14) that *any optical field with single-mode excitation is first-order coherent and satisfies the condition of Eq. (3-15).* Multi-mode coherent field is still first-order coherent and can be verified by the density operator defined in Eq.(3-11). The density operator for a multi-mode chaotic field is given as follows,

$$\hat{\rho} = \sum_{\{n_k\}} |\{n_k\}\rangle\langle\{n_k\}| \prod_k \frac{(\bar{n}_k)^{n_k}}{(1+\bar{n}_k)^{n_k+1}} \quad (3-16)$$

where $\bar{n}_k$ represents the average photon number in the kth mode. By substituting Eq. (3-16) into Eq. (3-14) we get the degree of first-order coherence for a multi-mode chaotic optical field as follows,

$$\gamma_{12}(\tau) = \frac{\sum_{\mathbf{k}} \bar{n}_{\mathbf{k}}\omega_{\mathbf{k}} \exp\{-i[\mathbf{k}\cdot(\mathbf{r}_1 - \mathbf{r}_2) - \omega_{\mathbf{k}}(t_1 - t_2)]\}}{\sum_{\mathbf{k}} \bar{n}_{\mathbf{k}}\omega_{\mathbf{k}}} \quad (3-17)$$

where the plane-wave mode functions appropriate to a cubical volume of side L has been used,

$$\mathbf{u}_{\mathbf{k}}(\mathbf{r}) = L^{-3/2}\hat{e}^{(\lambda)}\exp(i\mathbf{k}\cdot\mathbf{r}) \qquad (3-18)$$

Clearly from Eq. (3-17) we can see that, $|\gamma_{12}(\tau)|$ will strongly depend on the spatial or temporal separation and will exhibit maximum 1 if these two points coincide. When the optical modes are completely different at $\mathbf{r}_1$ and $\mathbf{r}_2$, $|\gamma_{12}(\tau)|$ vanishes and gives complete incoherence.

We will show by the following simple example that any field including a Fermion field (coherent or incoherent) could be first-order coherent in a certain condition.

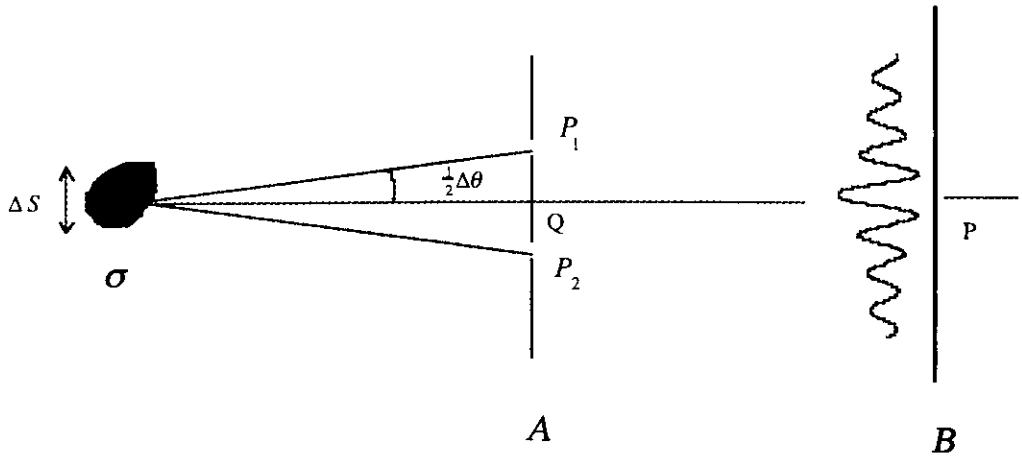

Fig. 3-1 Illustrating Youngs double slits experiment

The above Figure is well known Youngs double slits experiment. σ is the light source with transverse size Δs, a double slit is placed at plane A, and B is the observation plane. The angle opened by the double slits to the source is $\Delta\theta$. The visibility in the plane B reflects the field correlation $G^{(1)}(p_1, p_2)$ and is proportional to the degree of first-order coherence $\gamma_{12}(\tau)$ between p_1 and p_2. From classical optics we know that, no matter what kind of light source it might be, if $\Delta s \cdot \Delta\theta << \bar{\lambda}$ the visibility in the plane B is almost 100%, which implies that $|\gamma_{12}(\tau)|$ is almost unity and the field between p_1 and p_2 is completely first-order coherent. This means that the optical modes at p_1 and p_2 are exactly the same and the phase difference between p_1 and p_2 does not fluctuate.

3.4 Second-order coherence

Second-order coherence is a quantitative description of the two-photon correlation of a radiation field and belongs to the case of m=2 in Eq.(3-5). Its degree is defined as follows,

$$\Gamma^{(2)} = \frac{\left\langle \hat{\mathbf{E}}^{-}(\mathbf{r}_1,t)\hat{\mathbf{E}}^{-}(\mathbf{r}_2,t+\tau)\hat{\mathbf{E}}^{+}(\mathbf{r}_1,t)\hat{\mathbf{E}}^{+}(\mathbf{r}_2,t+\tau)\right\rangle}{\sqrt{\left\langle \hat{\mathbf{E}}^{-}(\mathbf{r}_1,t)\hat{\mathbf{E}}^{+}(\mathbf{r}_1,t)\right\rangle \left\langle \hat{\mathbf{E}}^{-}(\mathbf{r}_2,t+\tau)\hat{\mathbf{E}}^{+}(\mathbf{r}_2,t+\tau)\right\rangle}} . \quad (3-19)$$

In a Fermion field with same spin the second-order coherence vanishes at the same space-time point due to the Pauli principle. From the definition of Eq. (3-6) we can see, that if a field is second-order coherent its degrees of first-order coherence and second-order coherence should be simultaneously a constant, that is

$$|\gamma_{12}(\tau)| = 1, \quad (3-20)$$

and

$$\Gamma^{(2)} = 1. \quad (3-21)$$

It can be readily verified that coherent state satisfies the above two conditions and is second-order coherent. It should be noted that Eq.(3-21) alone does not always mean that the field is totally second-order coherent, because Eq.(3-21) also holds when the modes of the fields at $\mathbf{r}_1$ and $\mathbf{r}_2$ are completely different. In fact the complete second-order coherent field in the short-wavelength region is very rare except for the fields emitted from some artificial light sources such as lasers or FELs. Most of the fields we are familiar with belong to another kind of form, which is a so-called thermal field or in general chaotic field. Such a field is a statistically mixed states and its density operator has been given in Eq.(3-16). Obviously the probability of finding n photons (the photon statistics) in the kth mode is easily written as follows

$$p_n = \frac{1}{1+\bar{n}_k}\left\{\frac{\bar{n}_k}{1+\bar{n}_k}\right\}^n . \qquad (3-22)$$

In other words, the number of photons in the mode is distributed according to the powers of the parameter $\bar{n}_k/(1+\bar{n}_k)$. The Plank distribution for blackbody radiation furnishes an illustration of a density operator which has long been known to take the same form as Eq.(3-16). So this is the reason why the terminology of "thermal field" has been often used. However it is worth noting, in particular, that while the Plank distribution is characteristic of thermal equilibrium, no such limitation is implicit in the general form of the density operator Eq.(3-16). It will apply whenever the excitation has an appropriately random quality, no matter how far the radiator is from thermal equilibrium. Therefore the terminology of chaotic field is more general than that of thermal field. For any chaotic field its degree of second-order coherence can be decomposed into its degree of first-order coherence

$$\Gamma^{(2)} = 1 + |\gamma_{12}(\tau)|^2, \qquad (3-23)$$

where $\gamma_{12}(\tau)$ is defined by Eq.(3-14) and has an explicit form as Eq. (3-17) shows for a multi-mode chaotic field. Clearly the above $\Gamma^{(2)}$ is larger than or equal to unity, and will exhibit a bunching effect against space-time coordinates.

In addition to the coherent field and the chaotic field, there exists another interesting field called non-classical field [34]. For example if a field is in a photon number state $|n\rangle$ its degree of second-order coherence can be readily expressed as

$$\Gamma^{(2)} = 1 - \frac{1}{n} < 1 . \qquad (3-24)$$

This is called anti-bunching effect characterized by a sub-Poisson photon statistics.

The degree of second-order coherence for three typical optical fields is drawn in Fig. 3-2, where we can see that from the measurement of two-photon correlation, at least the chaotic field and the photon-number

squeezed field could be distinguished. If we measured a flat response like curve B in Fig. 3-2, we could say this field is second-order coherent and its photon statistics approaches to a Poisson distribution, where in general we need to measure coherence higher than the second-order coherence to check whether the field is totally coherent or not.

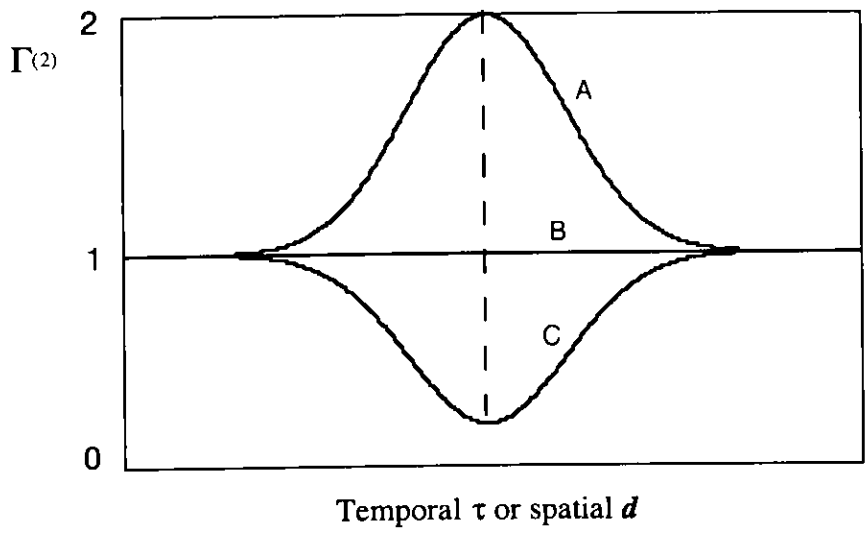

Fig. 3-2 Second-order coherence for three typical optical fields
A: chaotic, B: coherent, C: squeezed

4 A new intensity interferometer

A detailed description of the new apparatus will be presented in this chapter.

4.1 The optical system

4.1.1 Basic idea

To measure the intensity correlation, one important step is to realize the incident beam division. A conventional half-splitter mirror for visible light is not appropriate for soft X-ray region because it is not transparent in shorter wavelengths. The small beam size of undulator radiation suggests us to adopt the following diffraction splitting method.

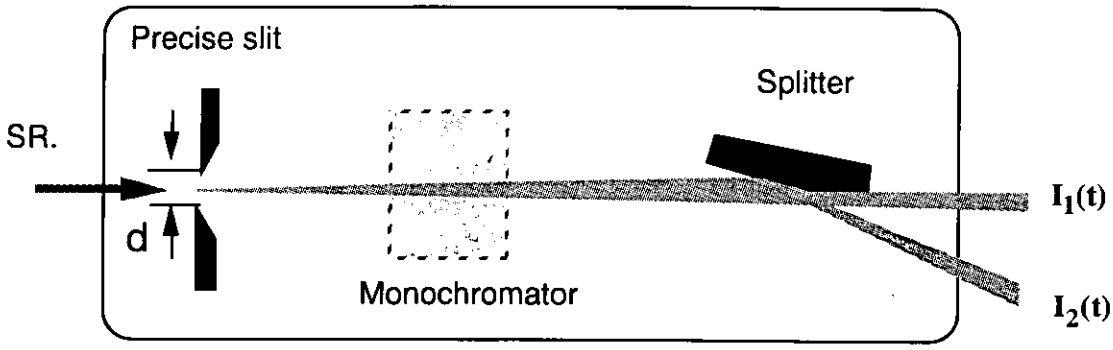

Fig. 4-1 Simplified diagram of optical beam division system for synchrotron radiation in VUV and soft X-ray region

As it is shown in Fig. 4-1, a precise slit diffracts incoming SR horizontally (or any direction, because the whole system can be rotated around the incoming axis), where the width d can be continuously adjusted by a micrometer with the accuracy of 0.8 μm. After going through a monochromator the diffracted incident light is divided into two beams by a splitter mirror.

Now let's give a simple quantitative analysis on the second-order coherence between $I_1(t)$ and $I_2(t)$. As Fig. 4-2 shows, o is the center of the

precise slit, d is its width. Incoming light propagates along z-direction. o' is the center of the diffracted beam at the splitter mirror. Due to the Fraunhofer diffraction we can easily express the field at point y as follows [30],

$$\begin{aligned} E(y) &= \frac{1}{L}\int_{-d/2}^{+d/2} E(x)\exp(ik\sqrt{L^2+(y-x)^2})dx \\ &= \frac{e^{ik(L+\frac{y^2}{2L})}}{L}\int_{-d/2}^{+d/2} E(x)\exp(-ik\frac{y}{L}x)dx, \end{aligned} \tag{4-1}$$

where L is the distance of oo', k is the wave vector, and x is the coordinate at the precise slit plane ox , and the term x^2 / L^2 has been neglected. We can further express the divided intensity $I_1(t)$ and $I_2(t)$ as follows,

$$I_1(t) = \int_0^{\infty} E(y)E^*(y)dy \tag{4-2}$$

and

$$I_2(t) = \int_{-\infty}^{0} E(y)E^*(y)dy \ . \tag{4-3}$$

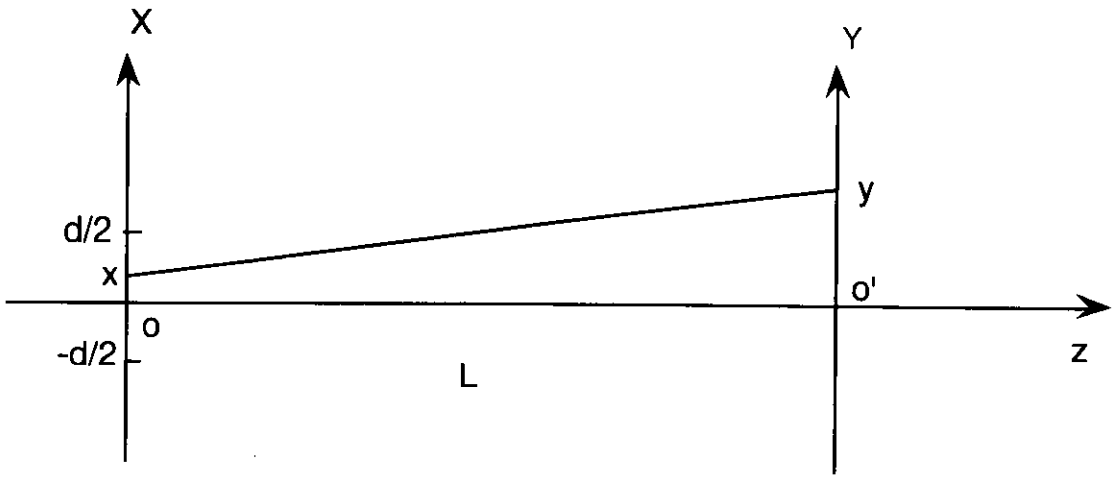

Fig. 4-2 Illustrating the intensity correlation between $I_1(t)$ and $I_2(t)$

Substituting Eq.(4-1) into Eq.(4-2) and Eq.(4-3), we get the second-order coherence between $I_1(t)$ and $I_2(t)$ as follows if we assume that SR is chaotic radiation,

$$\Gamma^{(2)}(d) = \frac{\langle I_1(t) I_2(t) \rangle}{\langle I_1(t) \rangle \langle I_2(t) \rangle} = 1 + |\gamma(d)|^2$$

$$= 1 + \frac{\int_{-d/2}^{d/2} \int_{-d/2}^{d/2} \left| \langle E^*(x_1) E(x_2) \rangle \right|^2 dx_1 dx_2}{\int_{-d/2}^{d/2} \int_{-d/2}^{d/2} \langle I_1(x_1) \rangle \langle I_2(x_2) \rangle \, dx_1 dx_2}, \qquad (4-4)$$

where x_i are the coordinates at the precise slit, $E(x_i)$ and $I(x_i)$ are the amplitude and the intensity of the optical field at x_i.

Eq. (4-4) implies that the intensity correlation between $I_1(t)$ and $I_2(t)$ is completely determinated by the field distribution at the plane of precise slit. If d is much smaller than the coherent size, the second term in Eq. (4-4) is nearly unity; if d is much larger than the coherent size, the field correlation between different the two points at precise slit will become very weak, and this makes the second term much smaller than unity but not zero due to the existence of auto correlation.

To give an explicit form of the relationship between the second-order coherence $\Gamma^{(2)}$ and the Fraunhofer slit width d, we use the following relationship to calculate the field correlation from the brightness [23] [37] [38][39].

$$\left\langle E^*(x + \frac{\xi}{2}) E(x - \frac{\xi}{2}) \right\rangle = \int d\phi \; B(x, \phi) \exp(-ik\phi\xi), \qquad (4-5)$$

where x and ξ are the coordinates at the precise slit and $B(x,\phi)$ is the brightness distribution at this slit and can be expressed as follows,

$$B(x,\phi) = B_0 \exp(-\frac{(\gamma x^2 + 2\alpha x\phi + \beta\phi^2)}{2\varepsilon}) \qquad (4\text{-}6)$$

where ε is the emittance of the stored beam, γ, α and β are the so-called Twiss parameters in accelerator physics and satisfies the following relation,

$$\gamma\beta - \alpha^2 = 1 \qquad (4\text{-}7)$$

Substituting Eq.(4-5) into Eq.(4-4), an approximate analytic solution could be solved, if we assumed that the precise slit has a Gaussian amplitude transmissive function such as $\exp(-x^2 / 2D^2)$, where the effective width D relates the real width d as $D = d / 2\sqrt{3}$, merely for the convenience of integral. The result is shown as follows,

$$|\gamma(d)|^2 = \frac{2}{\pi}\sqrt{\frac{d^2 + 24\Sigma^2}{(1+\Sigma^2/\sigma_c^2)d^2 + 24\Sigma^2}}\cos^{-1}\left(\frac{d^2}{1+2\sigma_c^2/\Sigma^2)d^2 + 48\sigma_c^2}\right), \qquad (4\text{-}8)$$

where d is the Fraunhofer slit width, Σ is the beam size and σ_c is the coherent size, at this slit. σ_c is defined as follows,

$$\sigma_c = \frac{\varepsilon_p \Sigma}{\sqrt{\varepsilon^2 - \varepsilon_p^2}}, \qquad (4\text{-}9)$$

where ε is the emittance of the stored beam and $\varepsilon_p = \lambda / 4\pi$.

Eq.(4-8) *is an important formula* to give a quantitative estimation of the excess two-photon correlation between the two divided light beams falling on the michrochannel plates. For a certain photon energy, if the beam size and the emittance are given, the dependence on the Fraunhofer slit width d, of the excess two-photon correlation, is deterministic. Fig.4-3 shows the theoretical curves for different emittance according to Eq. (4-8) and Eq. (4-4) , where it is assumed that the photon energy is 70 eV and the beam size Σ=80μm at the precise slit. The beam size is defined as follows and could be

measured experimentally by a wire scanner attached directly behind the precise slit.

$$\langle |E(x)|^2 \rangle = |E_0|^2 \exp(-\frac{x^2}{2\Sigma^2}) \tag{4-10}$$

From Fig.4-3 we can see that the photon bunching effect gets sharper and sharper as the emittance increases and detection of the bunching effect becomes more difficult because the total intensity passing the precise slit should be decreased.

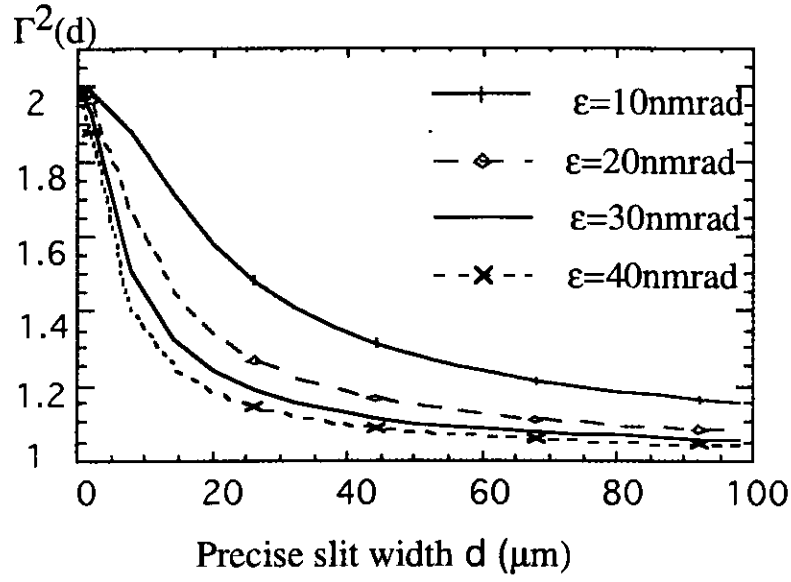

Fig.4-3 Theoretical estimation of $\Gamma^{(2)}(d)$ between $I_1(t)$ and $I_2(t)$
Beam size Σ=80μm is assumed at precise slit

4.1.2 Optical setup

The optical setup with the parameters designed is shown in Fig. 4-4, where (a) is the top view and (b) is the side view. The angle of $(\alpha+\beta)$ can be adjusted from 160° to 175° , and the outgoing length b of *the exit slit* can be adjusted from 108 *mm* to 216 *mm* to satisfy the beam converging condition, without breaking the high vacuum. In Fig. 4-4 (b) a piezoelectric translator (PZT) is installed on *the entrance slit* to modulate this slit width slowly and

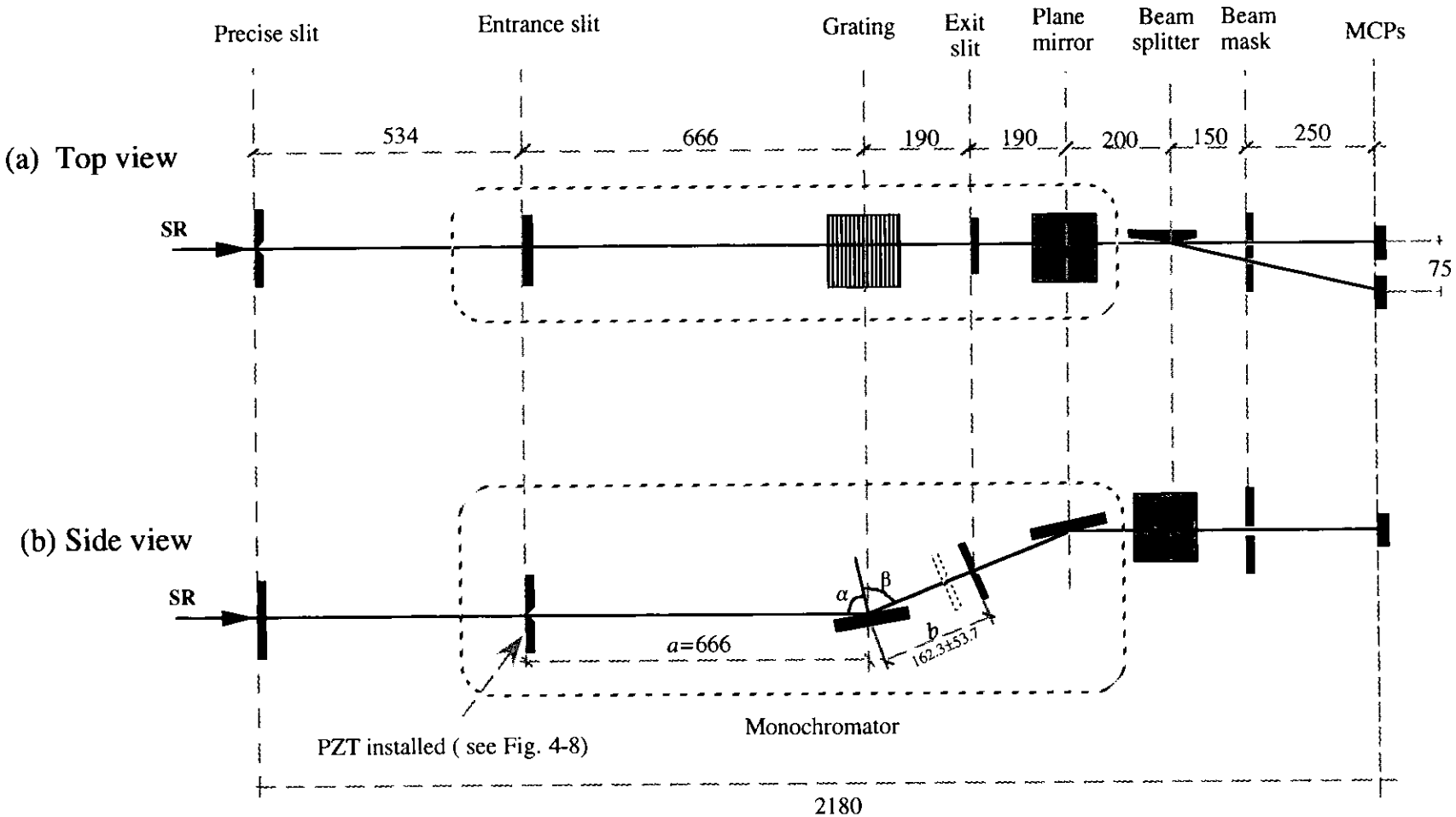

Fig. 4-4 Setup of the optical system (unit: *mm*)

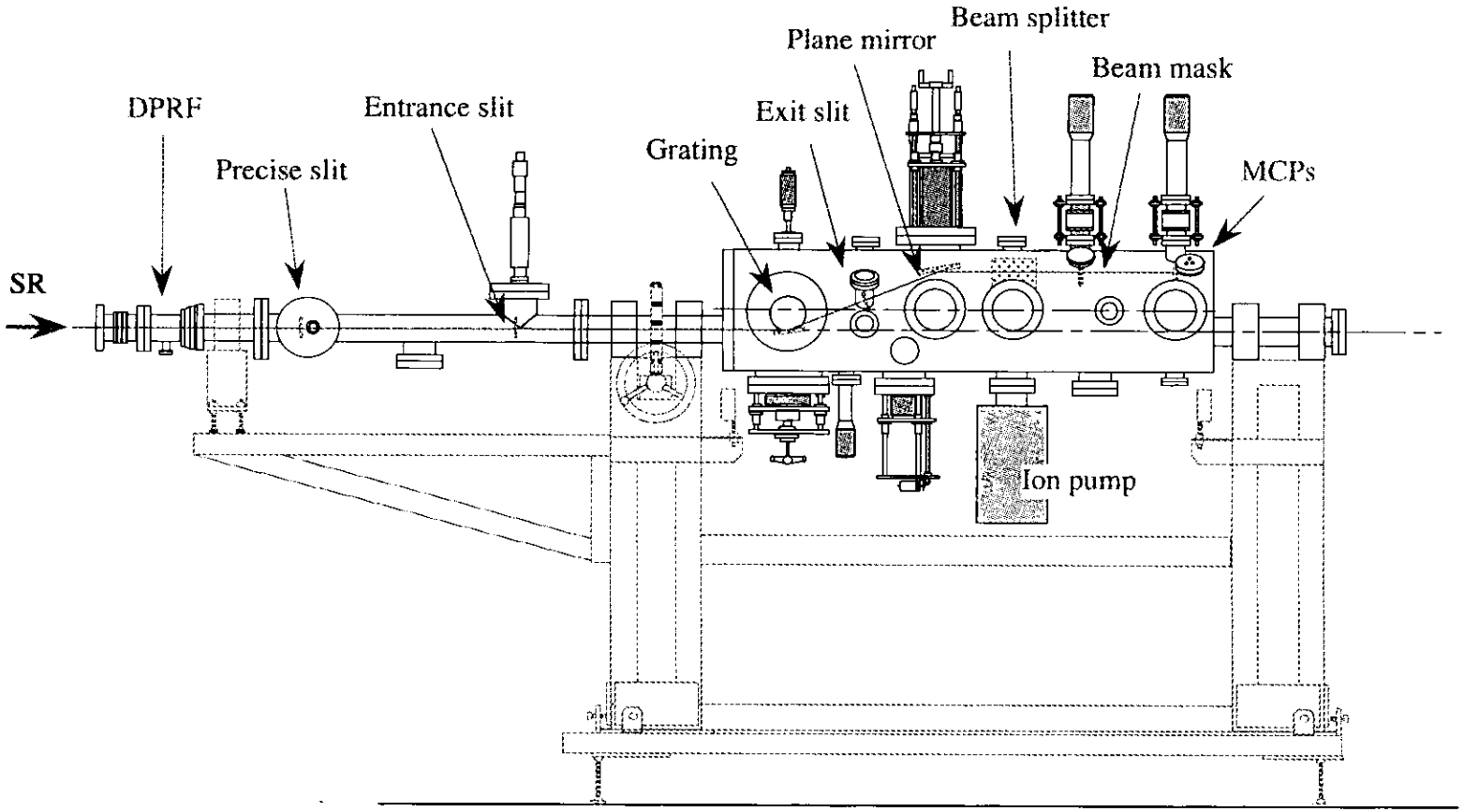

Fig. 4-5 Side view of the optical vacuum chamber

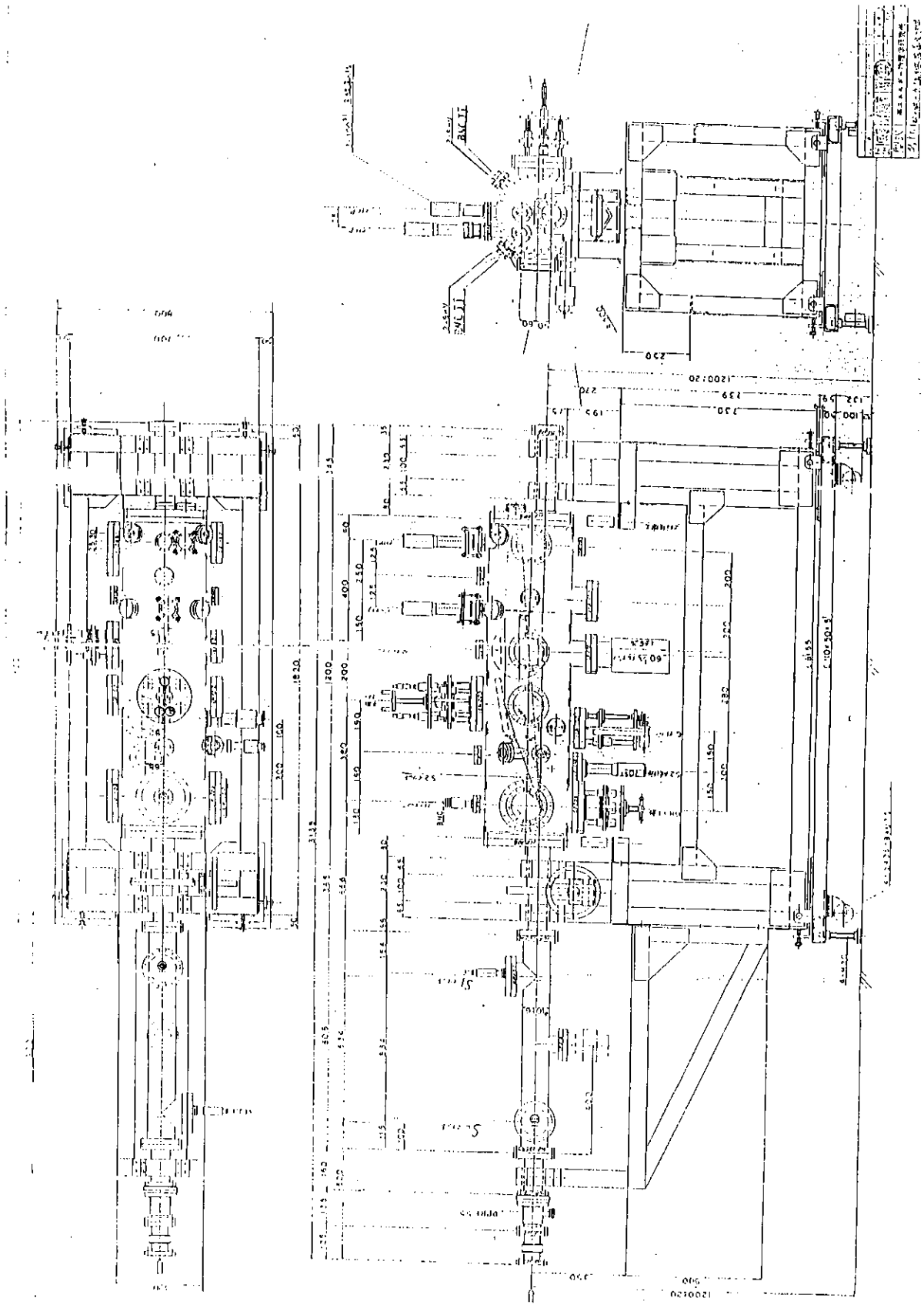

Fig. 4-6 Three-dimensional view of the design of the vacuum chamber

quasi-sinusoidally. All these elements are installed in a high vacuum chamber as it is shown in Fig. 4-5 . Now I will give a detailed description about its constituents.

• Main chamber

The parameters of the main chamber are shown in Fig. 4-6. The total length is 313.5 *cm* long and the high vacuum is maintained at UHV ($10^{-7} \sim 10^{-9} torr$) by a 20 *l/s* ion pump. This vacuum chamber, as it shown in Fig. 4-9 and Fig. 4-10, can be rotated around the incident optical axis by a differentially pumped rotary feedthrough (DPRF) to characterize the transverse coherence along an arbitrary orientation .

• Precise slit

The width d of this slit is controlled by a high-precision micrometer with the accuracy of 0.8 μm. It is used to diffract the incoming light and to change the spatial coherence of synchrotron radiation. The normalized excess two-photon correlation is measured as a function of this width d.

• Monochromator

The monochromator is an important component in this apparatus. In addition to make the incident light quasimonochromatic, it plays a role of coherence time modulation which will be shown later to be vital for the use of lock-in amplifier to suppress the accidental correlation, to suppress the white noise, and to extract the weak true two-photon correlation.

This mochromator consists of an *entrance slit*, a *spherical grating*, an *exit slit* and a *plane mirror*. The grating parameters are chosen as R=4m(radius of curvature) and N = 600 *l/mm* (groove density). To optimize this mono-chromator, we use the grating equation and the first-order converging condition as follows[40][41],

$$\sin(\alpha) - \sin(\beta) = -\frac{\lambda}{d} \qquad (4\text{-}11)$$

$$\frac{\cos^2(\alpha)}{a} + \frac{\cos^2(\beta)}{b} = \frac{\cos(\alpha) + \cos(\beta)}{R} \qquad (4\text{-}12)$$

where $d=1/N$, a is the incident length, b is the outgoing length, and the negative 1st-order diffraction has been used. After optimization the sum of α and β is fixed at 168.88° in the present study (but could be changed if needed without breaking the vacuum). As shown in Fig. 4-4, the incident length a is fixed as 666 *mm* and the outgoing length b varies between 108.6 *mm* and 216 *mm* to satisfy the first-order focussing condition for different photon energies, which can be scanned continuously from 60*eV* to 220*eV* with the resolution of $\lambda/\Delta\lambda$ ~1000 by rotating the angle of the grating, correspondingly changing α and β.

Table 4-1 Parameters of the Monochromator

Radius of curvature of the grating (R)	4000 *mm*
Groove density of the grating (N)	600 *l/mm*
α+β	168.88° (adjustable 160° ~ 175°)
Incident length (a)	666 *mm*
Outgoing length (b)	216 *mm* ~ 108.6 *mm*
Scanned photon energies	60 eV ~ 220 eV (206 Å ~ 56 Å)

The resolution of the monochromator is determined by the width of the entrance slit and exit slit in case that the total number of the grooves be regarded as an infinity. By differentiating Eq. (4-11), the coherence time can be expressed as follows,

$$\tau_c \equiv \frac{1}{|\Delta\nu|} = \frac{\lambda}{c} \cdot \frac{\sin(\beta)-\sin(\alpha)}{\cos(\alpha)|\Delta\alpha|+\cos(\beta)|\Delta\beta|} \qquad (4-13)$$

where $\Delta\alpha=d_1/a$, $\Delta\beta=d_2/b$, d_1 and d_2 are the widths of the entrance slit and exit slit respectively. The results are shown in Fig. 4-7. Clearly we can see that if the exit slit is fixed at 20μm, and the entrance slit is modulated between 50μm and 100μm, then nearly 30% modulation of the coherence time can be attained at a fixed wavelength.

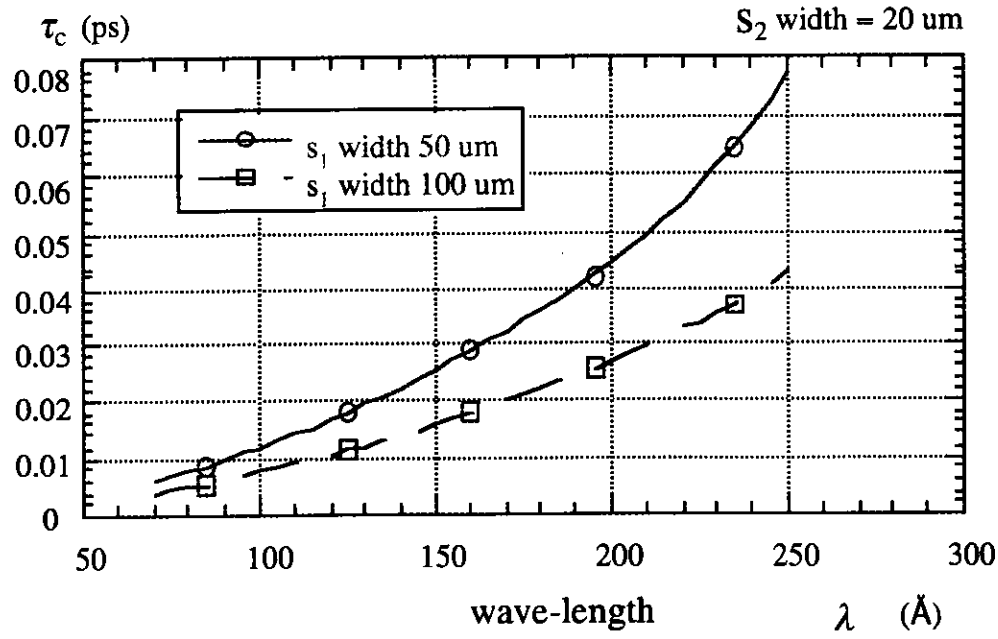

Fig. 4-7 Coherence time τ_c of the monochromator for different entrance slit width of 50μm and 100μm, where the exit slit width is fixed at 20μm. (S_1 - entrance slit, S_2 - exit slit)

The entrance slit width can be modulated slowly and quasi-sinusoidally by an installed piezoelectric translator (PZT, P-244.30) as is shown in Fig.4-8, for the purpose of coherence time modulation. The nominal expansion at the applied voltage of 1000 V is 40 μm for each PZT. In addition, the width can be adjusted manually by two micrometers with the accuracy of 1μm. The PZT parameters are given in Table 4-2.

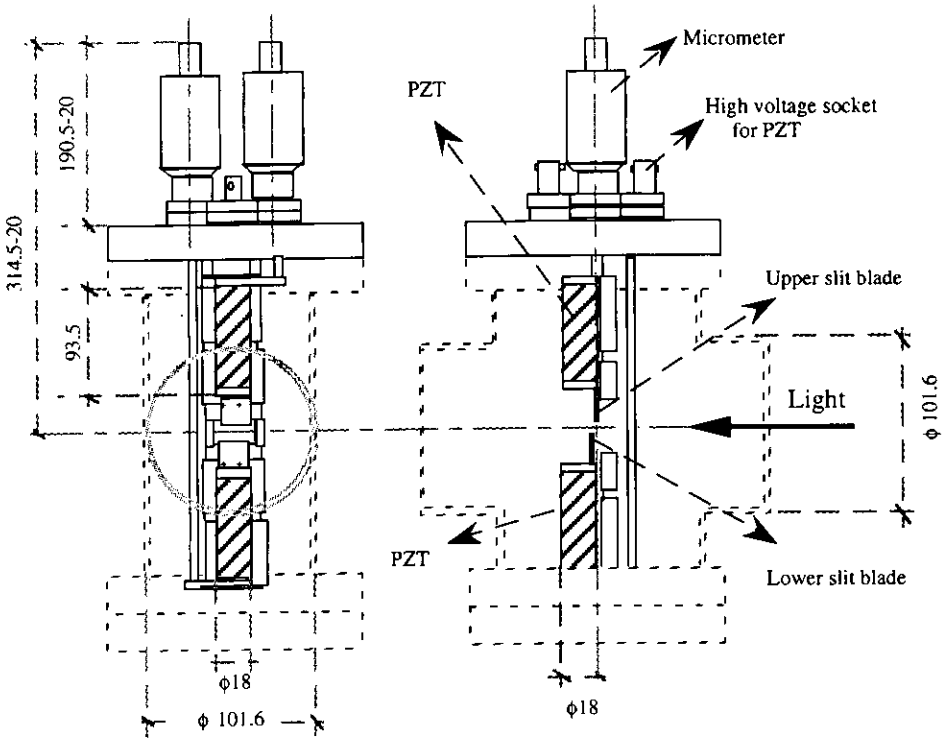

(a) (b)

Fig.4-8 Control system of the entrance slit installed in the main chamber (unit: *mm*).
(a) View from the upper stream, (b) side view

Table 4-2 P-244.30 stacked translator

Nominal expansion (at -1000 V)	40 *μm*
Max. expansion (at -1500 V)	60 *μm*
Resonant frequency	9 KHz
Stiffness	60 N/*μm*
Electrical capacitance	76 nF
Total length	93.5 *mm*
Weight	128/147 *g*
Temperature expansion	0.65 μm/K

(Physik Instrumente PI GmbH & Co.)

The exit slit could be adjusted manually by a similar micrometer with a accuracy of 1 μm. The plane mirror acts merely as a reflection mirror.

• Beam splitter

This is actually a plane mirror with a very sharp edge.

• Beam mask

This is used to smooth the divided two beams and to reject the unnecessary scattered light. In addition it could act as a " balancer" to adjust the incident intensities falling on the two microchannel plates.

• MCPs

The microchannel plate (HAMAMATSU F4655-10) acts as our fast-response photon detector Its rising time is 0.25 ns and falling time is 0.75 ns. The maximum linear output of this MCP is 1μA. The nominal gain at 2.4 KV is about 5×10^7.

Table 4-3 Important parameters of MCP assembly (F4655-10)

Efficient diameter	14.5 mm
Operation temperature	+10 °C ~ + 40 °C
Operation vacuum	1.3 x 10^{-3} Pa (1x 10^{-5} Torr)
dark current (2.4 kV)	3 cps/cm^2
Gain (2.4 kV)	5 x 10^7
Rising time	250 ps
Falling time	750 ps
Maximum linear output	1 μA

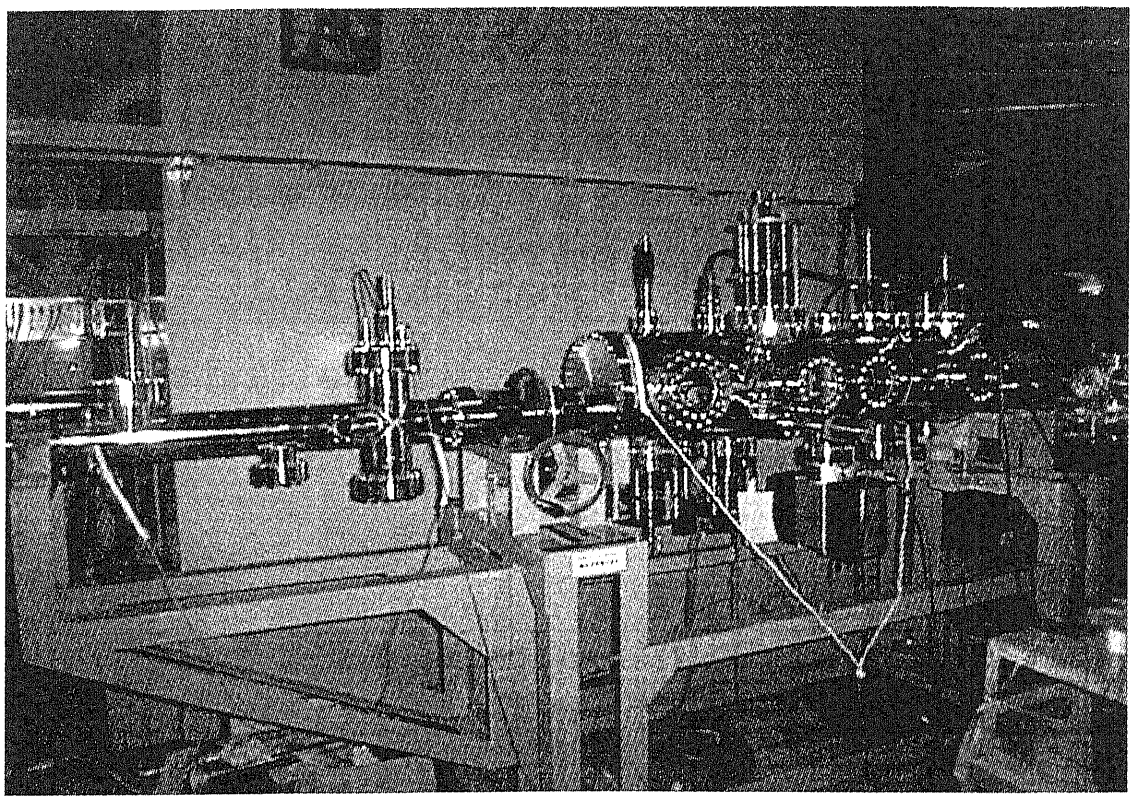

Fig. 4-9 Photograph of the side view of the optical vacuum chamber of the new intensity interferometer for soft X-ray synchrotron radiation

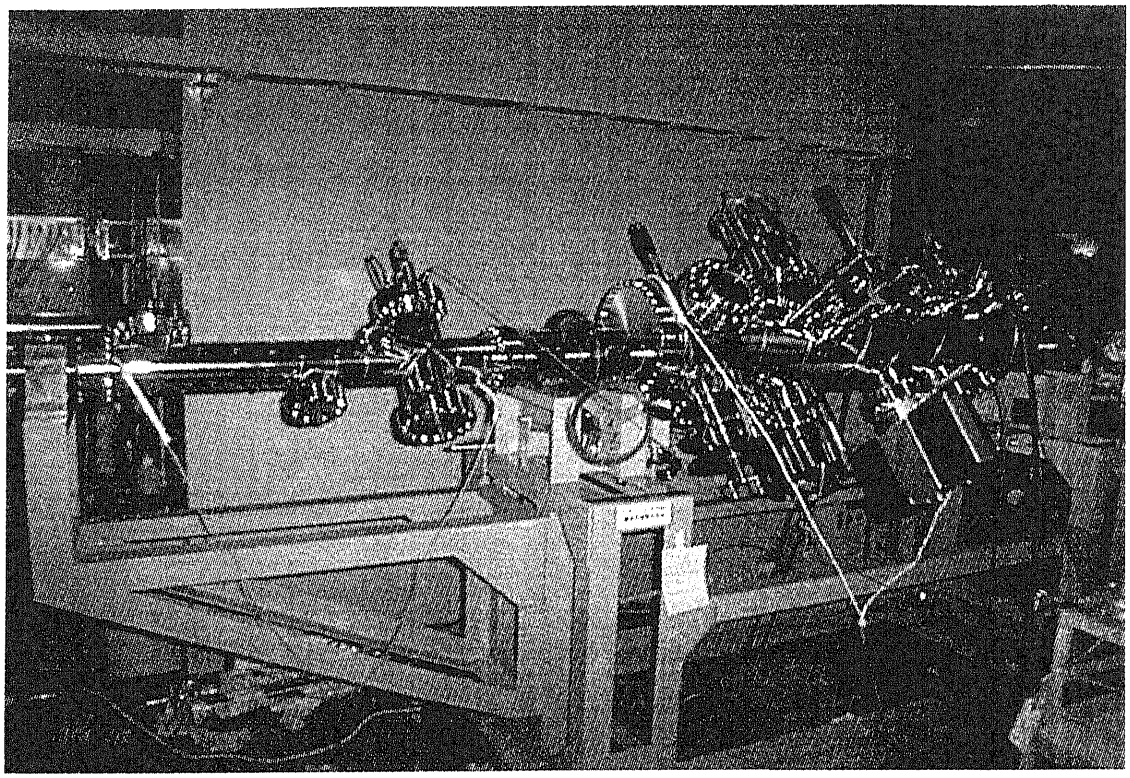

Fig. 4-10 Photograph of the side view of the optical vacuum chamber of the new intensity interferometer for soft X-ray synchrotron radiation The chamber is rotated 45 degrees around the incident optical axis.

4.2 The electric correlator

Just as we have mentioned above, the electric correlator plays an important role in the measurement of the correlation of intensity fluctuations of synchrotron radiation. This comes from two reasons. One is the limited bandwidth of any electronics, and the other is the bunch structures of the present light source. As it is well known that the intensity of a chaotic light source fluctuates with a very broad band (from dc component to the order of optical bandwidth $\Delta\nu$, i.e. inverse of coherent time τ_c). This is apparent because chaotic light looks stable only in the short period of coherence time τ_c. Limited bandwidth of electronics Δf (at best several GHz nowadays) cuts off most of the fluctuation components and makes the correlation, i.e. the multiplication of two wide band photoelectric currents, decrease by $\Delta f/\Delta\nu$ which is around the order of 10^{-5} in most actual cases. To measure such an extremely small correlation signal, Hanbury-Brown and Twiss borrowed the technique of "phase switching" from radio-astronomy and successfully observed the bunching effect from a stationary thermal light source of mercury arc nearly forty years ago. So now it seems that there is no severe difficulties in measuring such a small correlation signal for a stationary light source in case that the Bose degeneracy is not too small. But things will become much more complicated for a non-stationary light source such as synchrotron radiation. In the following sections we first review the outline of a conventional electric correlator for a conventional optical intensity interferometer using a linear electric current multiplier, and then consider the special properties of synchrotron radiation emitted from the Photon factory of KEK, and finally a new experimental proposal is presented based upon this basic electric correlator.

4.2.1 Outline of a conventional electric correlator

As Fig.4-11 shows, a conventional electric correlator operated in photo-electric current mode consists of three basic components: two fast response photon detectors and one linear multiplier. Such limitations as limited response time of photon detector and limited bandwidth of electric circuits

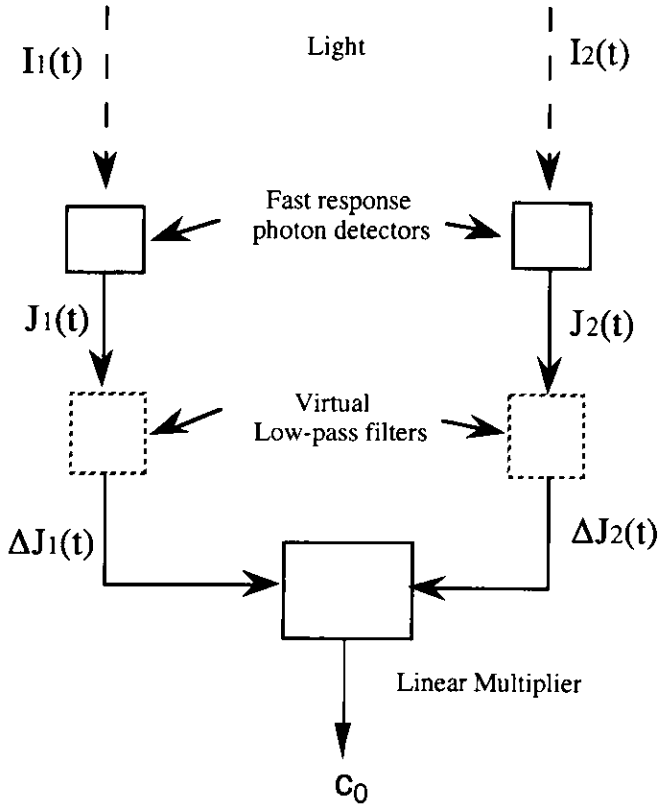

Fig.4-11 Outline of an elementary electric correlator

are represented by a virtual low pass filter in each arm. Now we consider a stationary light coming from a chaotic source. From Eq.(3-13) the excess two-photon correlation can be easily expressed as follows,

$$\frac{\langle \Delta I_1(t)\Delta I_2(t+\tau)\rangle}{\langle I_1(t)\rangle\ \langle I_2(t+\tau)\rangle} = |\gamma_{12}(\tau)|^2 , \qquad (4-14)$$

where τ is the time delay and $\gamma_{12}(\tau)$ is the first-order coherence. The fast response detector converts the light intensity fluctuation into photoelectric current fluctuation according to the semi-classical photoelectric theory [42],

$$J(t) = \alpha e I(t), \qquad (4-15)$$

where α is quantum efficiency of the detector, e is the charge of an electron. $I(t)$ is light intensity and $J(t)$ is output photoelectric current of the detector.

Clearly the multiplier output reflects the correlation information (spatial or temporal) of the two light intensities at each detector

$$\langle \Delta J_1(t)\Delta J_2(t)\rangle \propto \frac{\tau_c}{T_R}\langle \Delta I_1(t)\Delta I_2(t)\rangle \qquad (4-16)$$

where τ_c is coherence time, T_R is the average response time of the correlator and can be expressed as the inverse of the bandwidth of the virtual low pass filter. The reduction factor τ_c / T_R comes from the fact that the time response of any electric circuit is usually much slower than the coherence time. For example, in the present soft x-ray region, $\lambda = 17.7nm$, the resolution $\lambda / \Delta\lambda = 1000$, electric bandwidth $\Delta f = 1GHz$, then this reduction factor is around 10^{-6}. This is the main reason why two-photon correlation is difficult to detect, especially in the region of short wavelengths.

4.2.2 Time structure of synchrotron radiation

The system as shown in Fig. 4-11 works well for a stationary light source. However for non-stationary light such as synchrotron radiation much more attention must be paid to the bunch structure. Here "non-stationay" means that the light source fluctuates not only randomly but also systematically with some frequency components. Then the much larger accidental correlation would severely prevent us from observing the true two-photon correlation. Here the parameters of the PF storage ring of KEK are listed as follows for the correlator design.

Table 4-4 General parameters for the PF storage ring

Beam energy	2.5 GeV (0.75 - 3.0 GeV)
Initial beam current (multi-bunch)	400 mA (achieved 770 mA)
Beam emittance (design value)	36 nm*rad (horizontal) 0.4 nm*rad (vertical)
rf frequency	500.1 MHz
Circumference	87 m(bending radius=8.66m)
Beam lifetime	≥ 20 h (at I=400 mA)

Table 4-5 Beam parameters

Bunch length (r.m.s.)	1.0 cm
Synchrotron radiation loss per turn	400 keV
Horizontal betatron tune	9.85
Vertical betatron tune	4.20
Synchrotron tune	0.023
Momentum compaction factor	0.0061

Among those, the rf frequency and the circumference are most important parameters because they determine the time structure of synchrotron radiation. We illustrate this time structure as follows.

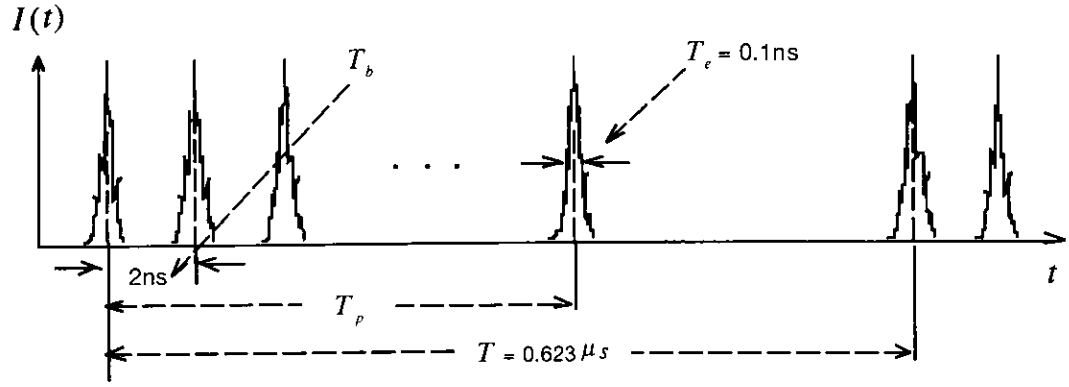

Fig.4-12 Time structure of synchrotron radiation at PF

The fluctuation at each pulse arises from the fact that synchrotron radiation is chaotic light and the photons emitted by any two electrons have no deterministic phase relationship. The pulse structure comes from the bunch distribution of the electron beam in the storage ring. Due to the partial filling of electron bunches in the storage ring, these pulses exhibit the repetition frequency not only at the rf frequency ($1/T_b = 500MHz$) but also exhibit macro-bunches repetition frequency (or so-called revolution frequency) at $1/T = 1.6MHz$, where cT is the length of one circumference ($187m$). Fig.4-13 shows the spectral characters of SR intensity. The slope line comes from the fluctuation at each pulse as is shown in Fig.4-12, and it has the Guassian shape and extends to the frequency of the order of $1/\tau_c$ (τ_c is coherence time)

provided that the light has a Gaussian spectral distribution in the central frequency ν_0. The sharp peaks come from the repetition frequencies of each bunch, macro-bunches, their harmonics and their coupling.

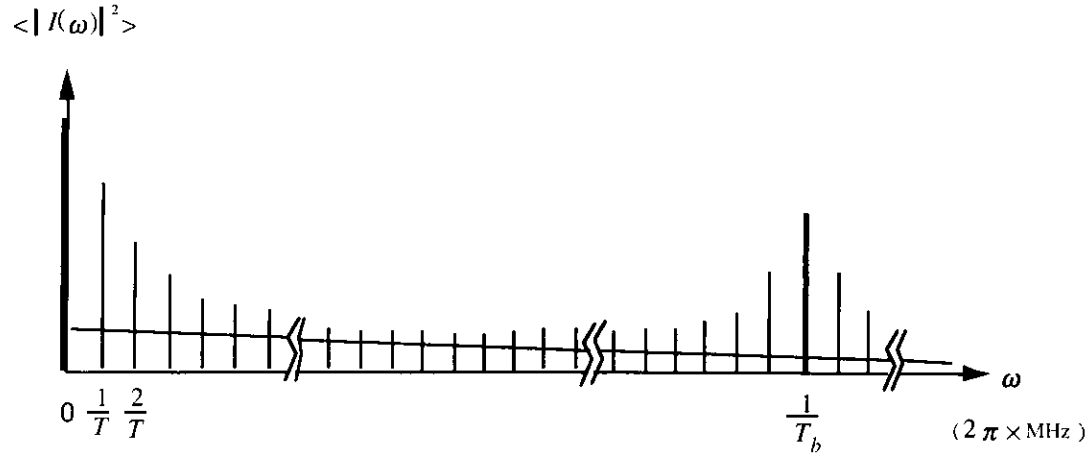

Fig. 4-13 Spectral density distribution of SR intensity

Fig.4-14 is a measured spectrum at the Photon factory by a *Tektronix 494AP programmable spectrum analyzer* and it is consistent with the theoretical prediction as is shown in Fig. 4-13 .

The above characteristic temporal and spectral structure of SR intensity distribution suggests us to consider such kind of non-stationary light as a pulse-modulated stationary thermal light. By using this model we have given a detailed theoretical analyses on the photoelectric correlation from the frequency domain (see **Appendix A**) and the result is as follows,

$$c_0 \propto \langle I_1 \rangle \langle I_2 \rangle (\tilde{A} + \kappa \frac{\tau_c}{T_R} |\gamma_{12}|^2), \qquad (4-17)$$

where $\langle I_1 \rangle$ and $\langle I_2 \rangle$ are the average light intensity at each detector, $(1+|\gamma_{12}|^2)$ is *the degree of 2nd-order coherence* as defined in Eq.(3-17), τ_c is the coherence time, $1/T_R$ is the bandwidth of electric correlator, The duty ratio $\kappa = (T_b/T_e) \times (T_{rev}/T_{cov}) >> 1$, where T_b, T_e, T_{rev} and T_{cov} are the bunch width, bunch separation length, revolution time and bunches partial filling length respectively, can cancel the reduction factor a little which may be the advantage of pulse structure of SR for the measurement of two-photon

correlation just as E. Ikonen predicted [13]. But on the other hand the pulse structure also gives rise to a great difficulty to observe the true two-photon correlation. That is just the first term $\tilde{A}$ in Eq.(4-17). It is defined as follows according to Eq.(A-37),

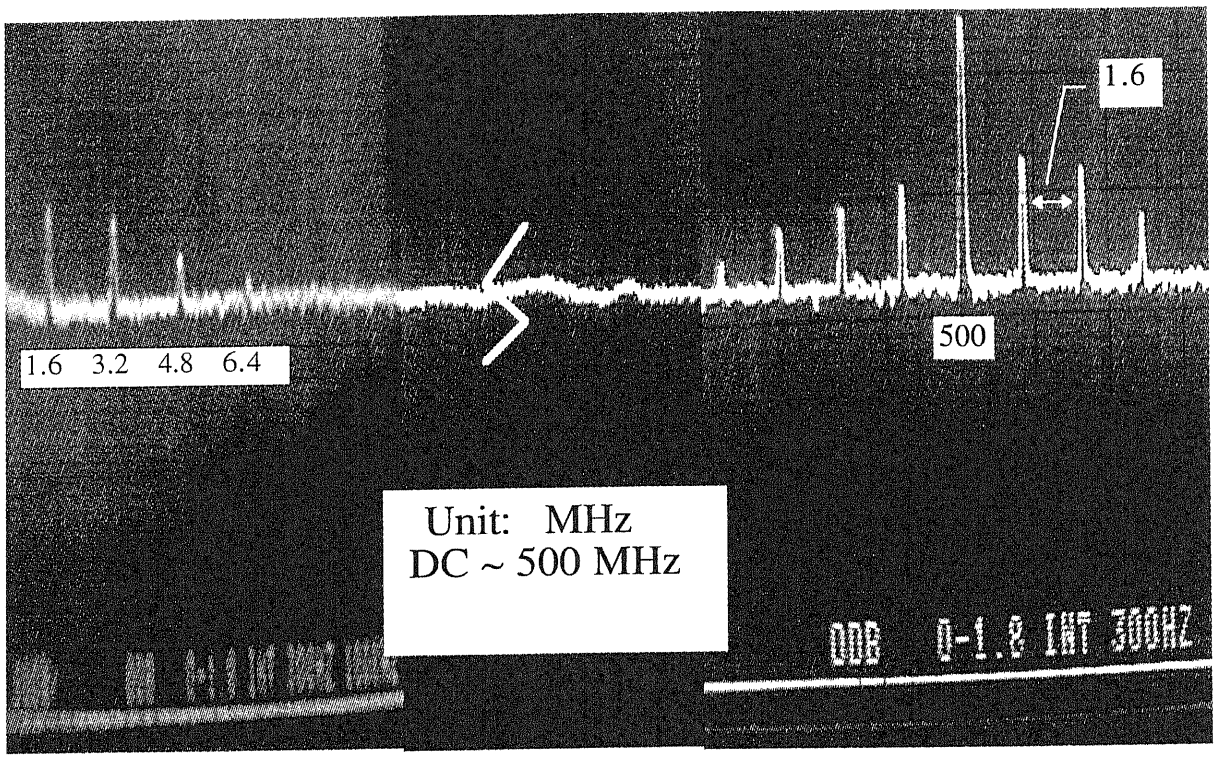

Fig. 4-14 Intensity spectrum of synchrotron radiation
(measured at the Photon factory, KEK, Japan by a Tektronix 494A programmable spectrum analyser)

$$\tilde{A} = \sum_{n=N_1}^{N_2} \left[\frac{\sin(n\pi \frac{T_{cov}}{T_{rev}})}{(n\pi \frac{T_{cov}}{T_{rev}})} \right]^2 \quad , \qquad (4-18)$$

where the integers N_1 and N_2 are the lower and the upper limit of the bandpass region of the correlator in units of the revolution frequency 1.6 MHz. we call $\tilde{A}$ accidental correlation or trivial correlation because it is just the summation of those sharp peaks in the band-pass region of the virtual low pass filter. This low pass filter could be regarded as a real filter if we think the response time of the detector and the linear multiplier as zero. And more its shape can be arbitrary. In Eq. (4-18) the filter function has been assumed as a square wave with the band-pass region from $1.6N_1$ (MHz)to $1.6N_2$ (MHz). This unuseful term $\tilde{A}$ usually has the magnitude much larger than the second term in Eq.(4-17).

4.2.3 A new correlator for SR

In order to measure the true two-photon correlation, the harmful term $\tilde{A}$ must be suppressed, because otherwise in such a strong background any variation of the true correlation information could not be resolved with present experiment precision.

One step to suppress the accidental correlation is to choose an appropriate filter. There are two requirements for characteristics of such a filter. First it has to pass those frequency signals including only high harmonics with small amplitude and small intercoupling. Second the bandwidth must be wide enough to measure such a weak signal. As an optimized choice a bandpass region was decided to be from $100MHz$ to $350MHz$, where the trivial term $\tilde{A}$ in Eq.(4-17) is suppressed to nearly the same order with the second term which makes it reasonable to observe the variation of the 2nd-order coherence as a function of different spatial positions.

To suppress further the accidental correlation $\tilde{A}$ and to remove the DC drift of such a broad band electric system, a novel modulation technique is adopted in this correlator. The entrance slit width of the monochromator is

selected as a modulated quantity because it strongly affects the coherence time and is easy to control. The width of entrance slit is actually modulated by a pair of piezoelectric translators very slowly at a frequency *f*. This modulation does modulate not only coherent length τ_c, but also the two intensities I_1 and I_2 in Eq.(4-17). Therefore when exact sinusoidal modulation of SR intensity and coherence time τ_c is achieved, the third harmonics *3f* of modulation frequency *f* corresponds to the true correlation as is shown in the second term in Eq.(4-17). Even when modulation of τ_c includes some higher harmonics, the true correlation appears only in the harmonics larger than *3f*. But when the intensity modulation is not sinusoidal we have to check whether it affects the 3f components of Eq.(4-17). Fig. 4-15 shows the principal diagram of this new electric correlator.

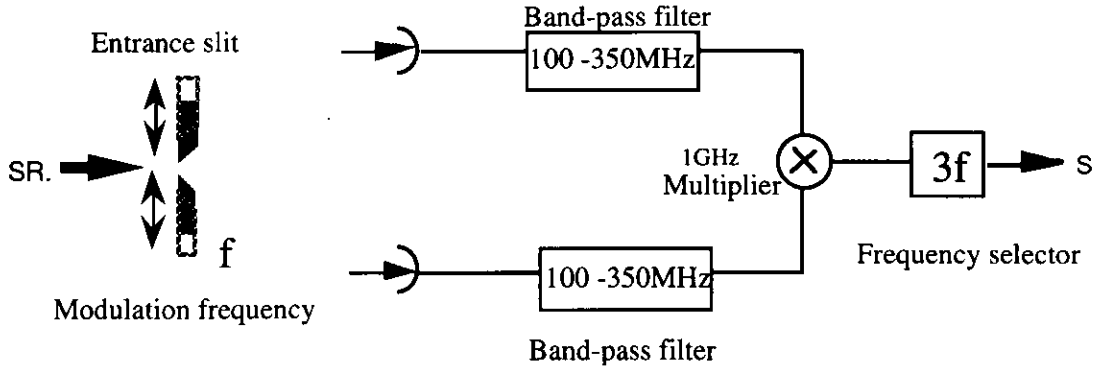

Fig. 4-15 Principal diagram showing how to extract true two-photon correlation

The block diagram of this correlator is shown in Fig.4-16. A pair of microchannel plates (*MCP,HAMAMATSU F4655-10*) are used as photon detectors due to its fast response time (0.75*ns*). A high pass filter(*SHF175*, 100~800*MHz*) and a low pass filter(300*k*~350*MHz*) constitute the bandpass filter. The double balanced mixer (*DBM, Mini-Circuits LRMS-5*) acts as a multiplier with broad band frequency response(5~1500*MHz*). All the high frequency components including 4 preamplifiers (EG&G ORTEC 9306, 1-GHz), DBM and bandpass filters are mounted on a board which is placed in a copper-electromagnetic shielding box. A temperature controller is installed

on this borad to control the temperature around $(40 \pm 0.1)^{\circ}C$. Fig.4-17 and Fig.4-18 show the photographs. In spite of the high gain of the amplifier A_1 and A_2, the true 2-photon correlation signal, i.e. the $3f$ signal, is deeply submerged in the strong thermal noise sea. Therefore *SR830 (DSP Lock-In Amplifier)* is employed to extract the weak signal through its high dynamic reserve. I_1 and I_2 are the low frequency (or DC) components which are used as the normalization of the signal output.

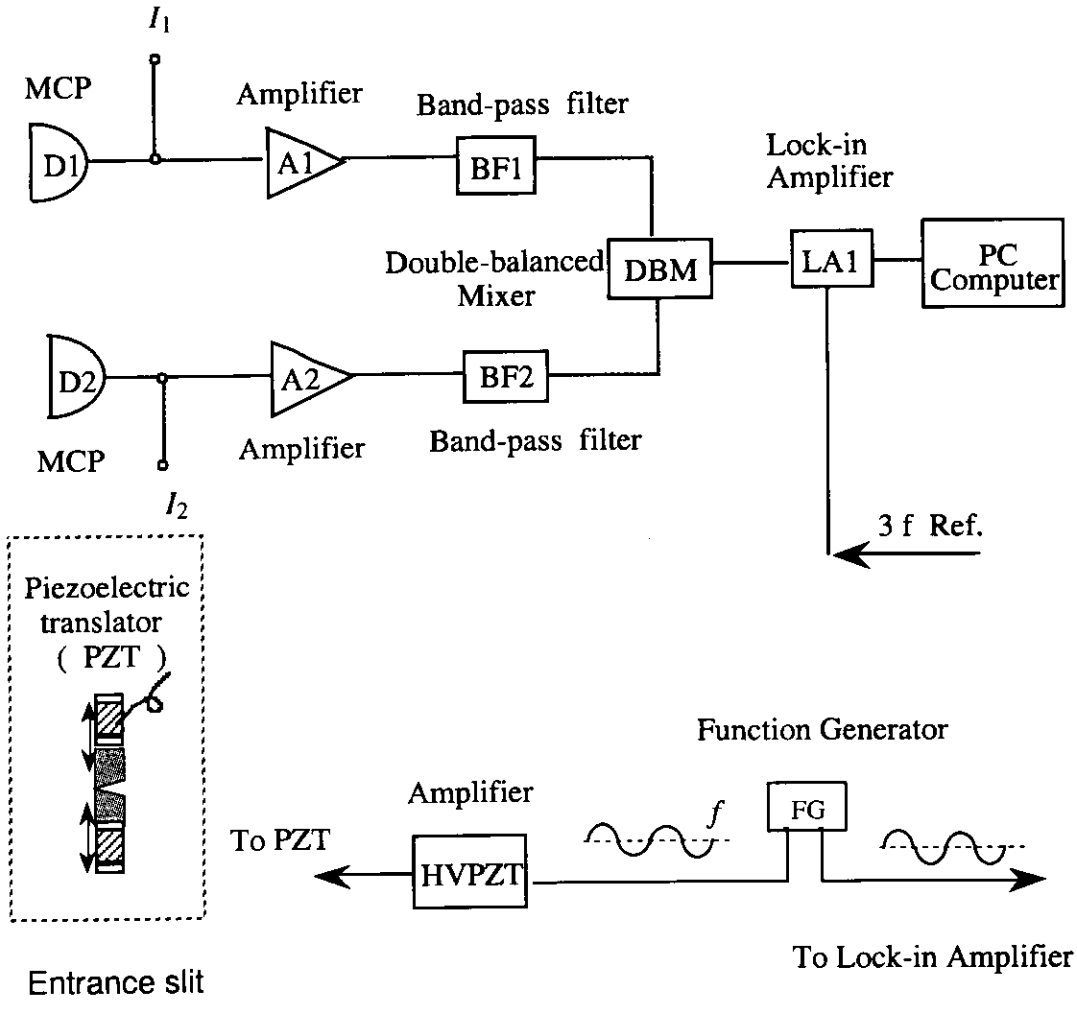

Fig. 4-16 Block diagram of electric correlator for SR

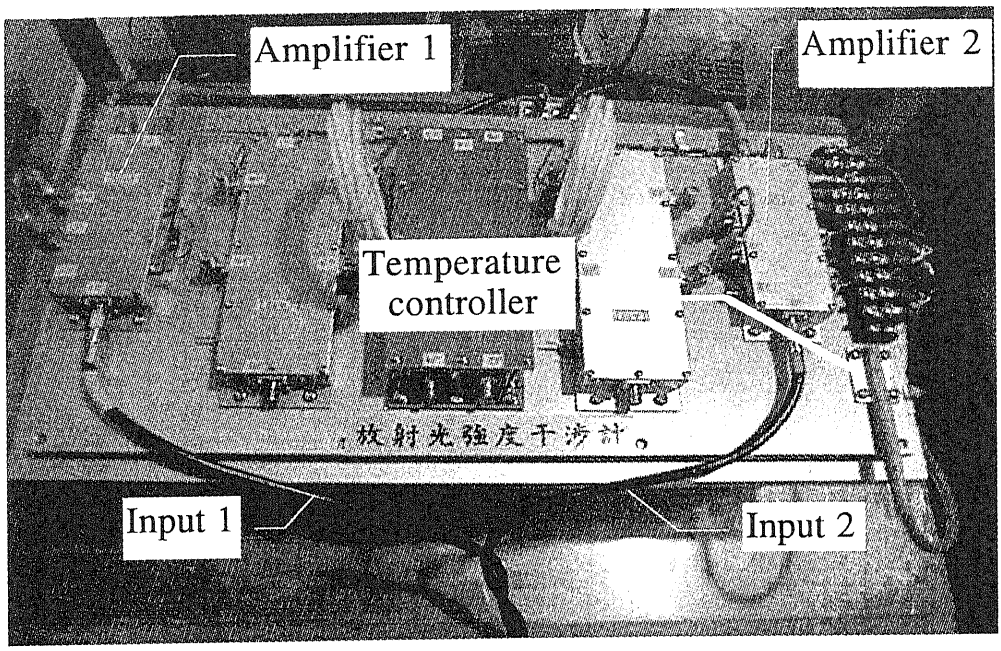

Fig. 4-17 Top view of the electric correlator

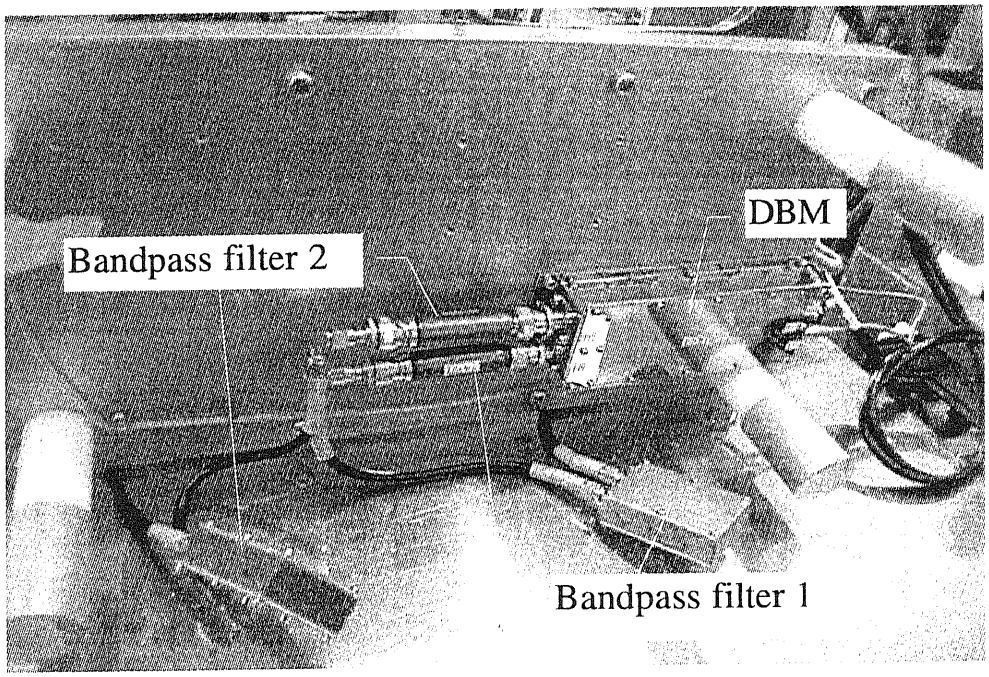

Fig. 4-18 Bottom view of the electric correlator

4.2.4 Photon number and S/N ratio

To estimate the S/N ratio of this new electric correlator it is necessary to estimate the photon number falling on the detectors.

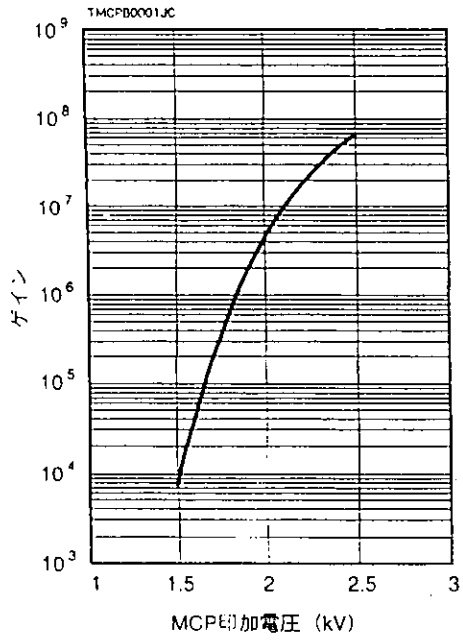

Fig. 4-19 Gain feature of MCP [43]

The gain characteristics of MCPs is shown in Fig.4-19. In the experiment the high voltage is fixed as 1800 V, and the output current is adjusted to about 100 nA (BL16B, PF). The gain was readily estimated to be of the order $G \sim 10^5$ from Fig.4-19. The quantum efficiency is about $\alpha \sim 0.02$ for the photons of 70eV. The photon number N falling on the detectors within unit time can be estimated as follows,

$$N = \frac{J_{DC}}{G\alpha e} \approx 10^9 \quad sec^{-1} \ . \qquad (4\text{-}19)$$

Considering the resolution $\lambda / \Delta\lambda \sim 1000$ for $\lambda = 17.7nm$ (70eV), and the coherence time is $\tau_c \sim 10^{-13} sec$, then the degeneracy parameter δ [44] is calculated as follows (the average photon number falling on the detector

within coherence time τ_c which is a quantity proportional to the Bose degeneracy [45]),

$$\delta = N\tau_c \sim 10^{-4} \qquad (4-20)$$

Obviously δ is the same as the Bose degeneracy n_B when only the diffraction limited part of the beam is detected. In Fig.4-11 the *wave noise* J_S at the output of the filter, which comes from photon fluctuation, is given by the equation [6],

$$\overline{J_S^2} = 2J_{DC}^2 \frac{\Delta f}{\Delta \nu}, \qquad (4-21)$$

where J_{DC} is the direct current component in signals, which is induced by the average intensity of the light. In addition the *shot noise* due to the finite charge of an electron is

$$\overline{J_n^2} = 2eJ_{DC}\Delta f. \qquad (4-22)$$

From a simple calculation we can find that in the present situation the *wave noise* is much smaller than the *shot noise*.

$$\frac{\overline{J_S^2}}{\overline{J_n^2}} = \alpha\delta << 1, \qquad (4-23)$$

where α is the quantum efficiency of photon detector, δ is the degeneracy parameter. According to the above analysis the ratio in Eq.(4-23) is about 10^{-6}.

The signal to noise ratio at the correlation output can be expressed as follows [6],

$$\frac{S}{N} = \alpha\delta\kappa|\gamma_{12}(0)|^2\sqrt{\frac{1}{2}T_0\Delta f}\ \ \Sigma, \qquad (4-24)$$

where T_0 is the measuring time, α is the quantum efficiency of photon detector, δ is the degeneracy parameter of light source, κ is duty ratio as defined in Eq.(4-17), Δf is the bandwidth of this electric correlator, Σ is the unexpected loss in the period of measuring time T_0.

Let us give a numerical estimation of Eq.(4-19). For our correlator, we assume $\Delta f = 250$ MHz, $\kappa \approx 20$ (see **Appendix A**), and $\Sigma \approx 0.5$, For a light source with Bose degeneracy $\delta \approx 10^{-4}$, we give a measuring time $T_0 = 2$ *hours*, then

$$\frac{S}{N} \approx 27. \qquad (4-25)$$

Therefore two-hour measurement can give an enough S/N ratio.

5 System tests

To ensure that this new intensity interferometer be reliable, a series of tests were performed.

5.1 Monochromator

The monochromator plays the roles of wavelength tuning and coherence time modulation. To demonstrate its resolution we measured the Aluminium transmittance spectrum by scanning photon energy with this monochromator. Fig.5-1 shows the *Al* $L_{II,III}$ absorption edge of an *Al* filter installed at BL12A.

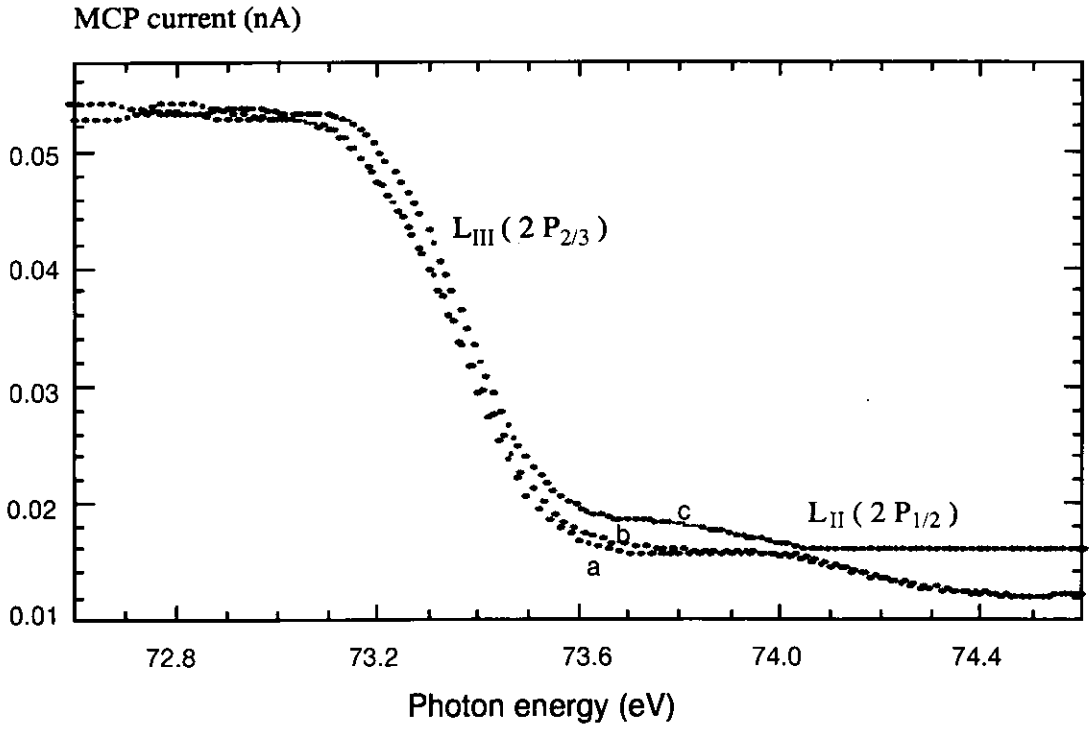

Fig.5-1 Transmittance spectrum of Aluminium scanned by the monochromator with different *Entrance-Exit* slit width pairs. Curve a: 40*μm*-40 *μm*, b:100 *μm* -40 *μm*, c:140 *μm* -100 *μm*

Curve *a*, *b* and *c* represent the transmittance spectrum scanned by the monochromator with different *Entrance-Exit* slit width pairs respectively.

The first step in Fig.4-1 comes from the L_{III} (73 eV) resonant absorption, the second one from L_{II}(74 eV) absorption. The data include the thermal broadening of the Fermi edge of Al, which is the order of 3.5 $K_B T$ and roughly equal to 80 meV at room temperature. The resolvable photon energy of this monochromator was estimated to be smaller than $0.1eV$. On the other hand Fig. 5-1 also gives a qualitative indication about the resolution of the monochromator. Clearly the relatively plainer curve c than curve a or b implies the fact that the resolution of this monochromator at the case of small slit width pair (40 μm -40 μm) is better than at other case (100 μm -40 μm or 140 μm -100 μm). In other words the coherence time $\tau_c(a)$ at case a is the longest one and $\tau_c(a) > \tau_c(b) > \tau_c(c)$. More exact estimation of the resolution would need some deconvolution considering the thermal broadening of the Fermi edge.

5.2 Time response of MCP

Microchannel plates are installed in the high vacuum chamber of this intensity interferometer and are our photons-electrons converters. Their response time is important for improving S/N ratio. Fig. 5-2 is measured by *IWATSU 400MHz storagecope*. The solid lines are Gaussian fitting results.

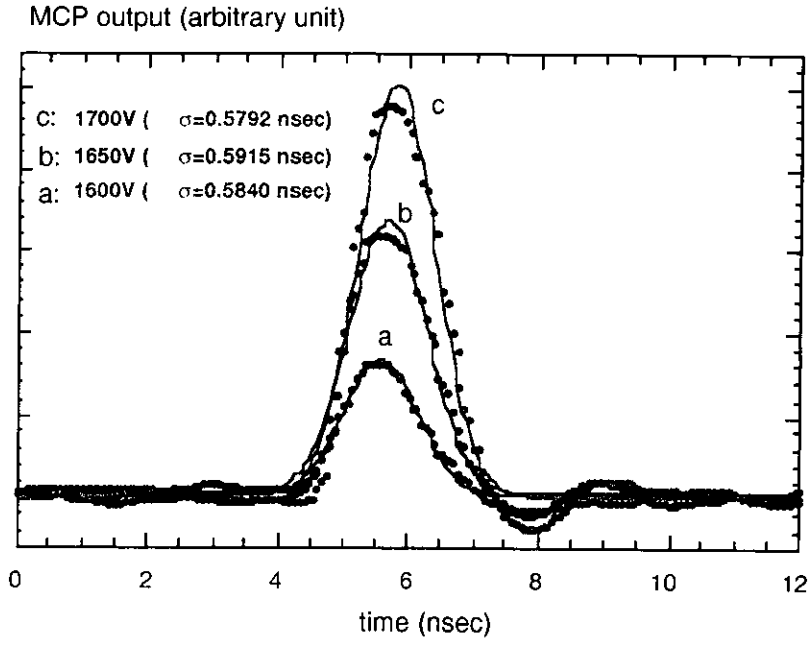

Fig. 5-2 MCP response pulses at various bias voltages

By increasing MCP bias voltage from $1600V$ to $1700V$, the response magnitude is linearly increased but the width is almost invariated, which corresponds to the response time of MCP. Due to the limited bandwidth of the storagecope (400 MHz) the measured value (about $1.2nsec$) is a little larger than the actual one ($0.75nsec$).

5.3 Intensity modulation

As it is shown in the last chapter sinusoidal modulation of light intensity is vital for suppressing false correlation.

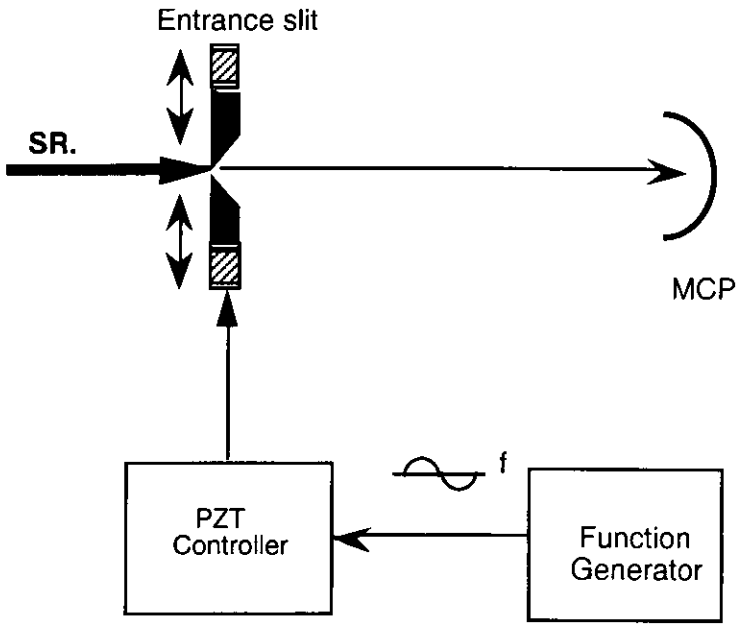

Fig. 5-3 Arrangement to modulate the slit width

Fig. 5-3 shows the simplified schematic diagram of this operation. Basically the waveform of analog output of the function generator (FG) is arbitrarily program-controlled, and an appropriate waveform can compensate the influences of hysteresis and nonlinearity of the piezoelectric translator (*PZT*) and the nonuniform distribution of SR. Then we can in principle produce precise sinusoidal modulation of SR intensity. But due to the instability of beam position the perfect compensation of nonlinearity is difficult to achieve. We estimate the effect of higher harmonics of the intensity modulation in Eq. (4-17) by comparing contributions due to the first and the

second term in the 3f components of Eq. (4-17). We found that the effect is negligible when undulator radiation is used and the higher harmonics is less than 10%. Therefore we just use the sinusoidal waveform output of the function generator.

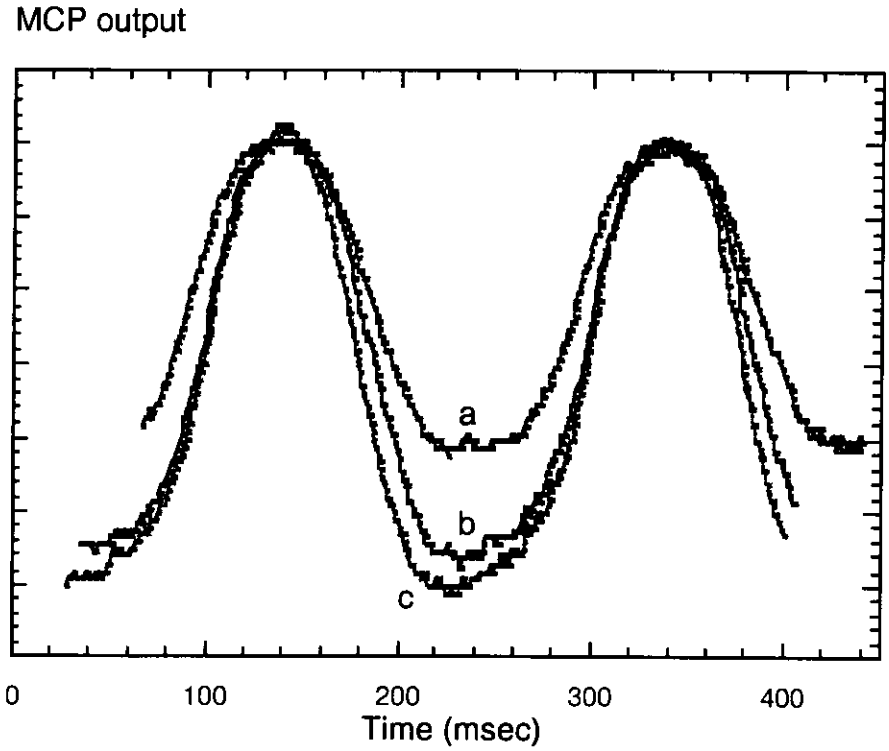

Fig. 5-4 Modulated intensity waveform of synchrotron radiation
5Hz modulation frequency, control input, a: 4.00Vpp, b: 5.6Vpp, c:6.4Vpp

Some examples of modulated SR intensity is shown in Fig. 5-4 at the fundamental frequency 5Hz with different peak to peak output voltage from FG. Table 5-1 shows their harmonic ratio of each curve. Apparently approximate sinusoidal intensity modulation can be achieved by appropriate selection of peak to peak voltage output of the function generator.

Table 5-1 Higher harmonics and their ratio. (*5Hz*-modulation frequency)

	5Hz	10Hz	15Hz	20Hz
4.0Vpp	1	0.062	0.085	0.023
5.6Vpp	1	0.123	0.062	0.031
6.4Vpp	1	0.182	0.053	0.037

5.4 DBM performance

Double balanced mixer (DBM) acts as the linear multiplier in the electric correlator of this intensity interferometer. By using the network analyzer we measured its performance with the two inputs Lo and RF in the same frequency.

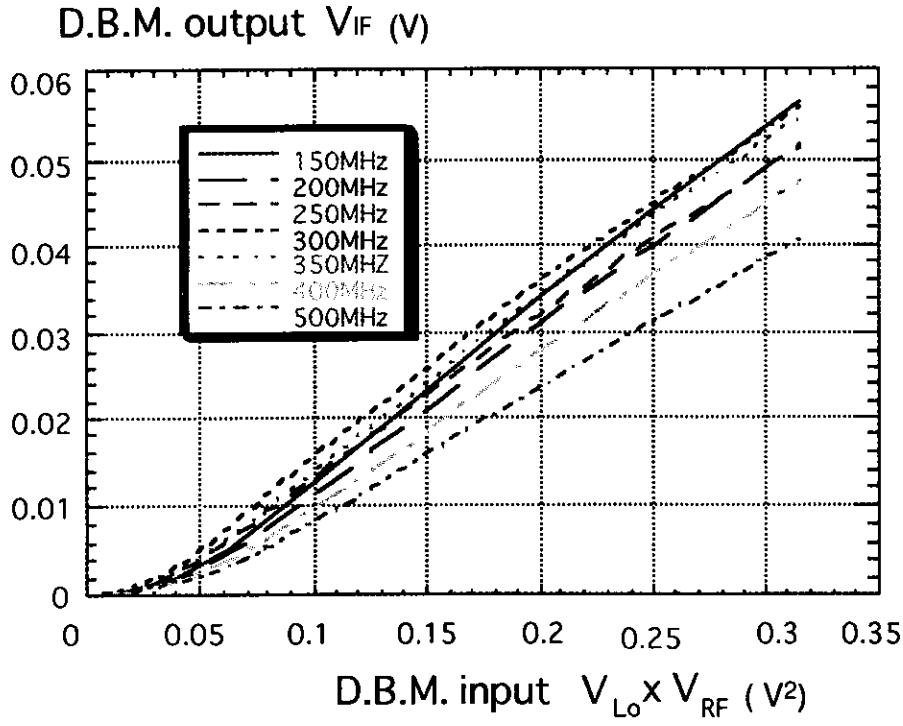

Fig. 5-5 DBM performance test

The measured results are shown in Fig. 5-5. We can see when each input is larger than $0.2V$, DBM can exhibit good linearity. Of course this is just a simple test of DBM operation. For actual case the output will be an integral effect because the input frequencies cover a continuous broad band which is the passing band of the bandpass filter in the correlator.

5.5 Noise characteristics

For such a high-gain ($120dB$) broadband ($250MHz$) electric correlator, the most important problem is to suppress the thermal noise and coherent noise.

The lock-in amplifier acts as the $3f$ selector in our correlator and it is sensitive only to such signals which oscillates at the same or some harmonic frequency as its reference input. Fig.5-6 show the working principle for a lock-in amplifier [46]. For a synchronously excited signal its modulated amplitude s and phase difference from the lock-in reference $\theta = \theta_{ref} - \theta_{sig}$ would be measured simultaneously. The averaged amplitude output can be calculated as follows for a long-time measurement.

$$\langle S \rangle = \sqrt{\langle S\cos\theta\rangle^2 + \langle S\sin\theta\rangle^2} \qquad (5\text{-}1)$$

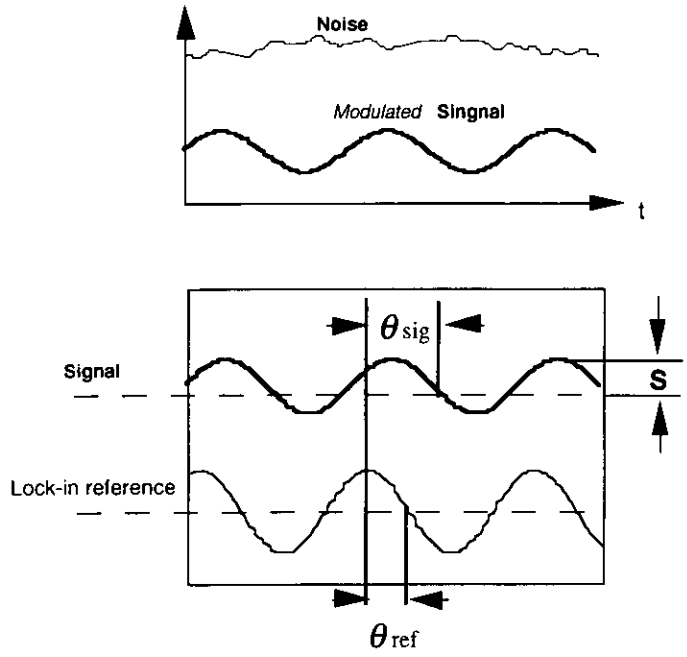

Fig.5-6 Illustrating the measuring principle of the Lockin amplifier

The measuring system is shown in Fig.5-7. If the two inputs are independently, or in other words uncorrelated, the correlator output is apparently only the thermal noise output, nevertheless this noise is not small but could be canceled through large sampling number N due to the relation of $S/N \sim N^{1/2}$ for white noise .

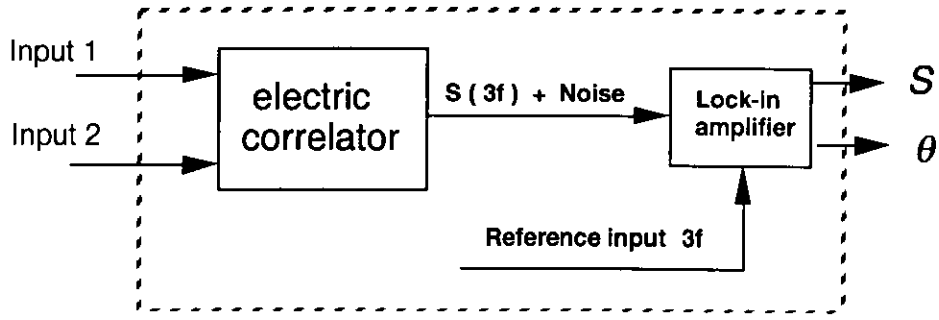

Fig.5-7 Illustrating the measuring system

The most serious problem might be the so-called coherent noise, which is the noise with the same oscillation frequency as the reference frequency and is the main cause of large DC drift. In fact great care has been taken to eliminate the influence of coherent noise. Fig.5-8 shows the typical averaged amplitude output for a noise by giving two independent inputs in Fig.5-7, and Fig.5-9 shows the locked noise-phase distribution. *It clearly shows that for a real noise the locked phase is randomly distributed and the locked averaged amplitude is time-decreasing.* Fig.5-8 also indicates that, at the sampling number around 20000, the white noise can be canceled to the order of several nanovolts, which is much smaller than the expected true correlation signal from undulator radiation.

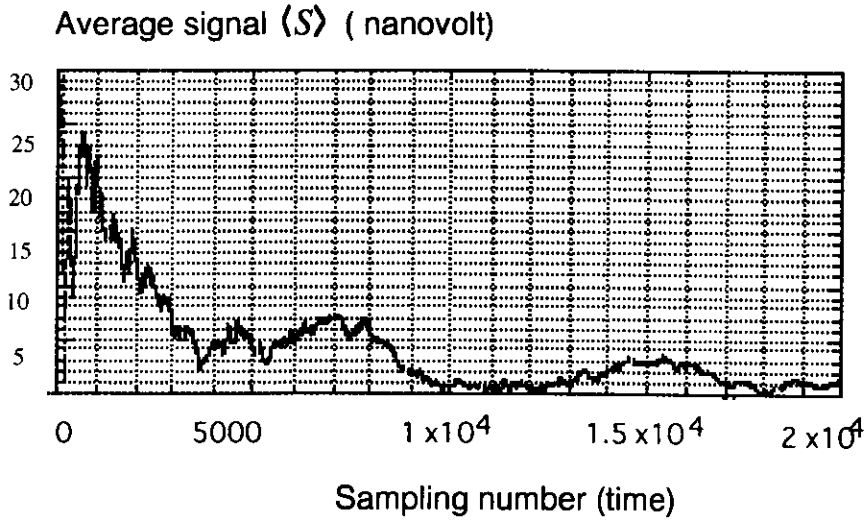

Fig. 5-8 Typical integral amplitude output for a noise

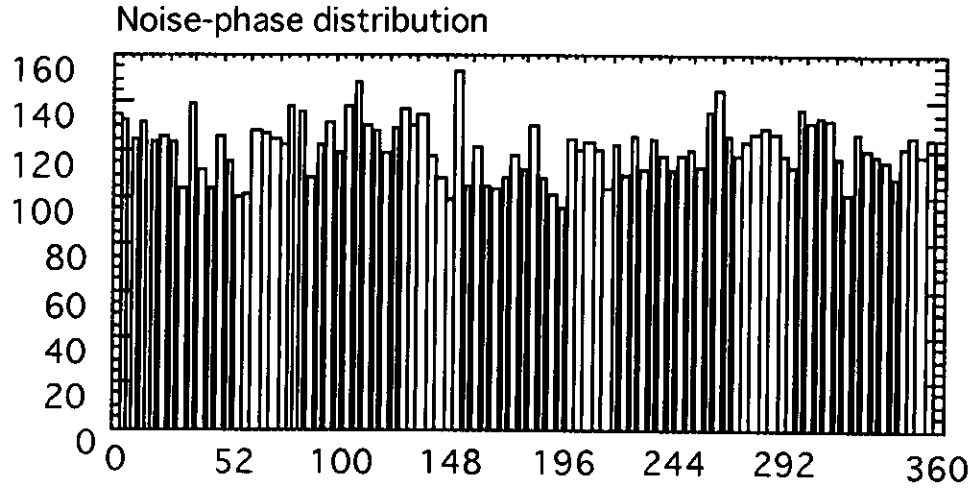

Fig. 5-9 The locked phase distribution for a noise

It is worth noting here that, if the two inputs in Fig. 5-7 are dependent or in other words correlated, the locked phase will have a Gaussian-like distribution centered at θ_{max} which is the locked phase with the maximum probability, but not random-distributed any longer. This θ_{max} is decided by the modulation system. Fig. 5-10 shows an example of the phase distribution for a real signal, where the outputs of the two MCPs illuminated by the $I_1(t)$ and $I_2(t)$ as shown in Fig.4-1 were used as the two inputs, and the width d of the precise slit was adjusted to 30μm.

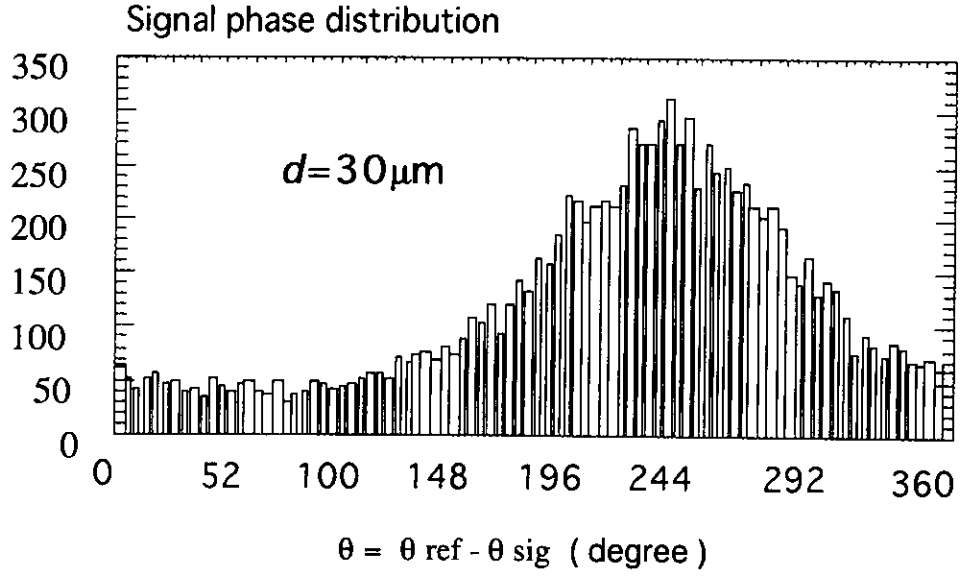

Fig. 5-10 The locked phase distribution for a signal

6 Experiment

In this chapter the experiment and its related data analyzing method are to be presented.

6.1 Experimental setup

The top view of the whole experimental system is shown in Fig. 6-1. The light source is undulator radiation at beam line BL16B of the Photon factory, KEK. The grating of beam line monochromator was placed at the *zero*th order, and its entrance slit and exit slit were kept fully open in order not to disturb the coherence properties of the light emitted from relativistic electron beam in the storage ring. The precise slit in our high vacuum chamber diffracts the incident synchrotron radiation horizontally, so the horizontal spatial two-photon correlation was measured. The bias voltage of MCPs was fixed at $1800V$ and their output currents were fixed at about $100nA$ at the beginning of each measurement by adjusting the incident light intensities. To balance the light intensities falling on the two MCPs, we adopted two ways. One was to adjust the beam mask in our vacuum chamber, the other was to adjust the exit slit of the beamline monochromator. The entrance slit of our monohcromator was modulated at a low frequency $f = 9.5Hz$. The low-frequency f-components of the MCPs outputs, that are $I_1(f)$ and $I_2(f)$, were measured by two analog lock-in amplifiers for the normalization because the intensity of synchrotron radiation is time-decreasing due to the damping effect of electron beam. The high-frequency parts of MCP output currents, after being amplified and filtered by the amplifiers and the bandpass filters, were multiplied by a double balanced mixer (DBM). The $3f$ component $S(3f)$ of the DBM output was detected by a digital lock-in amplifier. The phase information of the $3f$ signal was also recorded due to the characteristic of lock-in amplifier.

The photon energy was chosen at $70eV$. The exit slit was fixed at $50\mu m$, the entrance slit was modulated between $50\mu m$ and $100\mu m$, therefore the average resolution $\lambda/\Delta\lambda$ of our monohcromator was about 1000. The true two-photon correlation S was measured as a function of the horizontal width d of the precise slit. For each d value, the measuring time was 2 hours and the

sampling points were 10000. The beam size falling on the precise slit was also measured by a wire scanner directly attached behind this slit. The knowledge of the beam size is convenient for the theoretical estimation.

Finally the residual false correlation was measured at BL12A. This was done by changing the diffraction order of our grating monochromator to the *zero*th order, consequently the coherence time is zero and only residual false correlation is left in the signal $S(3f)$.

Table 6-1 Parameters of experimental setup

Light source	BL16B, PF (undulator radiation)
Photon energy	70 eV (first harmonics)
PZT modulation frequency	9.5 Hz
Variation of the entrance slit width	50 μm ~ 100 μm
Width of the exit slit	40 μm
Resolution of the monochromator	~ 0.1 eV
MCP bias voltage	- 1800 V
MCP output (in the beginning)	100 nA
Sampling points	10000
Measuring time	2 hours

Table 6-2 Comparison of Case A and Case B

Case A	The ***exit slit*** of beamline monochromator was used as an intensity **attenuator** of SR (vertically)
Case B	The ***beam mask*** was used as an intensity **attenuator** of SR

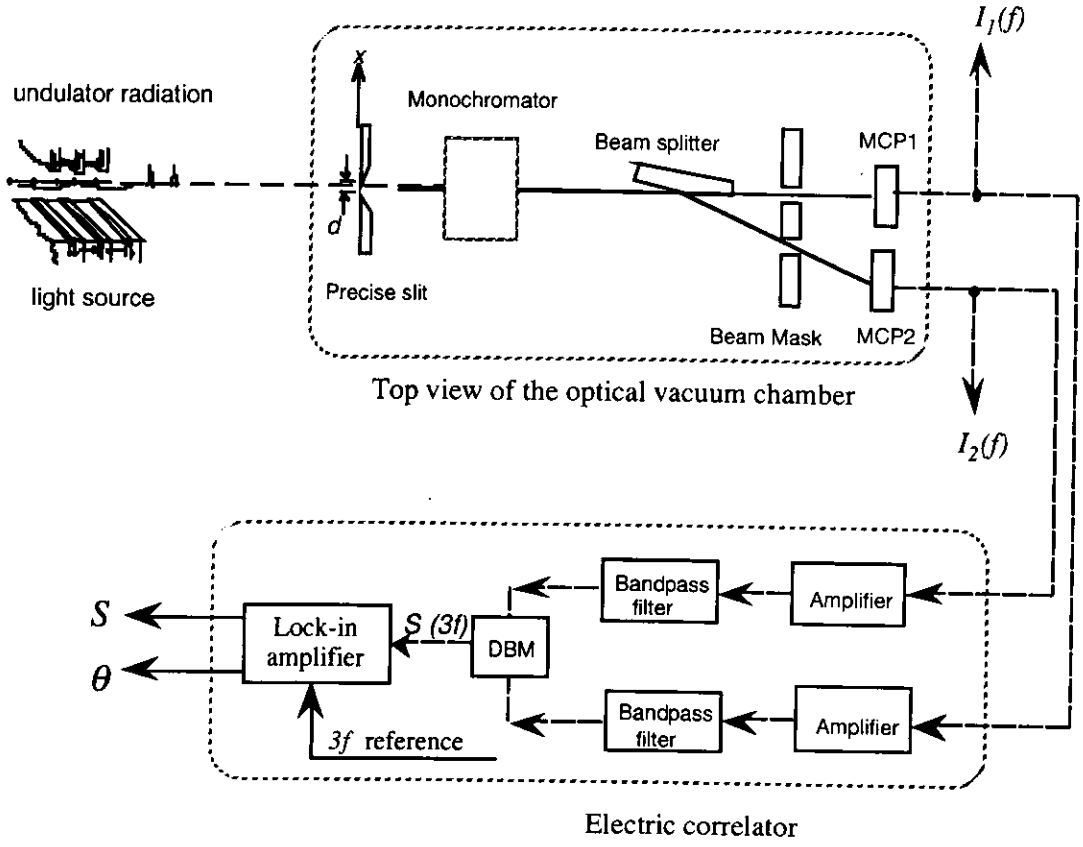

Fig. 6-1 Simplified diagram of the whole experimental system. $I_1(f)$, $I_2(f)$ and $S(3f)$ are simultaneously recorded and saved in each sampling time by a computer.

6.2 Statistical analysis on experimental data

6.2.1 Theoretical background [47]

This is going to explore a way to decide a statistical mean $\bar{X}$ and its error bar. For a random sample $X_1,X_2,...X_k$ from a normal distribution that is $n(\mu,\sigma^2)$, μ–mean, σ^2–variance of this statistics X_i, a question is how we can decide the confidence intervals for the maximum likelihood estimator $\bar{X}$ of μ, where

$$\bar{X} = \frac{1}{k}\sum_{i=1}^{k} X_i \qquad (6-1)$$

Case 1, if μ is unknown but σ^2 is known
then the statistics $\bar{X}$ also obey to a normal distribution $n(\mu,\sigma^2/k)$ and the statistics $(\bar{X}-\mu)/(\sigma/\sqrt{k})$ obeys to $n(0,1)$, thus the probability

$$\Pr(-2.576 < \frac{\bar{X}-\mu}{\sigma/\sqrt{k}} < 2.576) = 99\% \qquad (6-2)$$

or equivalently

$$\Pr(\bar{X} - 2.576\frac{\sigma}{\sqrt{k}} < \mu < \bar{X} + 2.576\frac{\sigma}{\sqrt{k}}) = 99\% \qquad (6-3)$$

The probability that the random interval $(\bar{X}-2.576\sigma/\sqrt{k}, \bar{X}+2.576\sigma/\sqrt{k})$ includes the unknown fixed point μ is 99%. The number 99% is called *confidence coefficient.*

Case 2, both μ and σ^2 are unknown
We define the variance of a random sample of size k as S^2,

$$S^2 = \frac{1}{k}\sum_{i=1}^{k} X_i^2 - \bar{X}^2 \qquad (6-4)$$

then the statistics $(\overline{X}-\mu)/(\sigma/\sqrt{k})$ obeys to the normal distribution $n(0,1)$, and kS^2/σ^2 obeys to Chi-square distribution χ^2(k-1). The random variable T, defined as follows, has a t-distribution with k-1 degrees of freedom whenever $\sigma^2>0$,

$$T=\frac{\overline{X}-\mu}{S/\sqrt{k-1}} \qquad (6-5)$$

t-distribution is written as follows,

$$g(t)=\frac{\Gamma((r+1)/2)}{\sqrt{\pi r}\ \Gamma(r/2)}\times\frac{1}{(1+t^2/r)^{(r+1)/2}} \qquad (6-6)$$

$$(-\infty<t<\infty)$$

$r-$ degrees of freedom

for $r>>1$, $g(t)$ approaches to normal distribution. For our case the degrees of freedom k=10000, So we can use the same formula as Eq.(6-3) just with S instead of σ.

Theorem Let $X_1, X_2, .. X_m$ be mutually stachastically independent random variables, which obeys the normal distribution $n(\mu_1,\sigma_1^2)$, $n(\mu_2,\sigma_2^2)$, ... and $n(\mu_m,\sigma_m^2)$ respectively. The random variable $Y=c_1X_1+c_2X_2+...c_mX_m$, where c_1, c_2 and c_m are real constants, is normally distributed with mean $\overline{Y}=c_1\mu_1+c_2\mu_2+...c_m\mu_m$ and variance $\sigma^2=c_1^2\sigma_1^2+c_2^2\sigma_2^2+...c_m^2\sigma_m^2$, That is

$$n(\sum^m c_i\mu_i,\sum^m c_i^2\sigma_i^2) \qquad (6-7)$$

Eq.(6-3) ***and*** **Eq.(6-7)** ***are important formulae for estimation of the mean, the standard deviation and the error bar.***

6.2.2 Data Analyses

For each fixed width d of the precise slit, we have k=10000 sampling points. The $S_i(3f)$, that is the measured signal in the ith time, can be decomposed into x_i and y_i which include the phase information. The low-frequency $1f$-component of MCP output are $I_{1i}(f)$ and $I_{2i}(f)$, then,

$$\bar{x} = \left\langle \frac{x_i}{I_{1i}(f) I_{2i}(f)} \right\rangle \qquad (6-8)$$

$$\bar{y} = \left\langle \frac{y_i}{I_{1i}(f) I_{2i}(f)} \right\rangle \qquad (6-9)$$

$$\langle x^2 \rangle = \left\langle \frac{x_i^2}{I_{1i}^2(f) I_{2i}^2(f)} \right\rangle \qquad (6-10)$$

$$\langle y^2 \rangle = \left\langle \frac{y_i^2}{I_{1i}^2(f) I_{2i}^2(f)} \right\rangle \qquad (6-11)$$

mean signal $$S = \sqrt{\bar{x}^2 + \bar{y}^2} \qquad (6-12)$$

mean phase $$\theta = \tan^{-1}\left(\frac{\bar{y}}{\bar{x}}\right) \qquad (6-13)$$

standard deviation $$\sigma = \frac{\sqrt{\langle x^2 \rangle + \langle y^2 \rangle - S^2}}{\sqrt{k-1}} \qquad (6-14)$$

If there are several independent measurements for a fixed width d, say m times (notes here for each measurement the number of sampling is k=10000), then according to Eq. (6-7) we get the final mean signal and its standard deviation as follows,

$$\bar{S} = \frac{1}{m} \sum_{j=1}^{m} S_j \qquad (6-15)$$

$$\overline{\sigma} = \frac{1}{m}\sqrt{\sum_{j=1}^{m}\sigma_j^2} \qquad (6-16)$$

Eq.(6-8) ~ Eq.(6-16) are the fundamental formulae for our data processing. The following table is calculated from the data measured at case A, where the exit slit of beamline monochromator was used as a light attenuator to keep the intensity falling on the MCPs almost the same for different precise slit widths d in the beginning of each measurement.

Table 6-3 Case A

Precise slit d (μm)	S ($\times 10^{-5}$)	θ (degree)	σ ($\times 10^{-5}$)	$\overline{S}$ ($\times 10^{-5}$)	$\overline{\sigma}$ ($\times 10^{-5}$)
10-1	1.09	-115.73	0.036		
10-2	2.63	-117.16	0.033		
		-116.45		1.86	0.024
15	1.83	-110.32	0.055	1.83	0.055
20-1	0.77	-113.06	0.037		
20-2	1.61	-121.82	0.023		
20-3	1.38	-114.65	0.046		
		-116.51		1.25	0.021
30-1	1.46	-121.48	0.025		
30-2	1.46	-124.82	0.062		
		-123.15		1.46	0.033
50-1	1.39	-135.36	0.038		
50-2	0.35	-124.12	0.028		
		-129.74		0.87	0.024
70	1.18	-117.06	0.021	1.18	0.021
100-1	0.73	-135.31	0.035		
100-2	1.44	-108.49	0.024		
		-121.90		1.08	0.021

The exit slit of beamline monochromator was used as a intensity attenuator.

Table 6-4 is from the datas measured at case B, where the beam mask in our vacuum chamber was used as the light intensity attenuator.

Table 6-4 Case B

Precise slit $d(\mu m)$	S ($\times 10^{-5}$)	θ (degree)	σ ($\times 10^{-5}$)	$\overline{S}$ ($\times 10^{-5}$)	$\overline{\sigma}$ ($\times 10^{-5}$)
10-1	2.01	-120.00	0.037		
10-2	1.58	-119.67	0.027		
		-119.80		1.80	0.023
20	1.16	-120.59	0.023	1.16	0.023
50-1	1.12	-118.90	0.015		
50-2	0.88	-117.27	0.047		
		-118.08		1.00	0.025
100	0.82	-123.80	0.017	0.82	0.017

The beam mask in our vacuum chamber acts as the light attenuator

Table 6-5 shows the residual false correlation measured at BL12A.

Table 6-5 Residual false correlation A

Measuring times	A ($\times 10^{-5}$)	θ_A (degree)	σ_A ($\times 10^{-5}$)	$\overline{A}$ ($\times 10^{-5}$)	$\overline{\sigma}_A$ ($\times 10^{-5}$)
1	0.627	-113.21	0.013		
2	0.409	-115.93	0.010		
3	0.625	-118.05	0.007		
4	0.165	-127.58	0.007		
5	0.107	-127.42	0.006		
6	0.155	-125.39	0.006		
		-121.26		0.348	0.0035

6.2.3 Normalized true two-photon correlation

From Eq.(4.17) we know that the normalized signal output is,

$$\bar{S}(d) = \bar{A} + \chi \cdot \kappa \frac{\tau_c}{T_R} |\gamma(d)|^2 \qquad (6-17)$$

where we have assumed that the incoming light is chaotic light and the second-order coherence is defined as $\Gamma^{(2)} = 1 + |\gamma(d)|^2$. Of course the second term in Eq.(6-17) will vanish if the light is totally coherent. The coefficient χ is decided by the characteristics of electric circuit. In experiment all the parameters of the electric correlator, the electronics were fixed, so χ is a constant. The first term $\bar{A}$ is the residual false correlation. We can express *the normalized true two-photon correlation* as follows,

$$\bar{C}(d) = \bar{S}(d) - \bar{A} \qquad (6-18)$$

$\bar{S}(d)$ is listed in Table 6-3 and Table 6-4, $\bar{A}$ is in Table 6-5. According to those datas $\bar{C}(d)$ are drawn in Fig. 6-2 and Fig.6-3. As Eq.(6-3) shows, the error bar represents the statistical confidence interval around the mean with 99% confidence coefficient.

According to the theoretical analysis of Eq.(4-8) we can express the theoretical normalized two-photon correlation as follows,

$$C_{Theo}(d) = \Lambda \sqrt{\frac{d^2 + 24\Sigma^2}{(1 + \Sigma^2 / \sigma_c^2) d^2 + 24\Sigma^2}} \cos^{-1}\left(\frac{d^2}{(1 + 2\sigma_c^2 / \Sigma^2) d^2 + 48\sigma_c^2} \right) \qquad (6-19)$$

where

$$\sigma_c = \frac{\varepsilon_p \Sigma}{\sqrt{\varepsilon^2 - \varepsilon_p^2}} \qquad (6-20)$$

where the influences of the electronics have been represented by a factor Λ. ε is the emittance of the stored beam and $\varepsilon_p = \lambda / 4\pi \cong 1.41 nmrad$ for 70eV. Σ is the horizontal beam size and has measured as Σ=77.9 μm as Fig. 6-4 shows. By adjusting carefully the two parameters Λ and ε in Eq.(6-19), we get the optimal fitting as the dotted lines show in Fig.(6-2) and Fig.(6-3) and the emittance ε is estimated at about 40 *nmrad.*

There are several possible reasons about the singular points in Fig.6-2. One is the horizontal-vertical coupling (H-V coupling). This is due to the reason that the horizontal direction of our vacuum chamber didnot coincide rigorously with the horizontal direction of beam line. During the beam time of this experiment the electron beam was run in low emittance. When we increased the precise slit width horizontally, the exit slit width of the beamline monochromator was inevitably decreased vertically in order to keep the light intensity falling on the detectors invariant. In fact the exit slit of beam line was decreased to the order of several tens of micrometers, which makes the light very coherent in the vertical direction. The severe vibration of beam position (instability) would randomly disturb this coupling, which makes the measured datas behave less regular. Another possible reason might be the electric correlator. Such a broadband high-gain electric circuit is extremely sensitive to the change of surrounding environment such as the temperature and the wind etc. even though we have used a electromagnetic shielding and a temperature controller. It might take a long time to reach its stable state.

To overcome these drawbacks we performed this experiment in case B, where the H-V coupling effect had been avoided by keeping the exit slit of beamline monochromator fully open. Of course the electric circuit might be more stable thermally than in case A because rather long time (several days) had passed, which is longer than the time constant to restore the system to be thermal equilibrium state.

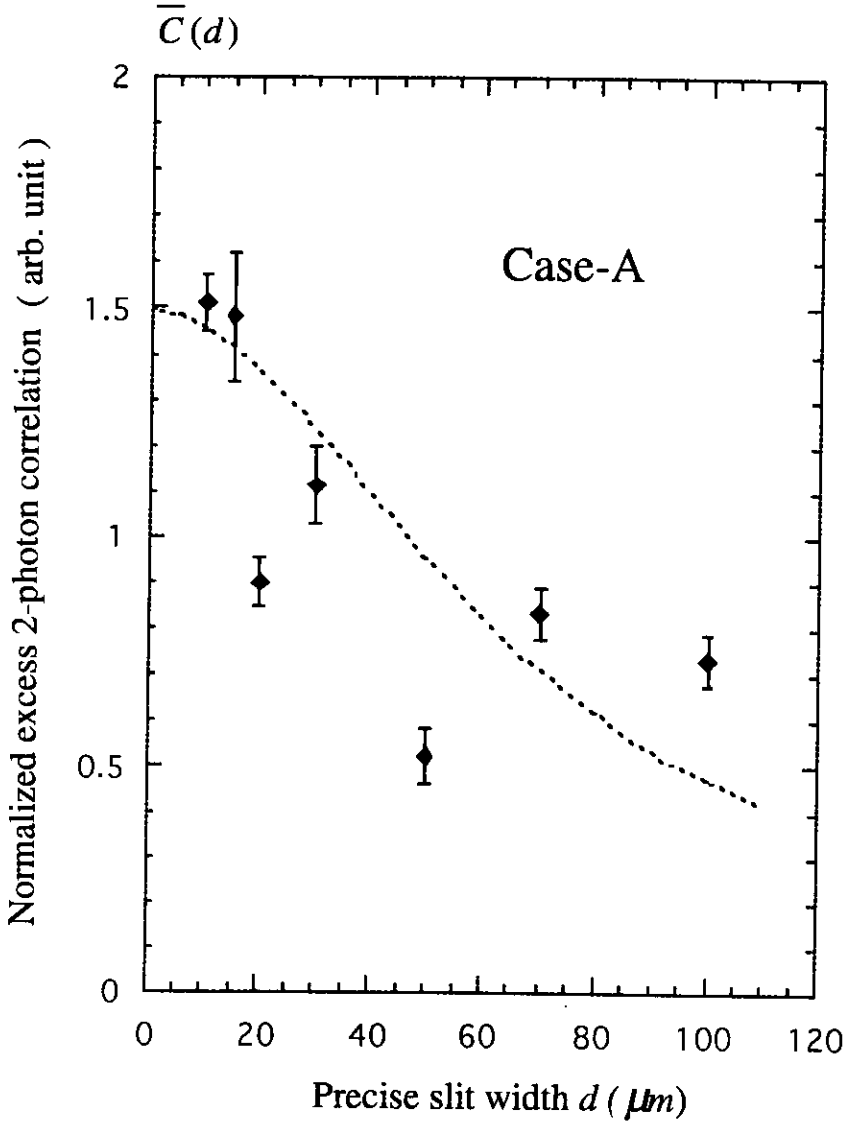

Fig. 6-2 Measured true two-photon correlation in case A

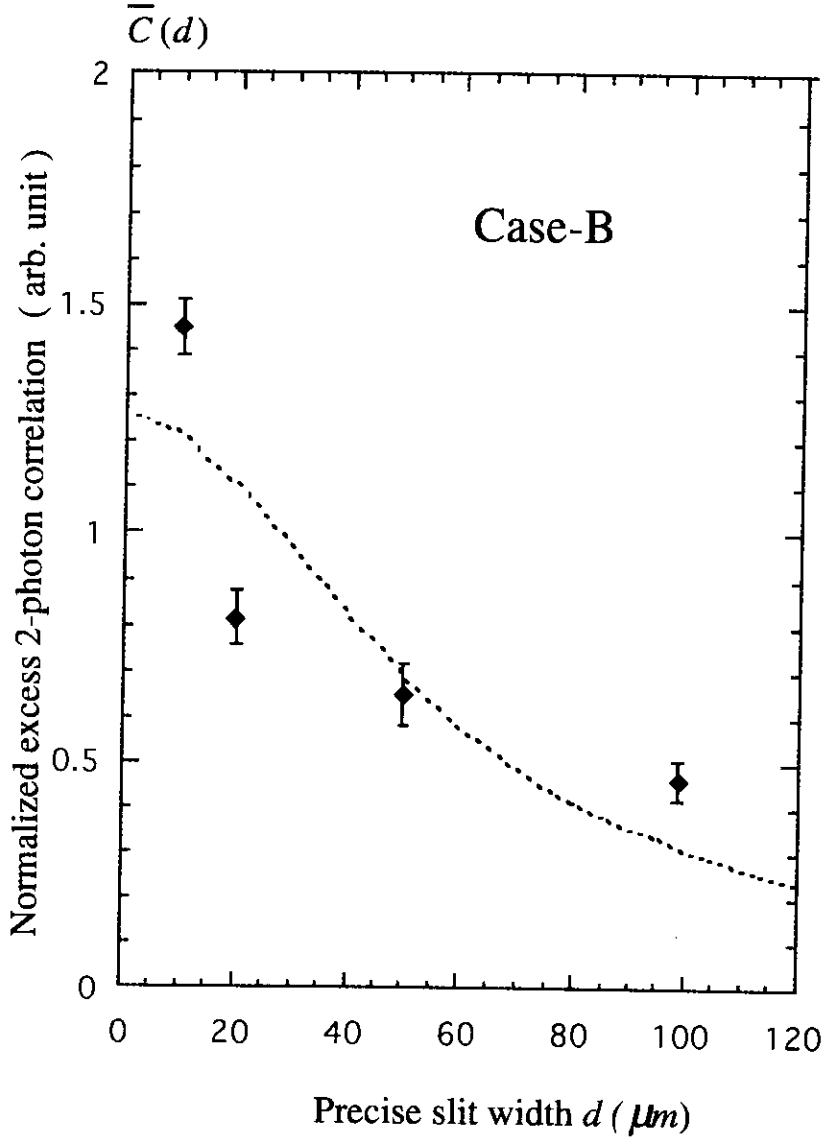

Fig.6-3 Measured true two-photon correlation

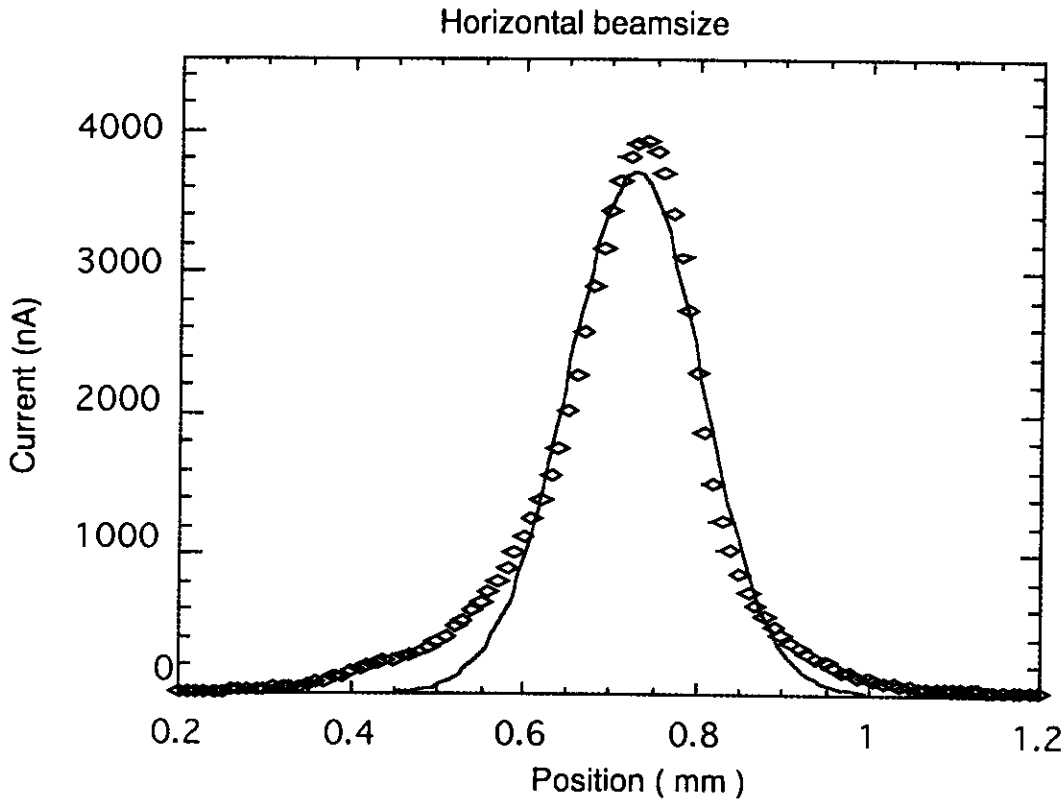

Fig. 6-4 Beam size measured directly behind the Precise slit
(Horizontal Σ=77.9 μm)

7 Discussions

In the last chapter the details of the experiment has been described. Related with the explicit photon-bunching effect shown in Fig.6-2 and Fig.6-3, We will argue in detail the properties of synchrotron radiation and some applications of this experiment.

7.1 Chaotic nature of synchrotron radiation

For a field of coherent radiation, photons obey a Poisson distribution, correspondingly the electrons emitted from the detector obey Poisson distribution too, which make the two photoelectric currents behave as mutually independent fluctuations, which are just the shot noises of classical electric currents. The important consequence is that the random coincidence of such two Poisson distributions does not depend on any temporal or spatial delay of observed points. In experiment it would give a flat response for the normalized true two-photon correlation $\overline{C}(d)$ no matter how we change the precise slit width d.

The explicit bunching effect shown in Fig.6-2 and Fig.6-3 indicates that there exists a positive correlation, rather than independent fluctuations, between the two photoelectric currents for a small spatial delay. This positive correlation and its strong dependence on the temporal or spatial delay are typical features of two-photon correlation of a chaotic light. For chaotic light second-order coherence is completely determined by the first-order coherence which is temporal or spatial delay dependent. In Fig.6-2 and Fig.6-3 we have fit the measured datas with a theoretical curve calculated from the absolute square of the first-order coherence and found they agree well, although there is a little discrepancy which is possibly caused by the theoretical approximation and the experimental error.

There are two basically equivalent interpretations on the chaotic origin of synchrotron radiation One is the classical wave-packet interference in time domain [19]. The classical wave packets emitted from neighboring two electrons can overlap and interfere but the phase difference is completely random due to the random distribution of the electrons in one bunch. If this interference is constructive, the intensity exhibits maximum; if it is

destructive, the intensity exhibits minimum, that would be zero. Therefore the observed intensity fluctuates randomly from zero to its maximum. The other interpretation is the shot noise of the stored current in the storage ring [48]. This can be understood in frequency domain by following simple consideration.

The electron beam current is constituted by moving electrons randomly arriving to the entrance of bending magnet:

$$j(t) = (-e)\sum_{k=1}^{N} \delta(t - t_k) \qquad (7-1)$$

where e is the charge of one electron, N is the number of electrons in one bunch, and t_k is the arrival time of the kth electron.

After average over an ensemble of bunches , we get the bunch profile function $F(t)$,

$$\langle j(t) \rangle = (-e)NF(t) \qquad (7-2)$$

$F(t)$ may be Guassian and expressed as follows if the bunch width is σ_T,

$$F(t) = \frac{1}{\sqrt{2\pi}\sigma_T} \exp(-\frac{t^2}{2\sigma_T^2}) \qquad (7-3)$$

The Fourier transform of the current in Eq.(7-1) is easily calculated as follows,

$$\tilde{j}(\omega) = \int_{-\infty}^{\infty} j(t) e^{i\omega t} dt = (-e)\sum_{k=1}^{N} \exp(i\omega t_k) \qquad (7-3)$$

So it clearly shows that the Fourier transform of the stored current is the sum of a large number of complex random phasor with random phase $\phi_k = \omega t_k$. For our case, $\omega\sigma_T >> 1$, then the phase ϕ_k can be considered to be uniformly distributed on interval $(\pi,-\pi)$. Therefore it becomes the famous random-walk problem. And the probability density distribution of $|\tilde{j}(\omega)|^2$ is given by the negative exponential distribution,

$$p(|\bar{j}(\omega)|^2) = \frac{1}{\langle |\bar{j}(\omega)|^2 \rangle} \exp\left(\frac{|\bar{j}(\omega)|^2}{\langle |\bar{j}(\omega)|^2 \rangle} \right) \qquad (7-4)$$

On the other hand from Maxwell equations the Fourier components of electric field of the synchrotron radiation can be written as follows,

$$\bar{E}(\omega) = A(\omega)\bar{j}(\omega) \qquad (7-5)$$

where A(ω) is the field emitted by one electron and is deterministic. Therefore the negative exponential distribution of stored current directly determines the negative exponential distribution of synchrotron radiation. Such a distribution is a feature of chaotic light.

Both the above interpretations are based on the assumption that the field emitted by one electron is a fully coherent field and can be coherent to any higher order.

7.2 Applications

The present new intensity interferometer has been operated successfully to extract the true two-photon correlation for non-stationary light source-synchrotron radiation. Some possible applications of this new experimental method are to be discussed in this section.

7.2.1 Measurement of instantaneous emittance

The emittance measurement is a traditional but an important theme in accelerator science[49]. It was found here, If it is known in advance that synchrotron radiation is a chaotic radiation, that from the measurement of the true two-photon correlation we can deduce its instantaneous emittance with the time scale of coherence time τ_c. To understand this we need a little deeper mathematic model.

First let us review the fact that the degree of first-order coherence could be decomposited into the product of spatial part and temporal part under the condition of cross-spectral purity, which is usually satisfied by the experimental conditions [9] [10]. We express this as follows,

$$\gamma_{12}(\tau) = \gamma_{12}(\mathbf{r})\gamma(\tau) \qquad (7-6)$$

where $\gamma_{12}(\mathbf{r})$ is a pure spatial coherence and $\gamma(\tau)$ is a pure temporal coherence. τ is the time delay. The temporal coherence $\gamma(\tau)$ is the Fourier transformation of the normalized spectral distribution function $F(\omega)$ of the light source according to the Wiener-Khintchine theorem.

$$\gamma(\tau) = \frac{1}{2\pi}\int_{-\infty}^{+\infty} F(\omega)\exp(-i\omega\tau)\ d\omega \qquad (7-7)$$

Fig.7-1 shows the form of $\gamma(\tau)$, where a Gaussian spectral distribution has been assumed.

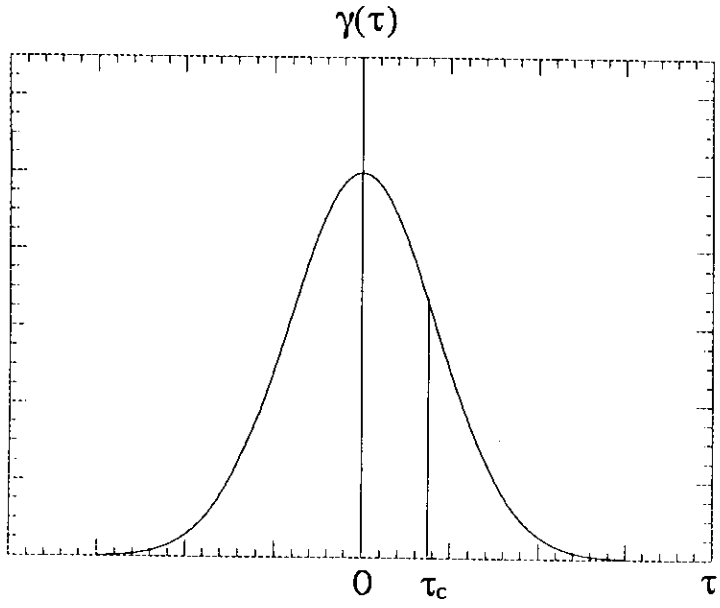

Fig. 7-1 Illustating the temporal coherence with Gaussian form

Here it is worth noting that the tempotal coherence usually happens within the temporal order of coherence time τ_c, no matter what kind of spectral distribution the light has. After the delay τ is getting larger than τ_c, the $\gamma(\tau)$will quickly decreases.

Now I will turn back to discuss the intensity correlation output from time domain.

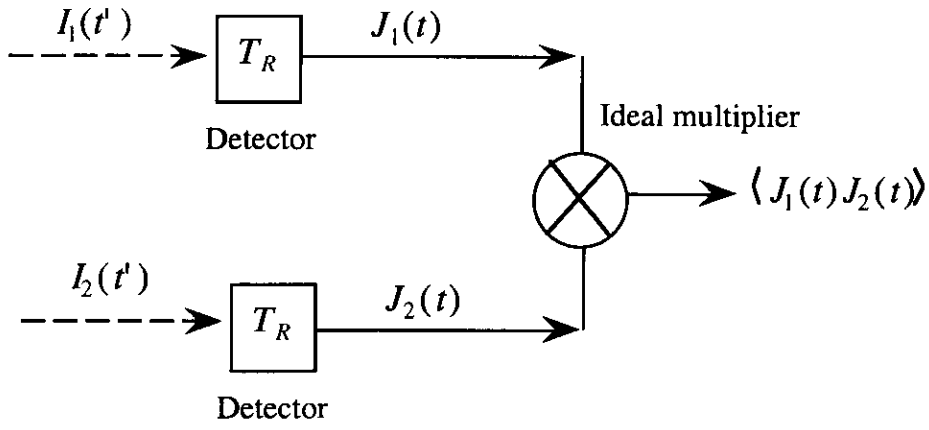

Fig.7-2 An equivalent electric correlator

The above figure shows an equivalent electric correlator, where the time response of this system has been represented by the response time T_R of the photon detectors and the multiplier is an ideal one with zero response time. The correlation of the two incident light intensities is expressed as follows,

$$\langle I_1(t')I_2(t'+\tau)\rangle = \langle I_1\rangle\langle I_2\rangle(1+|\gamma_{12}|^2|\gamma(\tau)|^2), \qquad (7-8)$$

where the cross-spectral purity of Eq.(7-6) has been used and we have used a simple notation γ_{12} instead of $\gamma_{12}(\mathbf{r})$. The induced eletric current from the detector with a response time T_R can be expressed as follows [42],

$$J_1(t) = \int_t^{t+T_R} I_1(t')dt' \qquad (7-9)$$

and

$$J_2(t) = \int_t^{t+T_R} I_2(t')dt', \qquad (7-10)$$

where the quantum efficiency has been assumed to be unity for simplicity. The output of the ideal multiplier can be written as

$$\langle J_1(t)J_2(t)\rangle = \int_t^{t+T_R} dt' \int_t^{t+T_R} dt''\langle I_1(t')I_2(t'')\rangle \qquad (7-11)$$

Therefore from Eq.(7-11) we can easily see that the tempral coherence term would be inevitably induced due to the response delay of the detectors, although we had expected to detect only the spatial coherence of the two incident lights. Eq.(7-11) can be further simplified to give an explicit form of physical meaning as follows,

$$\langle J_1(t)J_2(t)\rangle = \langle I_1\rangle\langle I_2\rangle T_R{}^2\left(1+\frac{|\gamma_{12}|^2}{T_R{}^2}\int_0^{T_R}2(T_R-\tau)|\gamma(\tau)|^2 d\tau\right) \quad (7-12)$$

If $T_R << \tau_c$, $|\gamma(\tau)|^2$ can be regarded as having a constant value and the second term can be easily integrated to be $|\gamma_{12}|^2$. If $T_R >> \tau_c$, which is our present case and also most common case nowadays for chaotic light, then we find,

$$\begin{aligned}&\int_0^{T_R}2(T_R-\tau)|\gamma(\tau)|^2 d\tau\\ &\approx\int_0^{\tau_c}2(T_R-\tau)|\gamma(\tau)|^2 d\tau \qquad (7-13)\\ &=T_R\tau_c,\end{aligned}$$

where the upper limit of the integrand has been changed to the coherence time τ_c by considering the characteristics of the temporal coherence. The following identity also has been used,

$$\int_{-\infty}^{\infty}|\gamma(\tau)|^2 d\tau=\tau_c \qquad (7-14)$$

The physical meaning of Eq.(7-13) is clear, which is that **we do not need to wait such a long time as response time T_R, but several coherence times τ_c are long enough to get the final stable state from the correlation output. In other words the correlation output from the ideal multiplier at time t is actually the average of the correlation of the two incident intensities within the time region of $t-\tau_c \sim t$. Therefore the two-photon correlation gives the instantaneous information of light source (emittance for synchrotron radiation) with the time scale of coherence time τ_c.** Formally the excessive part $|\gamma_{12}|^2$ of the second-order coherence is

merely the modulus square of its first-order coherence, but physically they are essentially different. The emittance information of synchrotron radiation estimated from the first-order coherence recorded all the historical paths experienced by the bunch during a period of the response time T_R of the photon detector and gives a "broadened" emittance; The second-order coherence can only remember its past history in a short period of coherence time τ_c. So the emittance from the second-order coherence may be more "real", more reasonable and may be smaller than the "broadened" emittance.

There also exist some other advantages about the measurement of two-photon correlation. Eq.(B-11) in **Appendix B** gives the expression of the degree of first-order spatial coherence for a generalized light source which might be transversely movable with time. We can see the phase disturbance between the light source and the observation plane falls into the imaginary part ϕ, which gives no contribution to the second-order coherence. This is the reason why the angular size of stars measured by HBT intensity interferometer is much more precise than by a Mechelson interferometer.

Eq.(7-13) also indicates that the attempt to measure temporal two-photon correlation is impossible if the response time of measuring system is much larger than the coherence time.

7.2.2 Diagnosis of incomplete FELs

The diagnosis of incomplete FELs, such as SASE, is apparent by using this method. Because if it is fully coherent light the normalized excess two-photon correlation would be a flat response, but not showing a photon-bunching effect.

8 Conclusions

(1) We have constructed a new intensity interferometer for soft X-ray synchrotron radiation based upon our new operating principle. The large background, that is the unuseful accidental correlation arising from the systematic time structure of the light, has been efficiently suppressed by a novel coherence-time modulation technique.

(2) This new apparatus works well for extracting the true two-photon correlation of soft X-ray synchrotron radiation. The DC drift, that is the thermal noise from the broadband high-gain electric correlator, has been canceled to almost zero compared with the signal output for a two-hour measuring time. The accidental correlation also has been suppressed to the magnitude of nearly 1/10 of the true correlation, which enable us to observe the apparent bunching effect.

(3) The measured explicit bunching effect implies that synchrotron radiation, even high-brilliance undulator radiation, is a chaotic radiation. Synchrotron radiation is a spontaneous radiation. The phase difference of the photons emitted by two neighboring electrons is usually determined by their distance, which is usually much larger than the observed photon wavelength. The significant fluctuation of this distance makes the superposed field amplitude emitted by a large amount of electrons in the bunch behave as a random walk with an average of zero. This is the chaotic nature of present synchrotron radiation.

(4) This experimental method provides a way to measure the instantaneous emittance of the stored beam with the time scale of coherence time τ_c,

(5) This method will be utilized for characterization of coherence properties of incomplete FELs, such as SASE. For a complete FEL it will give a total coherent radiation, therefore the measured normalized excess two-photon correlation will exhibit a flat response against any values of the precise slit width. Otherwise the photo-bunching effect will be observed.

9 Future prospect

So far this work has exhibited a preliminary success in the measurement of true two-photon correlation of soft X-ray synchrotron radiation based on our new idea. However the time does not seem long enough to perform some additional next steps after completing the present series of work, such as design, construction, test, experiment and analysis etc, within three years. Therefore there are still several efforts to be made in the future, which might be important for the evaluation of various light sources. Now I will discuss the problems to be performed in the future.

• Precise measurement of emittance of the stored beam

Two-photon correlation might be a potential way to measure the instantaneous emittance due to the discussion of section 7.2.1. The measured value of 40 *nmrad* estimated by fitting the measured data in Fig.6-2 and Fig.6-3 is actually too rough due to the few measured points (various d values in horizontal axis). It is clear that, the more points we measure, the more precise emittance we can obtain by fitting the experimental points to our theoretical calculation. In addition, it is very neccessary to explore a more precise theoretical model, for example, the finite temporal coherence in the plane of the precise slit might produce some bad influence on the spatial coherence of the two divided lights falling on the two MCPs.

For the theoretical verification of the above effect we need to measure the same group of points for various photon energies.

• Absolute measurement of the second-order coherence

Now it is time to explain why the vertical units in Fig. 6-2 and Fig. 6-3 are arbitrary. This experiment measured the excess part of two-photon correlation, that is $|\gamma_{12}(d)|^2$. The DC components have been cut out by the band-pass filters in each arm. We have no way to define its absolute value of the measured $|\gamma_{12}(d)|^2$ because we have no standard to calibrate. There exsits a pair of contradictions. If we tried to keep the DC components which is the background 1, the excess part $|\gamma_{12}(d)|^2$ would be too small to detect due to

the reduction factor τ_c / T_R; if we rejected the DC components, we would lose the standard to deduce its absolute value of the measured $|\gamma_{12}(d)|^2$. For our case this difficulty comes not only from the small coherence time τ_c, which is usually much smaller than the response time T_R of the measuring system for a chaotic light, but also from the non-stationary nature of synchrotron radiation. How to measure the absolute value of the second-order coherence for non-stationary light source will be a new exciting and challenging theme in the future.

The absolute measurement of the second-order coherence is very important for the precise quantitative evaluation of the coherence properties of light sources. It would become possible to characterize an intermediate state between a totally thermal state and a totally coherent state

• Checking the influence of betatron oscillation to chaotic SR

Because betatron oscillation is a high-frequency non-harmonic oscillation, its fundamental and higher harmonic oscillation frequencies might produce some contributions to the intrinsic chaotic nature of SR. If we have ways to measure the absolute second-order coherence, the influence of the betatron oscillation can be easily checked by correspondingly changing the lower limit of the bandpass filter in each arm. For example if the horizontal betatron oscillation frequency is 15 MHz, we can choose the lower limit of the bandpass filter as 5 MHz, 20 MHz, 40 MHz, 100 MHz etc., and measure the corresponding second-order coherence. The contributions of the betatron oscillation can be readily seen by comparing these data.

10 Acknowledgement

I would like to express my sincere gratitute to Professor T. Miyahara, who offered the opportunities for me to study here, to join this interesting but challenging theme, and I have benefited a lot by the continuous stimulated discussions with him, which are in fact the key of the smooth progress of this work. I want to thank especially Dr. Y. Takayama for his coorporation of this experiment from the beginning to the end. I also want to thank Professor T. Matsushita for his all kinds of help within the later two years. My great appreciations are also extended to Professor M. Ando, Professor S. Yamamoto, Professor J. Urakawa, Professor H. Hayano and Dr. H. Sugiyama, for their frequent attentions of the meeting of this project and for their much helpful advices. Professor K. Nasu gave some good suggestions about the writing of this thesis, Professor S. Kamada provided a useful unpublished reference paper, my deep thanks and appreciations go to all those mentioned above.

Appendix A

Derivation of the correlation output in the spectral domain

We first suppose that SR be intensity - modulated stationary thermal light, and its intensity can be expressed as follows,

$$I(t) = F(t)I_0(t) \qquad (A-1)$$

I_0 is conventional stationary thermal light. We can further express it with its complex amplitude $E(t)$,

$$I_0 = E^*(t)E(t) \qquad (A-2)$$

Time modulation function $F(t)$ is expressed as follows,

$$F(t) = F_1(t)F_e(t) \qquad (A-3)$$

$F_1(t)$, which comes from the ununiform distribution of electron bunches in the storage ring, is a rectangular wave with the repetition frequency 1.6MHz. $F_e(t)$ is a series of uniformly-distributed Guassian pulses with the repetition frequency 500Mhz. Fig.A-1 shows their shape in time domain with bunch width $T_e \approx 0.1ns$, bunch separation $T_b \approx 2ns$, bunches partial filling length T_{cov} and revolution time $T_{rev} \approx 625ns$. According to that, we can write them explicitly as follows,

$$F_1(t) = \sum_{n=-\infty}^{\infty} F_{10}(t - nT_{rev}) \qquad (A-4)$$

where

$$F_1(t) = F_{10}(t) = \begin{cases} 1 & (|t| \le \frac{1}{2}T_{cov}) \\ 0 & (|t| > \frac{1}{2}T_{cov}) \end{cases} \qquad (A-4a)$$

$$F_e(t) = \sum_{m=-\infty}^{\infty} \exp[-\frac{(t-mT_b)^2}{2T_e^2}] \ . \qquad (A-5)$$

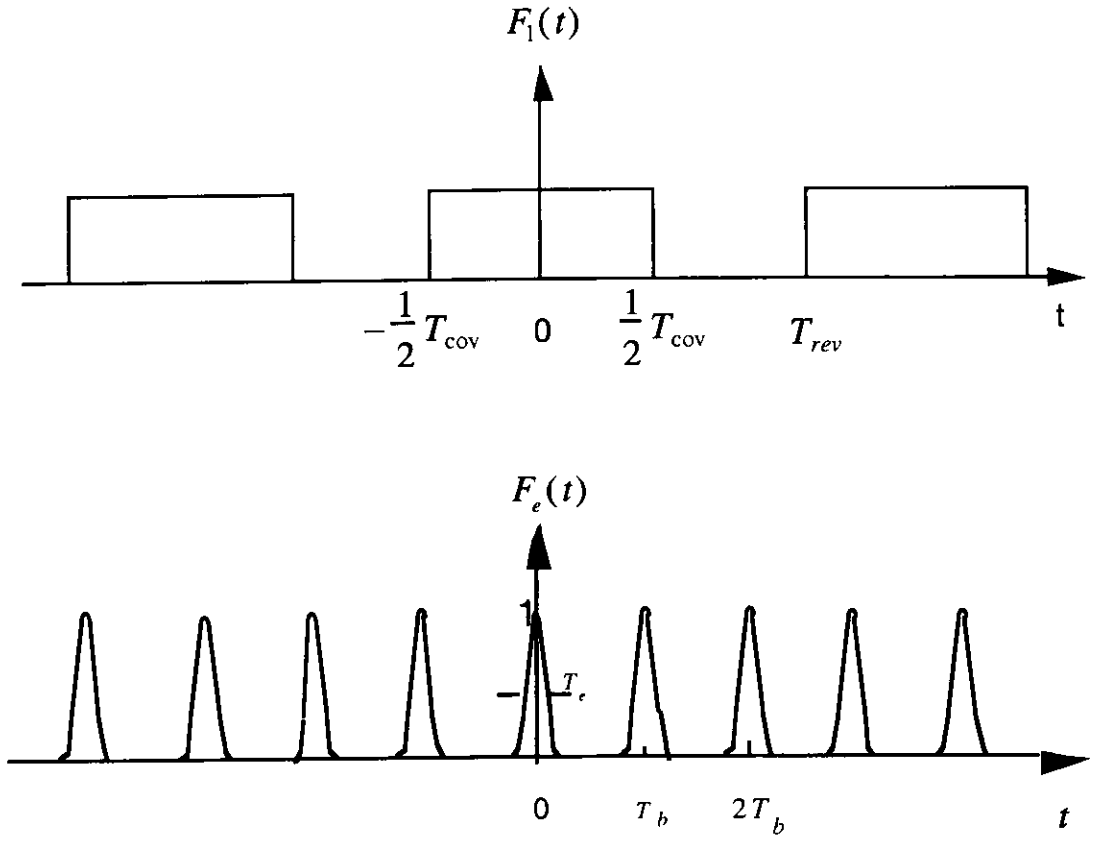

Fig.A-1

1. Spectral distribution of time modulation function

For the convenience of calculation, we present some basic formulae,

(1) For any periodic time function, such as

$$F(t) = \sum_{k=-\infty}^{\infty} F_0(t-kT) \ . \qquad (A-6)$$

Here T is the period. Its Fourier transformation has the form as

$$F(\omega) = (-1)^k \sum_{k=-\infty}^{\infty} \delta(\omega - k\omega_0) F_0(\omega) . \qquad (A-7)$$

$F_0(\omega)$ is the Fourier transformation of $F_0(t)$. ω_0 is the fundamental frequency and equals to $\omega_0 = \frac{2\pi}{T}$.

(2) For a multiplication of any two time functions such as

$$F(t) = F_1(t) F_2(t) , \qquad (A-8)$$

the Fourier transformation equals to the convolution of each Fourier transformation,

$$F(\omega) = F_1(\omega) \otimes F_2(\omega) = \int_{-\infty}^{\infty} F_1(\omega - \omega_1) F_2(\omega_1) d\omega_1 \qquad (A-9)$$

Thus from Eq.(A-9) and Eq(A-7), we get the spectral distribution of the time modulation function of Eq.(A-3) as follows,

$$F(\omega) = F_0 \sum_{n}^{\pm\infty} \sum_{k}^{\pm\infty} (-1)^{n+k} \frac{\sin(\frac{1}{2} T_m \omega_m n)}{T_m \omega_m n} \exp\left[-\frac{T_e^2}{2} (\omega - n\omega_m)^2 \right] \delta(\omega - n\omega_m - k\omega_B),$$

(A-10)

where

$$\omega_m = \frac{2\pi}{T_{rev}} \approx 2\pi \times 1.6 MHz \qquad (A-11)$$

$$\omega_B = \frac{2\pi}{T_b} \approx 2\pi \times 500 MHz \qquad (A-12)$$

and also $T_m = T_{cov}$

Expression (A-10) can be intuitively drawn as Fig. A-2 shows taking the consideration of $\frac{\omega_B}{\omega_m} \approx 312 >> 1$.

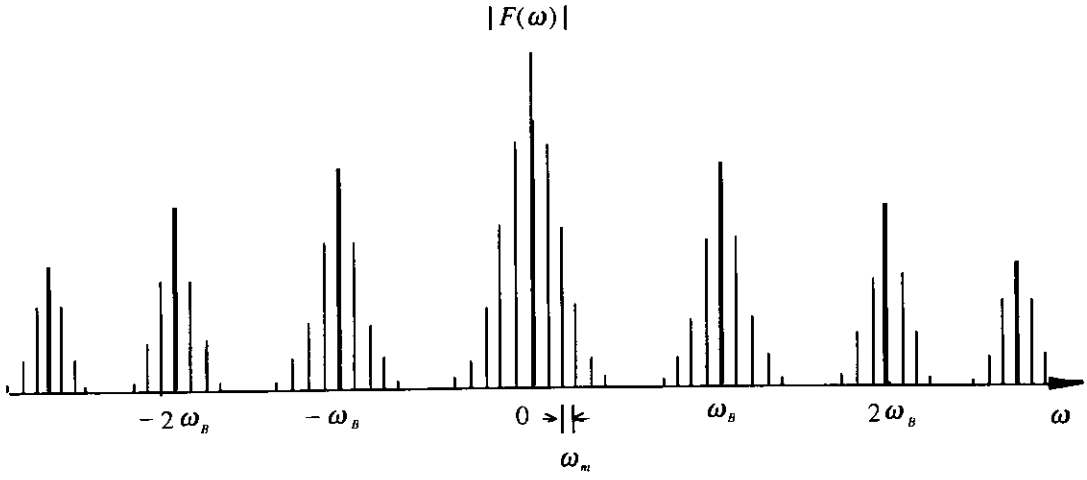

Fig. A-2 Spectral distribution of modulation function F(t)

2. Spectral distribution of the photoelectric current for an ideal detector

According to semiclassical theory photoelectric current is proportional to the incident optical intensity, i.e.

$$J(t) = \alpha e I(t) . \qquad (A-13)$$

Substitute Eq.(A-1), Eq.(A-2) and Eq.(A-10) into Eq.(A-13) and then transform it into the spectral domain, we get,

$$J(\omega) = e\alpha \iint F(\omega - \omega_1 + \omega_2) E(\omega_1) E^*(\omega_2) d\omega_1 d\omega_2, \qquad (A-14)$$

where e is the charge of an electron, α is the quantum efficiency of the detector. $E(\omega)$ is the Fourier transformation of the complex amplitude of the incident optical field.

3 . Low-pass filter and the average electric current

We suppose that the low-pass filter in the electric correlator be the following shape as is shown in Fig.(A-3), where only those frequencies which lie between ω_1 and ω_2 can pass this filter.

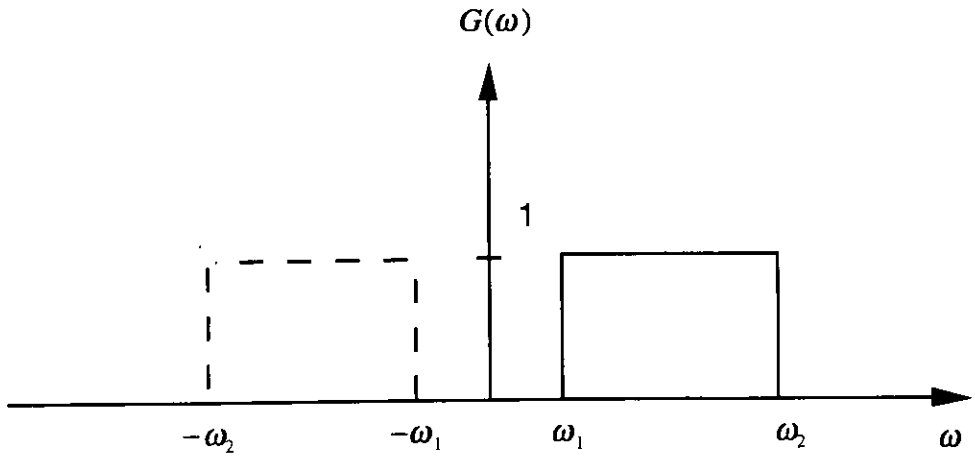

Fig. A-3 General low-pass filter shape

$$G(\omega)=\begin{cases}1 & (\omega_1<|\omega|<\omega_2)\\ 0 & else\end{cases}. \qquad (A-15)$$

With this filter, we can write the restricted electric current in the time domain as follows,

$$J_F(t)=e\alpha\iiint F(\omega-\omega_1+\omega_2)G(\omega)E(\omega_1)E^*(\omega_2)e^{-i\omega t}d\omega_1 d\omega_2 d\omega \qquad (A-16)$$

On the other hand, the spectral density of this stationary thermal light can be regarded as having a Guassian distribution for the simplicity of calculation,

$$<E(\omega)E^*(\omega')>=\frac{I_0}{\sqrt{2\pi}\omega_c}e^{-\frac{(\omega-\omega_0)^2}{2\omega_c^2}}\delta_{\omega,\omega'}, \qquad (A-17)$$

where I_0 is the DC component, ω_0 is the central frequency of this quasi-monochromatic optical field, and the coherent time τ_c can be expressed as

$$\tau_c = \frac{2\pi}{\omega_c} \ . \qquad (A-18)$$

With the Van Cittert—Zernike theorem, Eq.(A-17) can be easily generalized to the case of different two space points, i.e.

$$< E_1(\omega)E_2^*(\omega') >= \frac{\sqrt{\overline{I_1}}\sqrt{\overline{I_2}}}{\sqrt{2\pi}\omega_c} e^{-\frac{(\omega-\omega_0)^2}{2\omega_c^2}} \gamma_{12}(0)\delta_{\omega,\omega'} \ . \qquad (A-19)$$

The mutual degree of the first-order coherence $\gamma_{12}(0)$ is defined as follows,

$$\gamma_{12}(0) = \frac{< E_1(t)E_2^*(t) >}{< E_1(t)E_1^*(t) >< E_1(t)E_2^*(t) >} = \frac{< E_1(t)E_2^*(t) >}{\sqrt{\overline{I_1}}\sqrt{\overline{I_2}}} \ . \qquad (A-20)$$

$\gamma_{12}(0)$ is decided by the properties of light source and geometric structure of the experimental system.

Based upon those previous facts, we can easily estimate the average electric current of Eq(A-16),

$$< J_F(t) >_t = 0 \ , \qquad (A-21)$$

where < > represents the ensemble average over the optical field, subscript t indicates the time average. This result is obvious due to the DC-cut nature of this filter.

4 Correlation output

The correlation output of the two restricted electric current signals is

$$< J_{F1}(t)J_{F2}(t) >= (e\alpha)^2 \int_{-\infty}^{\infty} \cdots \int_{-\infty}^{\infty} d\omega_a d\omega_b d\omega_1 d\omega_2 d\omega_3 d\omega_4 e^{-i\omega_a t - i\omega_b t} \times$$

$$F(\omega_a - \omega_1 + \omega_2)F(\omega_b - \omega_3 + \omega_4)G(\omega_a)G(\omega_b) < E_1(\omega_1)E_1^*(\omega_2)E_2(\omega_3)E_2^*(\omega_4) >$$

(A-22)

We note the fact that,

$$< E_1(\omega_1)E_1^*(\omega_2)E_2(\omega_3)E_2^*(\omega_4) >$$
$$= V_{11}(\omega_1)V_{22}(\omega_3)\delta_{\omega_1,\omega_2}\delta_{\omega_3,\omega_4} + V_{12}(\omega_1)V_{12}^*(\omega_2)\delta_{\omega_1,\omega_4}\delta_{\omega_2,\omega_3},$$

(A - 23)

where we use the simple notation,

$$V_{ij}(\omega_k) =< E_i(\omega_k)E_j^*(\omega_k) > . \qquad (A\text{-}24)$$

Substitute Eq.(A-24) into Eq.(A-23), we find that the output result includes two parts,

$$< J_{F1}(t)J_{F2}(t) >= A + B \quad , \qquad (A - 25)$$

where

$$A = (e\alpha)^2 \int_{-\infty}^{\infty} \ldots \int_{-\infty}^{\infty} d\omega_a d\omega_b d\omega_1 d\omega_3 e^{-i\omega_a t - i\omega_b t} F(\omega_a)F(\omega_b)G(\omega_a)G(\omega_b)V_{11}(\omega_1)V_{22}(\omega_3),$$

(A - 26)

and

$$B = (e\alpha)^2 \int_{-\infty}^{\infty} \ldots \int_{-\infty}^{\infty} d\omega_a d\omega_b d\omega_1 d\omega_2 e^{-i\omega_a t - i\omega_b t} \times$$
$$F(\omega_a - \omega_1 + \omega_2)F(\omega_b - \omega_2 + \omega_1)G(\omega_a)G(\omega_b)V_{12}(\omega_1)V_{12}^*(\omega_2).$$

(A - 27)

A can be easily integrated by using Eq.(A-10),(A-15),(A-17) ,(A-24)

$$A \approx (e\alpha)^2 \overline{I_1}\,\overline{I_2} {F_0}^2 \sum_{n=N_1}^{N_2} \left[\frac{\sin(\frac{1}{2}T_m\omega_m n)}{\frac{1}{2}T_m\omega_m n} \right]^2 \quad , \qquad (A - 28)$$

where

$$N_1 = \frac{\omega_1}{\omega_m} \qquad (A-29)$$

and

$$N_2 = \frac{\omega_2}{\omega_m} \quad . \qquad (A-30)$$

We have performed the time average over A and assumed that the bandwidth of our electric circuit is smaller then ω_B (500MHz).

The calculation of Eq.(A-27) is a little complicated. First we make such substitution as follows ,

$$\begin{cases} \omega_\rho = \omega_1 - \omega_2 \\ \omega_s = \omega_1 + \omega_2 \end{cases} , \qquad (A-31)$$

and then integrate B over ω_ρ. Thus Eq.(A-27) can be simplificated as follows,

$$B = (e\alpha)^2 \frac{\overline{I_1}\,\overline{I_2}}{2\sqrt{\pi}\omega_c} |\gamma_{12}(0)|^2 \times$$

$$\iiint e^{-i\omega_a t - i\omega_b t} F(\omega_a - \omega_s) F(\omega_b + \omega_s) G(\omega_a) G(\omega_b) e^{-\frac{\omega_s^2}{4\omega_c^2}} d\omega_a d\omega_b d\omega_s .$$

(A-32)

Considering only the DC component and the fact $\omega_B / \omega_m >> 1$ and bandwidth $\omega_2 < 500MHz$, we arrive to

$$B \approx (e\alpha)^2 \frac{\overline{I_1}\,\overline{I_2}}{2\sqrt{\pi}\omega_c} |\gamma_{12}(0)|^2 F_0^2 \sum_{n=-\infty}^{\infty} \sum_{k=-\infty}^{\infty} \left(\frac{\sin(\frac{1}{2} T_m \omega_m n)}{T_m \omega_m n} \right)^2 e^{-(kT_e\omega_B)^2} \times$$

$$\int_{-\infty}^{\infty} |G(\omega)|^2 e^{-\frac{(\omega - n\omega_m - k\omega_B)^2}{4\omega_c^2}} d\omega \quad .$$

(A-33)

The integral part can be approximately integrated owing to the relation of $\omega_B / \omega_c \approx 10^{-5}$,

$$\int_{-\infty}^{\infty} |G(\omega)|^2 e^{-\frac{(\omega - n\omega_m - k\omega_B)^2}{4\omega_c^2}} d\omega \approx \int_{-\infty}^{\infty} |G(\omega)|^2 d\omega = 2(\omega_2 - \omega_1) = 2\omega_T \text{ ,(A - 34)}$$

where ω_T is the electric bandwidth. Another approximation can be achieved as follows,

$$\sum_{n=-\infty}^{\infty} \left(\frac{\sin(\frac{1}{2} T_m \omega_m n)}{T_m \omega_m n} \right)^2 \approx \frac{1}{T_m \omega_m} \int_{-\infty}^{\infty} \frac{\sin^2(\frac{1}{2}x)}{x^2} dx = \frac{1}{4} \frac{T_{rev}}{T_{\text{cov}}} \text{ , (A - 35)}$$

and

$$\sum_{n=-\infty}^{\infty} e^{-(kT_e \omega_B)^2} \approx \frac{1}{T_e \omega_B} \int_{-\infty}^{\infty} e^{-x^2} dx = \frac{1}{2\sqrt{\pi}} \frac{T_b}{T_e} . \qquad \text{(A - 36)}$$

Finally we get the important correlation output as follows,

$$< J_{F1}(t) J_{F2}(t) >_t \approx \overline{J_1}\,\overline{J_2} \left(\sum_{n=N_1}^{N_2} \left[\frac{\sin(\frac{1}{2} T_m \omega_m n)}{\frac{1}{2} T_m \omega_m n} \right]^2 + \frac{1}{8\pi} \frac{T_{rev}}{T_{\text{cov}}} \frac{T_b}{T_e} \frac{\omega_T}{\omega_c} |\gamma_{12}(0)|^2 \right),$$

(A - 37)

where $\overline{J_1}$ and $\overline{J_2}$ are average electric currents of each branch and expressed as follows,

$$\overline{J_1} = e\alpha \overline{I_1} F_0 , \qquad \text{(A - 38)}$$

and

$$\overline{J_2} = e\alpha \overline{I_2} F_0 . \qquad \text{(A - 39)}$$

Eq.(A-37) is a very important result. The first term in its expression is what we call trivial (or unuseful) correlation, which has nothing to do with the

properties of the intrinsic photon statistics.The main purpose of our design of an electric correlator is to suppress this harmful correlation. The second term is the real correlation of photon fluctuations. The duty factor $T_{rev}/T_{\mathrm{cov}} \sim 1$, $T_b/T_e \sim 20$ for the case of bunch distribution at the storage ring of Photon factory, KEK. The ratio of electric bandwidth to optical coherent bandwidth of $\omega_T/\omega_c \sim 10^{-5}$ is the main barrier for us to extract this so tiny useful signal. So we should enhance the electric band as we can as possible.

B Generalization to the Van Cittert-Zernike theorem

Now we consider the case that the light source has some transverse motion, what will affect the first-order coherence degree γ_{12} between the observation point P_1 and P_2?

As Figure B-1 shows, σ is the light source, which is the transverse electron distribution in the $\zeta - \eta$ plane. P_1 and P_2 are two points in the observation x-y plane A. The linear dimensions of σ is much smaller compared to the distance oo'. Electron bunch is moving along z-axis and its longitudinal distribution in the $\eta - z$ plane is shown in Figure B-2.

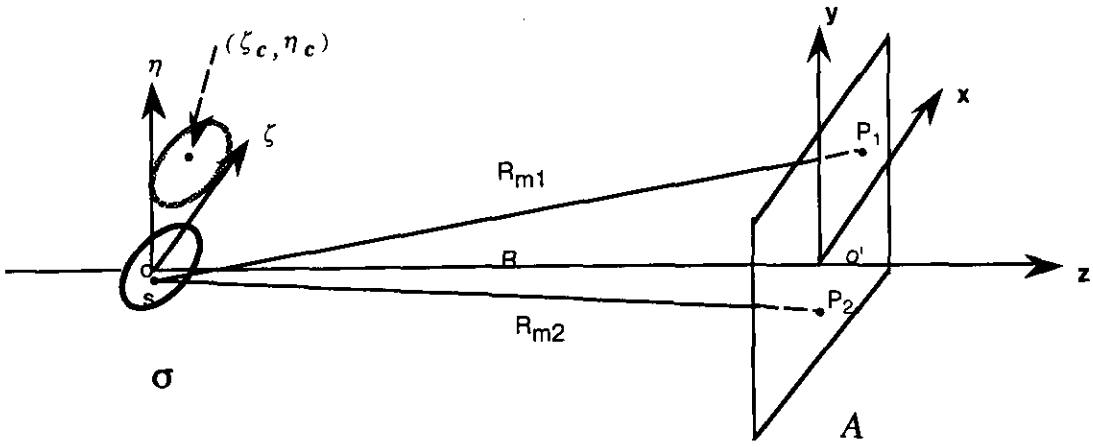

Fig. B-1 Illustrating the generalization of VAN CITTERT-ZERNIKE theorem

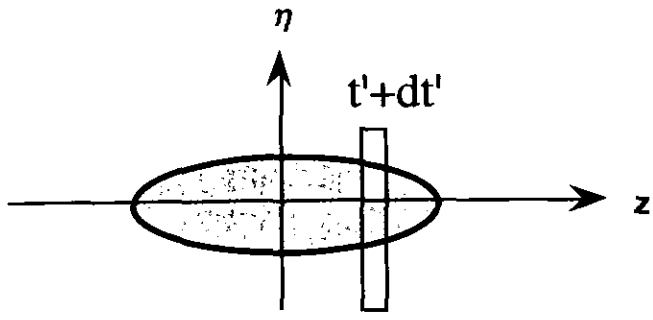

Fig. B-2 Longitudinal electron bunch distribution

If the light source has no any transverse motion relative to the observation points, γ_{12} can be easily estimated from the conventional Van Cittert Zernike theorem. Now we consider the case that the bunch center in the $\zeta - \eta$ plane could be movable with time.

First we suppose the spectral distribution emitted by an electron be Gaussian, that is,

$$E_m(\omega) = E_m(0)\exp(-\frac{(\omega-\omega_0)^2}{4\omega_c}) \ , \qquad (B-1)$$

where m stands for the mth electron, ω_0 is central frequency, ω_c is spectral bandwidth and its inverse is coherence time $\tau_c = 2\pi / \omega_c$. The electrons' intensity distribution in the $\zeta - \eta$ plane can be expressed as,

$$\rho(\zeta,\eta,t') = I[\zeta - \zeta_c(t'), \eta - \eta_c(t'), t'] \ B(t'), \qquad (B-2)$$

where t' is the emitter time, $B(t')$ is the brightness at time t'. $\zeta_c(t'), \eta_c(t')$ are the center coordinates of the transverse bunch distribution at time t'.

The optical field at P_1 and P_2 can be expressed as follows,

$$E_1(t) = \sum_m E_{m1}(t), \qquad E_2(t) = \sum_m E_{m2}(t) \ . \qquad (B-3)$$

$E_{m1}(t)$and $E_{m2}(t)$ are the fields at P_1 and P_2 due to the mth electron. Because the fields emitted by different electrons are assumed to be statistically independent, the field correlation function can be simplified to the following,

$$\langle E_1^*(t)E_2(t)\rangle = \sum_m \langle E_{m1}^*(t)E_{m2}(t)\rangle \qquad (B-4)$$

$E_{m1}(t)$and $E_{m2}(t)$ can be expressed as follows,

$$E_{m1}(t)=\frac{1}{R_{m1}}\int d\omega E_m(\omega)e^{-i\omega(t-t')+ikR_{m1}} \qquad (B-5)$$

and

$$E_{m2}(t)=\frac{1}{R_{m2}}\int d\omega E_m(\omega)e^{-i\omega(t-t')+ikR_{m2}} \quad . \qquad (B-6)$$

Substituting Eq.(B-5) and Eq.(B-6) into Eq.(B-4), considering the wave vector k is nearly unchanged with respect to ω within the bandwidth ω_c, then we get,

$$\langle E_1^*(t)E_2(t)\rangle=\sum_m \frac{4\pi\omega_c^2|E_m(0)|^2}{R_{m1}R_{m2}}\exp[-\frac{1}{2}\omega_c^2(t-t')^2+i\bar{k}(R_{m2}-R_{m1})], \qquad (B-7)$$

where the average wave vector is $\bar{k}=\omega_0/c$. We can further perform the ensemble average of Eq.(B-7) in the $\zeta-\eta-t'$ plane by using the intensity distribution function Eq.(B-2) and the summation over m is replaced by the integral over $\zeta-\eta$ plane. Then we get,

$$\langle E_1^*(t)E_2(t)\rangle=const.e^{i\psi}\iint I(\zeta,\eta)\exp[-i\bar{k}(p\zeta+q\eta)]d\zeta d\eta$$

$$\times B(t)\int\exp\{-\frac{1}{2}\omega_c{}^2(t-t')^2-i\bar{k}[p\zeta_c(t')+q\eta_c(t')]\}\ dt' \quad , \qquad (B-8)$$

where p,q and ψ are expressed as,

$$\psi=\frac{\bar{k}[(x_1^2-x_2^2)+(y_1^2-y_2^2)}{2R} \quad , \qquad (B-9)$$

and

$$p = \frac{x_1 - x_2}{R}, \qquad q = \frac{y_1 - y_2}{R} \quad , \tag{B-10}$$

where x_1, y_1 and x_2, y_2 are the coordinates of P_1 and P_2 in the x-y plane. From Eq.(B-8) we can readily get the coherence degree as follows,

$$\gamma_{12} = \frac{\langle E_1^*(t)E_2(t)\rangle}{\sqrt{\langle E_1^*(t)E_1(t)\rangle\langle E_2^*(t)E_2(t)\rangle}} \tag{B-11}$$

$$= \frac{e^{i\psi}\iint I(\zeta,\eta)\exp[-i\bar{k}(p\zeta + q\eta)]d\zeta d\eta}{\iint I(\zeta,\eta)d\zeta d\eta} \times f_c \quad ,$$

where

$$f_c = \frac{\omega_c}{\sqrt{2\pi}}\int \exp\{-\frac{1}{2}\omega_c{}^2(t-t')^2 - i\bar{k}[p\zeta_c(t') + q\eta_c(t')]\}\ dt' \quad . \tag{B-12}$$

f_c is so-called transverse motion factor.

C The radiation field emitted from an accelerated relativistic electron

In this part we try to derive the radiation fields emitted from an relativistic electron moving in the bending magnet and the undulator from Maxwell equations.

C-1 General radiation formula

The Maxwell equations are written as follows,

$$\begin{aligned}
&\nabla \times \mathbf{E}(\mathbf{x},t) + \frac{\partial \mathbf{B}(\mathbf{x},t)}{\partial t} = 0 \\
&\nabla \cdot \mathbf{B}(\mathbf{x},t) = 0 \\
&\nabla \times \mathbf{B}(\mathbf{x},t) - \frac{1}{c^2}\frac{\partial \mathbf{E}(\mathbf{x},t)}{\partial t} = \mu_0 \mathbf{i}(\mathbf{x},t) \\
&\nabla \cdot \mathbf{E}(\mathbf{x},t) = \frac{1}{\varepsilon_0}\rho(\mathbf{x},t)
\end{aligned} \quad , \qquad (C\text{-}1)$$

where **E** is electric field [V/m], **B** is magnetic flux density [T], **i** is electric current density [A/m^2], ρ is charge density [C/m^3], μ_0 is magnetic permeability [H/m], ε_0 is dielectric constant of vacuum [F/m], **x** is position [m], t is time [sec] , and c is light speed [m/sec].

Let us introduce **scalar and vector potential** ϕ and **A**,

$$\begin{aligned}
\mathbf{E}(\mathbf{x},t) &= -\frac{\partial \mathbf{A}(\mathbf{x},t)}{\partial t} - \nabla\phi(\mathbf{x},t) \\
\mathbf{B}(\mathbf{x},t) &= \nabla \times \mathbf{A}(\mathbf{x},t)
\end{aligned} \qquad (C\text{-}2)$$

with the Lorentz gauge condition

$$\nabla \cdot \mathbf{A}(\mathbf{x},t) + \frac{1}{c^2}\frac{\partial \phi(\mathbf{x},t)}{\partial t} = 0 \qquad (C\text{-}3)$$

After some algebra, potentials are given in **Wave equation** in case of Cartesian coordinate system.

$$\left(\Delta - \frac{1}{c^2}\frac{\partial^2}{\partial t^2}\right)\phi(\mathbf{x},t) = -\frac{1}{\varepsilon_0}\rho(\mathbf{x},t)$$
$$\left(\Delta - \frac{1}{c^2}\frac{\partial^2}{\partial t^2}\right)\mathbf{A}(\mathbf{x},t) = -\mu_0\mathbf{i}(\mathbf{x},t) \qquad (C-4)$$

where Δ is Laplacian in Cartesian coordinate system

$$\Delta = \frac{\partial^2}{\partial x^2} + \frac{\partial^2}{\partial y^2} + \frac{\partial^2}{\partial z^2} \qquad (C-5)$$

When charge and current densities are given, the scalar and vector potentials will be formally integrated out as follows,

$$\phi(\mathbf{x},t) = \frac{1}{4\pi\varepsilon_0}\int_{-\infty}^{\infty}dt'\int_{-\infty}^{\infty}d\mathbf{x}'\frac{\delta\left(t - t' - \frac{|\mathbf{x}-\mathbf{x}'|}{c}\right)}{|\mathbf{x}-\mathbf{x}'|}\rho(\mathbf{x}',t')$$
$$\mathbf{A}(\mathbf{x},t) = \frac{\mu_0}{4\pi}\int_{-\infty}^{\infty}dt'\int_{-\infty}^{\infty}d\mathbf{x}'\frac{\delta\left(t - t' - \frac{|\mathbf{x}-\mathbf{x}'|}{c}\right)}{|\mathbf{x}-\mathbf{x}'|}\mathbf{i}(\mathbf{x}',t') \qquad (C-6)$$

where δ Dirac's delta function.

Now let's express the charge and the current densities produced by a point charge moving along an arbitrary orbit $\mathbf{x}' = \mathbf{r}(t')$,

$$\rho(\mathbf{x}',t') = e\delta^3(\mathbf{x}' - \mathbf{r}(t'))$$
$$\mathbf{i}(\mathbf{x}',t') = e\delta^3(\mathbf{x}' - \mathbf{r}(t'))\frac{d}{dt'}\mathbf{r}(t') \qquad (C-7)$$

then the redarded potential for a moving point charge is given as follows by substituting Eq.(C-7) into Eq.(C-6),

$$\phi(\mathbf{x},t)=\frac{e}{4\pi\varepsilon_0}\int_{-\infty}^{\infty}dt'\,\frac{\delta\left(t-t'-\dfrac{|\mathbf{x}-\mathbf{r}(t')|}{c}\right)}{|\mathbf{x}-\mathbf{x}'|}$$

$$\mathbf{A}(\mathbf{x},t)=\frac{\mu_0 e}{4\pi}\int_{-\infty}^{\infty}dt'\,\frac{\delta\left(t-t'-\dfrac{|\mathbf{x}-\mathbf{r}(t')|}{c}\right)}{|\mathbf{x}-\mathbf{x}'|}\frac{d}{dt'}\mathbf{r}(t') \qquad (C-8)$$

The trajectory of the electron is shown in Fig.C-1, where t' is emitter time.

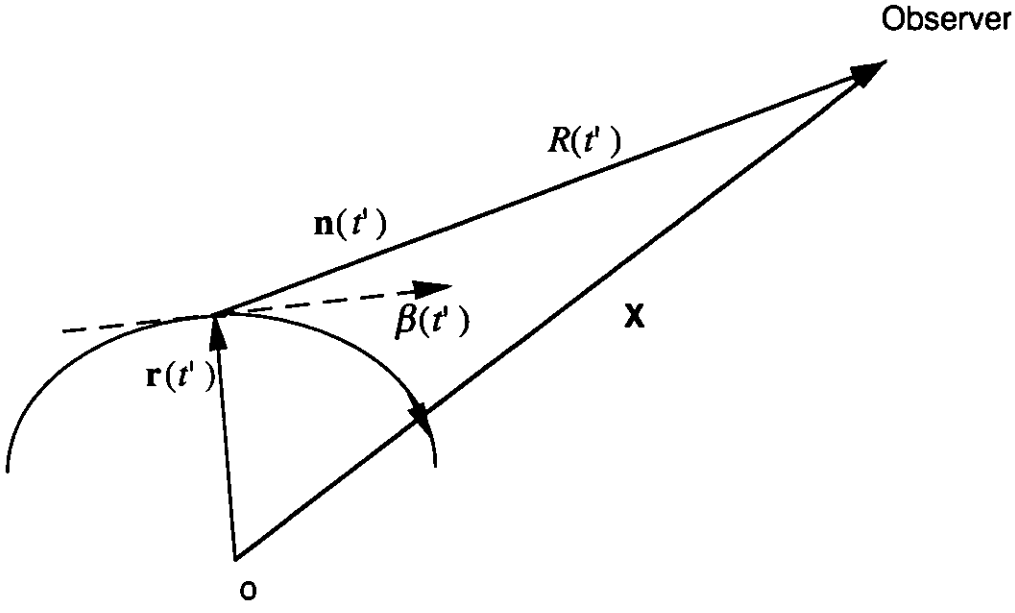

Fig. C-1 The electron trajectory and a stationary observer

Let's introduce a new notation,

$$\mathbf{R}(t')=\mathbf{x}-\mathbf{r}(t')$$

$$\mathbf{n}(t')=\frac{\mathbf{x}-\mathbf{r}(t')}{|\mathbf{x}-\mathbf{r}(t')|}=\frac{\mathbf{R}(t')}{R(t')} \qquad (C-9)$$

then the observer time is given as

$$t=t'+\frac{R(t')}{c} \qquad (C-10)$$

Also introduced is the scale-change factor $\kappa(t')$

$$\kappa(t') \equiv \frac{dt}{dt'} = 1 - \mathbf{n}(t') \cdot \bar{\beta}(t') \qquad (C-11)$$

where $c\beta(t')$ is the velocity of the electron, and we note here that $\bar{\beta}$ is a vector. The algebra to derive **Lienard-Wiechert potential** as follows,

$$\begin{aligned} \phi(\mathbf{x},t) &= \frac{e}{4\pi\varepsilon_0} \frac{1}{\kappa(t')R(t')} \\ \mathbf{A}(\mathbf{x},t') &= \frac{e}{4\pi\varepsilon_0 c} \frac{\bar{\beta}(t')}{\kappa(t')R(t')} \end{aligned} \qquad (C-12)$$

From Eq.(C-2) and (C-12) we can readily get the **electric field at the observer** as follows,

$$\mathbf{E}(\mathbf{x},t) = \frac{e}{4\pi\varepsilon_0}\left[\frac{\mathbf{n}}{\kappa R^2} + \frac{1}{c\kappa}\frac{d}{dt'}\left(\frac{\mathbf{n}-\bar{\beta}}{\kappa R}\right)\right] \qquad (C-13)$$

where the quantities within the square brackets are to be evaluated at the emitter time t'. Sometimes it is useful to give the **Feynmann's expression** [50] for the emitted field at the observer if we consider the time relationship $t'(t)$ according to Eq.(C-10).

$$\mathbf{E}(\mathbf{x},t) = \frac{e}{4\pi\varepsilon_0}\left[\frac{\mathbf{n}}{R^2} + \frac{R}{c}\frac{d}{dt}\left(\frac{\mathbf{n}}{R^2}\right) + \frac{1}{c^2}\frac{d^2}{dt^2}\mathbf{n}\right] \qquad (C-14)$$

C-2 Far-Field Limit

The expression of Eq.(C-13) or (C-14) simplifies in the far-field limit,

$$\begin{aligned} &\mathbf{x} = \mathbf{n}R_0, \\ &R_0 \to \infty \\ &|\mathbf{r}(t')| / R_0 \to 0 \end{aligned} \qquad (C-15)$$

Then the electric field at the observer is simplified as follows,

$$\mathbf{E}(\mathbf{x},t) = \frac{e}{4\pi\varepsilon_0 c^2 R_0}\left[\mathbf{n}\times\left(\mathbf{n}\times\frac{d^2}{dt^2}\mathbf{r}(t'(t))\right)\right] \qquad (C-16)$$

Fourier transformation of Eq.(C-16) gives the emitted spectral distribution as follows,

$$\begin{aligned} \mathbf{E}(\mathbf{n}R_0,\omega) &= \frac{1}{\sqrt{2\pi}}\int_{-\infty}^{\infty}\mathbf{E}(\mathbf{x},t)e^{i\omega t}dt \\ &= \frac{e}{2\sqrt{2\pi}\varepsilon_0 c R_0}(-i)\mathbf{A}(\omega) \end{aligned} \qquad (C-17)$$

$$\mathbf{A}(\omega) \equiv \frac{\omega}{2\pi}\int_{-\infty}^{\infty}dt'\,\mathbf{n}\times\left\{\mathbf{n}\times\bar{\beta}e^{i\omega t(t')}\right\} \qquad (C-18)$$

Now things get so simple for the exploration of the emitted electric field at the observer. The only job we need to do is to find its trajectory distribution with time and then integrate Eq.(C-18).

C-3 Motion of the electron in an external magnetic field

The equation of motion for an electron in an external magnetic field is

$$m\gamma_e\frac{d\mathbf{v}}{dt'} = e\mathbf{v}\times\mathbf{B} \qquad (C-19)$$

where m is the rest mass and $\gamma_e = 1/\sqrt{1-\beta^2}$ is the electron energy normalized by the electron rest mass and is a constant in the external magnetic field **B**. The velocity $\mathbf{v}(t') = c\bar{\beta}(t')$.

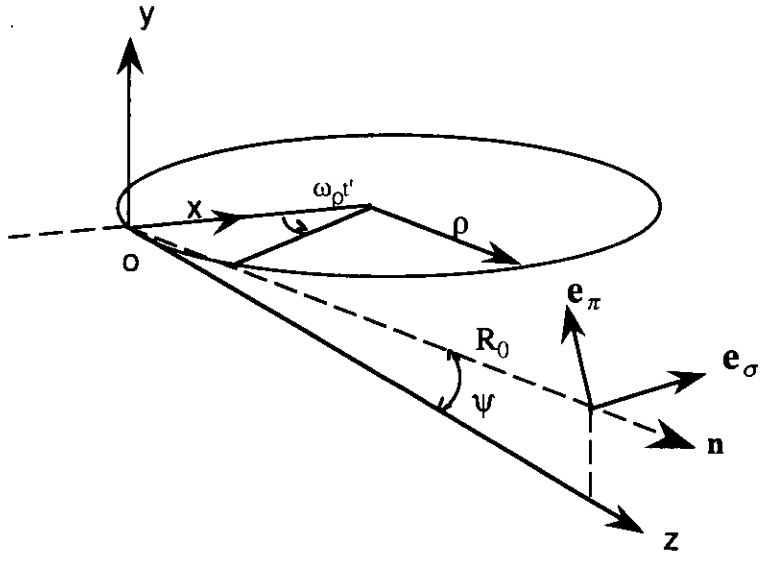

Fig. C-2 The orbit and coordinate system for bending-magnet radiation

First let's consoder the case of bending magnetic field, which is expressed as follows,

$$\mathbf{B} = (B_x, B_x, B_x) = (0, B, 0) \qquad (C-20)$$

The solution of Eq.(C-19) that satisfies the initial conditions is

$$\begin{aligned} \mathbf{r}(t') &= \rho\big(1-\cos(\omega_\rho t'), 0, \sin(\omega_\rho t')\big) \\ \bar{\beta}(t') &\equiv \dot{\mathbf{r}}(t')/c = \beta\big(\sin(\omega_\rho t'), 0, \cos(\omega_\rho t')\big) \end{aligned} \qquad (C-21)$$

where the bending radius and angular frequency are defined as,

$$\rho \equiv \frac{m_e \gamma_e c\beta}{eB}, \qquad \omega_\rho \equiv \frac{c\beta}{\rho} \qquad (C-22)$$

The initial conditions in Fig.C-2 are

$$\begin{cases} x(0)=0 \\ \dot{x}(0)=0 \end{cases} \quad and \quad \begin{cases} z(0)=0 \\ \dot{z}(0)=c\beta \end{cases} \qquad (C-23)$$

Under the approximations of $\omega_\rho t' << 1$, $1/\gamma_e << 1$ and small angle $n \approx (0, \psi, 1-\psi^2/2)$, the relation between emitter time and observer time is given as,

$$t(t') = \frac{1}{2}\left(\frac{1}{\gamma_e^{\,2}} + \psi^2\right)t' + \frac{\omega_\rho^{\,2} t'^{\,3}}{6} \qquad (C-24)$$

From Eq.(C-24) and Eq.(C-18) we can get the final result as it has been given in Eq.(2-2).

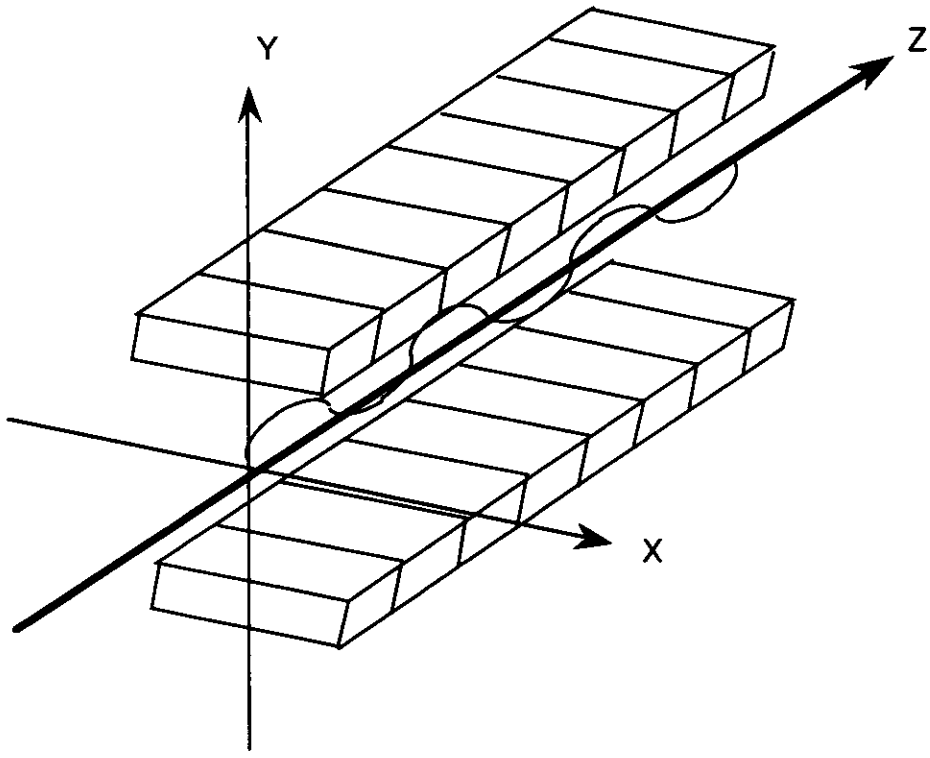

Fig. C-3 The orbit and coordinate system for undulator radiation

Another example is undulator magnetic field, which is expressed as,

$$\mathbf{B} = (B_x, B_x, B_x) = (0, -B_0 \sin(2\pi z / \lambda_u), 0) \qquad (C-25)$$

where λ_u is the period of the undulator. The electron orbit could be readily obtained as follows,

$$\frac{1}{c}\mathbf{r}(t') = \left(-\frac{K}{\gamma_e}\frac{1}{\omega_u}\sin(\omega_u t'), 0, \left(1 - \frac{1+K^2/2}{2\gamma_e^2}\right)t' - \frac{K^2}{8\gamma_e^2}\frac{1}{\omega_u}\sin(2\omega_u t') \right) \qquad (C-26)$$

where the undulator parameter K and the orbit frequency have been introduced,

$$K \equiv \frac{eB_0\lambda_u}{2\pi m_e c}, \qquad \omega_u = \frac{2\pi c}{\lambda_u} \qquad (C-27)$$

The coordinate system gives the observer pointing unit vector

$$\mathbf{n} = (\cos\psi\sin\phi, \sin\psi, \cos\psi\sin\cos\phi) \approx \left(\phi, \psi, 1 - \frac{1}{2}(\phi^2 + \psi^2)\right) \qquad (C-29)$$

Then the relation between the emitter time and the observer time is

$$t(t') = t' - \left(-\frac{K}{\gamma_e}\frac{1}{\omega_u}\sin(\omega_u t') \right)\phi - \left(1 - \frac{1}{2}(\phi^2 + \psi^2)\right) \times \left\{ \left(1 - \frac{1+K^2/2}{2\gamma_e^2}\right)t' - \frac{K^2}{8\gamma_e^2}\frac{1}{\omega_u}\sin(2\omega_u t') \right\} \qquad (C-30)$$

Eq.(C-30) and Eq.(C-18) give the final result described in Eq.(2-8).

References

[1] R. Hanbury Brown and R.Q. Twiss (1956a), *Nature* 177, 27-29.

[2] R. Hanbury Brown and R.Q. Twiss (1956b), *Nature* 178, 1046.

[3] R. Hanbury Brown and R.Q. Twiss (1957), *Proc.Roy.Soc.* (London) A242, 300.

[4] R. Hanbury Brown and R.Q. Twiss (1958), *Proc.Roy.Soc.* (London) A248, 199.

[5] R. Hanbury Brown and R.Q. Twiss (1958), *Proc.Roy.Soc.* (London) A248, 222.

[6] R. Hanbury Brown, *The intensity Interferometer*, Taylor and Francis, London,1974.

[7] R.J. Glauber (1963), *Phys.Rev.Letters,* 130, 2529-2539.

[8] R.J. Glauber (1963), *Phys.Rev.Letters,* 131, 2766-2788.

[9] L.Mandel and E.Wolf, *Optical coherence and quantum optics,* Cambridge University Press, New York, 1995.

[10] J. Perina, *Coherence of light,* D. Reidel Publishing Company, Dordrecht/Boston/Lancaster, 1985.

[11] M.L. Goldberger, H.W.Lewis, K.M.Watson (1963), *Phys.Rev.* 132, 2764

[12] E.V. Shuryak (1975), *Sov.Phys. JETP* 40, 30-31

[13] E.Ikonen (1992), *Phys.Rev.Letters* 68, 2759-2761

[14] E.Gluskin, I.McNulty and P.J.Viccaro (1992), *Nuc.Instr.Methods,* A319, 213-218

[15] E.Gluskin, I.McNulty , L.Yang, K.J.Randall, Z.Xu and E.D.Johnson (1994), *Nuc.Instr.Methods,* A347, 177-181

[16] L.Yang, I.McNulty and E.Gluskin (1995), *Rev.Sci.Instrum.* 6(2), 2281-2283

[17] Y.P.Feng, I.McNulty, Z.Xu and E.Gluskin, *LS Note* 258, 1997.

[18] E.Gluskin, "Intensity Interferometer and its application to Beam diagnostics", in 1991 *IEEE Particle Accel. Conf.*, (IEEE, New York, 1991), 2, 1169.

[19] T. Miyahara (1998), *J.Synchrotron Rad.* 5, 305-308.

[20] R.Z.Tai, Y.Takayama, T. Miyahara, S. Yamamoto, H. Sugiyama, J. Urakawa, H.Hayano and M.Ando(1998), *Rev.Sci.Instrum.* to be submitted

[21] Y. Kunimune, Y.Yoda, K.Izumi, M.Yabashi, X.W. Zhang, T. Harami, M.Ando, S.Kikuta (1997) *J.Synchrotron Rad.* 4, 199-203.

[22] D. Kleppner, *Physics Today*, August 1997, 11-13.

[23] K.J. Kim, *Characteristics of Synchrotron Radiation*, AIP Conference Proceedings, 184 vol 1: 565-632.

[24] A lecture on *the Generation Mechanism of Synchrotron Radiation* by S. Kamada in 1996.

[25] T. Miyahara, *Jpn. J. Appl. Phys.*, Vol 25, No.11 (1986), 1672.

[26] P. Meystre and M.Sargent, *Element of Quantum Optics* (second edition), Spring-Verlag Berlin Heidelberg 1990,1991.

[27] R. Loudon, *The Quantum theory of Light*, Oxford Science Publication 1973.

[28] T.C. Marshall, *Free-Electron Lasers*, Macmillan Publishing Company 1985.

[29] Max Cornacchia for the LCLS Design Study Group, *Performance and Design Concepts of a Free Electron Laser Operating in the X-ray Region*, SLAC-PUB-7433, March 1997.

[30] J.M. Buzz, A. Prokhorov(Editor-in-chief), P. Sprangle, and K. Wille. *Research Trends in Physics: Coherent Radiation and Particle Accelaration*, pp.106-115, La Jolla International School of Physics, The Institute for advanced Physics Studies, La Jolla, California, 1992.

[31] N. Wax, (Ed.)(1954). *Selected papers on noise and stochastic process*, Dover, New York.

[32] M. Sands, *The Physics of Electron Storage Rings, An Introduction*, 1970, Standford Linear Accelarator Center Report SLAC-PUB-121.

[33] P.A.M. Dirac, *The Principle of Quantum Mechanics*, Oxford University Press, 1958.

[34] U. Leonhardt, *Measuring the quantum state of light*, Cambridge University Press, 1997.

[35] O. Hirota, *Squeezed Light*, Elsevier Science Publisher B.V.(1992).

[36] M. Born and E. Wolf, *Principles of Optics*, sixth edition, Pergamon press, Oxford.1980

[37] Y. Takayama, Doctorate dissertation 1998, *Comprehensive determination of the coherence of synchrotron radiation in soft X-ray region.*

[38] Y. Takayama, R.Z. Tai, T. Hatano, T. Miyahara, W. okamoto and Y. Kagoshima, " *Measurement of the coherence of synchrotron radiation*", J. Synchrotron Rad. (1998). 5, 456-458.

[39] K.J. Kim, "*Brightness, coherence and propagation characteristics of synchrotron radiation*", Nuclear Instruments and Methods in Physics Research A 246 (1986) 71-76.

[40] T. Miyahara, 2nd School on the Fundamentals and the Techniques of Synchrotron Radiation, in Japanese, pp. 110-121.

[41] A.G. Michette, *Optical System for Soft X Rays*, Plenum Press, New York and London, 1986.

[42] L. Mandel, *Fluctuations of light beams*, Progress in Optics, Ed. E.Wolf, North-Holland, Amsterdam, 1963, pp. 181.

[43] Operating Manual for MCP Assembler F 4655-10 (Hamamatsu 1996)

[44] J.W. Goodman, *Statistical Optics*, John Wiley & Sons, Inc. New York, 1985.

[45] T. Miyahara and Y. Kagoshima, " *Importance of wave-optical correction to geometrical ray tracing for high brilliance beamline*" , Rev. Sci. Instrum. 66(2), February 1995.

[46] SRS Standford Research Systems, *SR830 DSP Lock-in amplifier operating manual and programming reference.*

[47] V.Hogg, A.T.Craig, *Introduction to mathematical statistics*, 4th edn, Macmillan Publishing Co.,Inc.1978.

[48] J. Krzywinski, E.L. Saldin, E.A. Schneidmiller and M.V.Yurkov *A new method for ultrashort electron pulse-shape measurement using synchrotron radiation from a bending magnet*, TESLA-FEL 97-03

[49] A. Ogata, "*Emittance Measurement in Electron Rings*", KEK Proceedings 95-7, September 1995 A.

[50] R.P. Feynman, *The Feynman lecture on Physics*, Addison-Wesley Pub. Co. Reading, Mass., 1963.

Publications and Presentations

1. Y, Takayama, R.Z. Tai, T. Hatano, T. Miyahara, W. Okamoto and Y. Kagoshima, " Measurement of the coherence of synchrotron radiation", *J. Synchrotron Rad.* (1998). 5, 456-458.

2. Y, Takayama, R.Z. Tai, T. Hatano, T. Miyahara, W. Okamoto and Y. Kagoshima, " Measurement of coherence of the synchrotron radiation", *The 6th International Conference on Synchrotron Radiation Instrumentation* (SRI.'97), Himeji, Japan, Aug.4-8,1997.

3. R.Z. Tai, Y. Takayama, T, Miyahara, S. Yamamoto, H. Sugiyama, K. Tsuchiya, M. Ando, J, Urakawa and H. Hayano, " Measurement of the second-order coherence of synchrotron radiation". *The 53rd Annual Meeting of the Physical Society of Japan,* Toho University & Nihon University, March 30~April 2, 1998.

4. R.Z. Tai, Y. Takayama, T, Miyahara, S. Yamamoto, H. Sugiyama, J. Urakawa, H. Hayano and M. Ando, " Measurement-II of the second-order coherence of synchrotron radiation", *Sectional Meeting of the Physical Society of Japan,* University of Ryukyus & Okinawa International University, Sep. 25~28, 1998.

5. R.Z. Tai, Y. Takayama, T, Miyahara, S. Yamamoto, H. Sugiyama, J. Urakawa, H. Hayano and M. Ando, " Measurement of True Two-Photon Correlation of Soft X-rays with Time Structure by Cancellation of False Correlation". *12th International Conference on Vacuum Ultraviolet Radiation Physics*(VUV-XII), August 3-7, 1998, Grand Hyatt Hotel, San Francisco, California, USA .

6. R.Z. Tai, Y. Takayama, N.Takaya, T, Miyahara, S. Yamamoto, H.Sugiyama, J. Urakawa, H. Hayano and M. Ando, " A novel intensity interferometer for synchrotron radiation in the VUV and soft x-ray region". Submitted to *Rev. Sci. Instrum.*(1999)

7. R.Z. Tai, Y. Takayama, N.Takaya, T, Miyahara, S. Yamamoto, H. Sugiyama, J. Urakawa, H. Hayano and M. Ando, " Chaotic nature of the stored current in an electron storage ring detected by a novel two-photon correlator for synchrotron radiation". Submitted to *Physical Reveiw A* (1999).